UNIVERSITY OF CALIFORNIA, MERCED

DATA-DRIVEN ROBUST CONTROL OF UNDERACTUATED MECHANICAL SYSTEMS USING IDENTIFICATION OF FLAT OUTPUT AND ARTIFICIAL INTELLIGENCE

by

Shangjie Ma

A thesis submitted in partial satisfaction of the
requirements for the degree of
Doctor of Philosophy

in

Mechanical Engineering

Committee in charge:
Professor Jian-Qiao Sun, Chair
Professor YangQuan Chen
Professor Reza Ehsani
Professor Roummel Marcia

The thesis of Shangjie Ma is approved:

Jian-Qiao Sun, Chair	Date
YangQuan Chen	Date
Reza Ehsani	Date
Roummel Marcia	Date

University of California, Merced

To my parents, my brother, and my love, Tiffany.

ACKNOWLEDGEMENTS

Life is a journey, and I am fortunate to own a special experience in the journey - an experience in the pursuit of truth and wisdom. Looking back over the past few years, the path I have walked through made me more humble and more aware of myself, which certainly would become one of the most valuable treasure in my life. Here, I am so grateful to my mentor Prof. Jian-Qiao Sun, my colleagues and my friends. Without their support, I would not be where I am today.

CURRICULUM VITAE

Education

B.S. in Mechanical Engineering, China University of Mining and Technology (Xuzhou, China), 2016.

M.S. in Mechanical Engineering, University of California San Diego (La Jolla, CA), 2018.

Ph.D. in Mechanical Engineering, University of California Merced (Merced, CA), 2021.

Honors

China National Scholarship, the Ministry of Education (China), 2013

Outstanding Graduate, China University of Mining and Technology (Xuzhou, China), 2016.

Mechanical Engineering Bobcat Fellowship, University of California Merced, 2019, 2020, 2021

Publications

Ma SF, Leylaz G, Sun JQ (2021) "Data-driven robust tracking control of underactuated mechanical systems using identified flat output and active disturbance rejection control ". *International Journal of Control*, 1-17.

Ma SF, Leylaz G, Sun JQ (2021) "Identification of differentially flat output of underactuated dynamic systems ". *International Journal of Control*, 1-17.

Leylaz G, Ma SF, Sun JQ (2021) "An optimal model identification algorithm of nonlinear dynamical dystems with the algebraic method ". *Journal of Vibration and Acoustics* **143**(2), 021002.

Laredo D, Ma SF, Leylaz G, Schütze O, Sun JQ (2021) "Automatic model selection for fully connected neural networks ". *International Journal of Dynamics and Control* **8**(4), 1063-1079.

Chi W, Ma SJ, Sun JQ (2020) "A hybrid multi-degree-of-freedom vibration isolation platform for spacecrafts by the linear active disturbance rejection control ". *Applied Mathematics and Mechanics (English Edition)*, 41(5), 805-818.

TABLE OF CONTENTS

LIST OF FIGURES

LIST OF TABLES

LIST OF SYMBOLS

n degrees of freedom of UMS
$x, \mathbf{x}$ state (vector)
$\mathbf{x}_\delta$ state vector near equilibrium point
$y_f, \mathbf{y}_f, y_l^{2n}, y_{f_1}$ flat output (vector)
$u, \mathbf{u}$ control input
r relative degree
r_f filter parameter
c_i coefficient in expression of flat output
y_l linear combination of incremental outputs
ω frequency variable
$H_1(j\omega), H_1(s)$ H_1 estimation of transfer function
s_l limit of slope of the transfer function in log-log plot
r_l absolute value of s_l
W_b data set in chosen frequency band in FOID
s_i slope of each subset of data set W_b
ϕ swing angle of Furuta pendulum
ψ, φ swing angle of rotary crane pendulum
θ angular position of Furuta pendulum and rotary crane pendulum
ϕ_δ Incrementalvariableof ϕ nearequilibirumpoint
$\psi_\delta, \varphi_\delta$ Incremental variable of ψ, φ near equilibirum point
θ_δ Incremental variable of θ near equilibirum point
C_r^* optimal ratio in FOID and FOID-Net
C_r ratio of two weights in FOID and FOID-Net
r^* optimal relative degree in FOID
J_r Rotary arm moment of inertia about its center of mass
J_p Pendulum moment of inertia
m_p Mass of pendulum
L_h Half length of pendulum
L_r Total length of rotary arm
g Gravitational acceleration
η_g Gearbox efficiency
K_g High-gear total gear ratio
η_m Motor efficiency
τ torque provided by motor

k_t Motor current-torque constant
k_m Motor current-torque constant
R_m Motor armature resistance
$q, \mathbf{q}$ generalized coordinates chosen for UMSs
$\dot{q}, \dot{\mathbf{q}}$ generalized velocities chosen for UMSs
$\xi(t)$ total disturbance in ADRC
$\tilde{\xi}(t$ estimate of disturbance in ADRC
J_λ cost function for LASSO
$\mathbf{C}_m$ MIMO controllability matrix
b_0 nominal control gain select in ADRC
G_D filter for TD layer in FOID-Net
$\mathbf{W}_f$ weight vector of flat output layer
$\mathbf{W}_p$ the weight matrix of state output layer
$\mathbf{W}_m$ the weight matrix of mirror layer
α learning rate for Adam
$\mathcal{L}_2, \mathcal{L}_3, \mathcal{L}_4, \mathcal{L}$ loss functions for FOID-Net

Subscripts and Superscripts
$\widehat{\ }$ Estimated values
$\dot{}$ First-order derivative with respect to time
$\ddot{}$ Second-order derivative with respect to time
$\dddot{}$ Third-order derivative with respect to time
(i) i-th order derivative with respect to time

ABSTRACT

Underactuated mechanical system (UMS) is a special class of mechanical systems that play an important role in a wide variety of engineering applications. UMSs typically show a great difficulty in analysis and control design because of complex nonlinearity and loss of capability to configure arbitrary motions in some directions. Flatness-based control and active disturbance rejection control (ADRC) approach has been an active research topic about dealing with control problems of UMSs. Flatness, as a useful property of a class of dynamical systems, called flat systems, guarantees that all the states and inputs of them can be parameterized by a set of differentially independent coordinates, called flat output. The trajectory planning and tracking control of flat systems can be greatly simplified by prescribing the desired references in 'flat space' without any other constraints except for necessary initial and final conditions. Despite its merits in control design, flatness is not a universal property of nonlinear dynamical systems and normally is not effortless to be characterized. Additionally, most UMSs are not inherently flat, i.e., not feedback linearizable, either statically or dynamically. The emerging framework that combines flatness of tangent linearization and ADRC has been experimentally proved feasible and robust for a large class of UMSs in recent years. While this approach continues to extend to more engineering applications, data-driven control design based on the flatness and ADRC has drawn attention of us, as fully detailed model information for flat output characterization is expensive and normally unavailable in control design. With few numbers of input-output measurements and little knowledge of the underlying UMSs, a data-driven approach for this framework enables an efficient, without modeling process, and systematic feedback control design for a class of UMSs with similar dynamical structures. Specifically, we first focus on the identification of flat output of nonlinear UMSs' tangent linearization using only input-output data collected. The identified flat outputs are naturally applied to the flatness-based control and ADRC framework, where several issues, such as trajectory planning and identification of state-flat output relations, are discussed and solved when extensive model information is no longer available.

Frequency domain algorithms (FOID, MFOID) and time domain algorithm (FOID-Net) are proposed to solve flat output identification (FOID) problem of nonlinear UMSs. FOID and MFOID leverages the estimated transfer function of various flat output candidate in chosen frequency band to identify their relative degrees

which is proved closely related to flatness of linearized UMSs. No detailed mathematical model of the system is needed. Flat output candidate is written as a linear combination of measured outputs. An optimal linear combination is identified so that the candidates achieve the highest relative degree. When the relative degree is equal to the order of the system, the output is flat. We have also developed data handling strategies to obtain the best estimate of the relative degree in the presence of measurement noise, high-frequency dynamics and Nyquist digitization effect. MFOID is an extension of FOID to deal with a special case of flat output of MIMO UMSs. The proposed algorithms are validated by numerical examples and an experimental study of a rotary crane system. The FOID-Net is a neural work framework designed to use time series data to estimate flat output out of linearized systems. We introduce the tracking differentiator into training of neural network which generates the time derivatives of flat output candidates and filter the noisy states. The idea of FOID-Net is based on the essential feature of flat systems that all states and inputs can be expressed by linear or nonlinear functions of flat coordinates. The training method, simulations of Furuta pendulum and a fourth-order nonlinear UMSs are discussed.

A framework of designing data-driven robust tracking control based on identified flat output and sparse identification is proposed. Reduced linearized model are proposed to show that the number of components of linear flat outputs can be further reduced. Flat outputs can be identified by FOID algorithm or FOID-Net. Technique of sparse regression is applied to identify the relationships between flat output and system states, which reduces the order of the well-known extended state observer (ESO) and thereby make the ESO more effective for both trajectory planning and tracking in terms of the flat output. When FOID-Net is applied, the flat output-state relations can be directly found by weight matrix of well trained layer. The proposed control scheme is validated by experimental studies of a rotary crane system in which a rest-to-rest tracking control is implemented.

Chapter 1

INTRODUCTION

1.1 Background

1.1.1 Underactuated Mechanical System

Underactuated mechanical system (UMS) is a special class of mechanical systems that play an important role in a wide variety of engineering applications. Many mechanical systems are UMSs, such as robot manipulators, helicopters, satellites and underwater vehicles. Underactuation basically refers to the feature that there are more degrees of freedom of the system than number of distinct and decoupled control inputs it has. This characteristic forces the motions of UMSs to being restricted in their configuration space, which can be the nature of some dynamical systems, a result of actuator failure or intentional design for flexibility and cost reduction. UMSs are usually difficult to analyze and to control even if the accurate mathematical models of them are available. When external forces and internal unknown dynamics, treated as general disturbances, affect the motion of the system, the stabilization or tracking control design can even become more challenging. There has been a major interest in developing control strategies for stabilization and tracking of UMSs in the past decades [1–4].

1.1.2 Differential Flatness and Flat Output

Flatness, as a property of nonlinear dynamical systems, has been used extensively in trajectory planning and tracking control. The flat system guarantees that a class of outputs, called flat outputs [5], exists such that all other system variables, including control inputs, can be expressed in terms of them and their finite number of time derivatives. The full parameterization of all system variables allows the dynamics of the nonlinear flat system to be rewritten completely with flat outputs such that the general difficulty of motion planning in nonlinear control design, approximation and integration of differential equations, is avoided. We are able to transform the system to a trivial form of integrals with flat output variables. Any other constraints on the systems could be also transformed by the flat coordinates and become the limits of the trajectories of flat output variables. It has been proved that a special class of mechanical control systems whose motion is described by Lagrange Equations and have special structures are differentially flat [6]. To leverage

the features of flatness, the flat output is normally identified first with a provided mathematical model of nonlinear flat system. However, the characterization of differential flatness and flat outputs of nonlinear system, even if with accurate model information, is generally a challenging problem, which has become one of the main obstacles to applying flatness-based control. Further, utilizing flatness becomes impracticable when the flat outputs do not exist since many nonlinear systems are not inherently or strictly flat.

1.1.3 Flatness-based Control and Active Disturbance Rejection Control

With characterized flat output variables, the trajectory planning and tracking control for nonlinear flat systems could be solved straightfowardly, hence the name flatness-based control. The concentration of our work is identification of flat outputs of a class of nonlinear UMSs without explicit models and use them in flatnes-based control design. Unfortunately, most underactuated mechanical systems are non-differentially flat, which seems to cause the concept of flatness to be useless in this scope. Although the direct application of flatness may fail, a framework of combining the flatness of the tangent linearization of the system and active disturbance rejection control (ADRC) is introduced recently to deal with the challenge of output reference trajectory tracking control of non-flat UMSs [7]. The tangent linearization of UMSs around arbitrary equilibrium point, if controllable, has been proved differentially flat and can take advantage of all the properties of flatness for control design. The approximation error of tangent linearization, internal and external disturbances, known as total disturbances, is compensated online by a properly configured extended-state observer(ESO) from ADRC framework. The ADRC has a good robustness of cancelling the real-time disturbances and mismatch of system parameters within a large range, thus the closed-loop system can operate far from the equilibrium point where it was supposed to operate around due to 'linear' assumption. However, the accuracy of characterization of flat output variable from the mathematical equations is still important, even if the linearization and other approximation error can be presumably compensated by the ESO. A large discrepancy existing in flat output variable's expression could easily result in the failure of ESO, because of the numerical instability and disqualification of estimating the huge variation in signals, and lead to instability and other undesirable behaviors of the closed-loop system.

1.1.4 Problem Formulation

We notice the characterization of the flatness and flat output variables, or short flat outputs, are almost model-based approaches. When model is available, the characterization process of flatness and find its flat is not trivial work generally, and sometimes it needs to tailor the existing models to simplified or reduced models so that the flat outputs could be found. With controllable tangent linearization of

nonlinear system and ADRC framework, the flat output characterization can rely on mathematical tools from linear system theories, although reduction of models sometimes are still needed to obtain flat output in a nice form, however, the model is still quite necessary to initiate the control design in the first place.

In this thesis, we first aim to design several data-driven algorithms using tools and concepts from machine learning and deep learning to identified the flat output for those tangent linearization of nonlinear UMSs for flatness-based control design. The identification of flat output does not require explicit equation of motions and only take input-output measurements from the underlying systems. As a result, the designed algorithms should find the best expression of flat output in terms of the linearized system states around certain equilibrium point where it is controllable. Secondly, the result of proposed flat output identification algorithms can be incorporated into a new framework where we only use input-output data to design robust tracking control for nonlinear UMSs based on ADRC. The algorithms need to additionally identifies the relations between flat coordinates, the flat output and its finite time derivatives, and linearized original system states which would be extremely useful in trajectory design in tracking control. This problem in linear system theory is also known as finding the controllability canonical form, or Brunovsky's Form. The performance of the ESO also needs to be improved when the system is faced with heavy noise.

1.2 Literature Review

1.2.1 Flatness and Flat Output Characterization

The characterization of differential flatness and flat outputs is a critical and challenging problem for flatness-based control design. Linear controllable systems can be proved to be flat [5]. The flat output of linear systems can be derived by polynomial matrices [8]. Sufficient and necessary conditions for existence of flatness of nonlinear systems are discussed in plenty publications [9–13]. These studies have not led to the development of methods for systematically computing and verifying the flat outputs. [14] proposed an approach by eliminating variables to construct flat outputs for lumped parameter nonlinear systems with an arbitrary number of inputs. [15] and [16] introduced generalized moving frame structure equations and generalized Euler-Lagrange operator to characterize the flatness of nonlinear systems. [17] have studied the characterization of flat outputs of MIMO controllable linear time-invariant discrete- and continuous-time systems, and developed a quick computational test to claim whether an output candidate is flat. [18] modeled the system by differential algebraic equations (DAE) and proposed a numerical method to characterize the flatness of complex nonlinear systems. However, the characterization of flatness and flat outputs highly depend on the availability and accuracy of the mathematical model of the system and is unreliable when uncertainties such as unmodeled dynamics and unknown disturbances are considered. In the recent years,

the data-driven method of finding the flat output has not been fully researched and discovered.

1.2.2 Flatness-based ADRC Design

Sira-RamirezLuviano-JuarezCortes-Romero2012 proposed a linear active disturbance rejection control scheme for Chua's circuit based on its differentially flatness. The flat output is found by inspecting the state-space model of the circuit, and validated by the dynamics of the equations. A smooth output reference signal is designed specifically for the tracking control, and generalized proportional integral(GPI) observer, a variant of ESO, is designed to compensate the internal and external disturbances. The circuit system is naturally differentially flat without approximation. The robustness with control gain parameters of ADRC is also shown in the work. The burden of GPI or ESO is relatively light compared with the case where controllable tangent linearization of system is introduced. [19] worked on the flatness-based ADRC design for buck-converter DC-motor combinations with a normalized average flat model. The unknown, exogenous, time-varying load current are considered as main disturbance for the system. The flatness is not exact but the dynamics can be compensated by the proposed GPI observers so the system could track the given reference velocities. Similar work for Thomson's ring model and permanent magnet synchronous motor can be in [20–22]. All of the flatness is characterized based on common models or transformed models.

For underactuated mechanical systems, [23] introduced tangent linearization model of Furuta pendulum and GPI observers for its tracking control design. The model of Furuta pendulum is nonlinear naturally, while in their work the model is linearized around the unstable equilibrium point and hence become flat system without damping terms in the model. The flat output is found based on the linearized model and verified. One important technique used in its GPI design is that the second-order derivatives of flat output is not taking from observers directly but an intermediate signals that constitute the second-order derivatives of flat output is introduced. The signals are linear combinations of the rotary angle of pendulum arm and the swing angle of pendulum. This is important model information they need to guarantee the GPI, or ESO, does not fail to provide useful and noise-attenuated feedback states. Tracking control with ADRC of ball and beam system is included in [24] where a class of underactuated systems that have the same form of model are considered. Although they are not feedback linearizable, i.e., non-flat, the controllable tangent linearization still leads to successful tracking control design thanks to ADRC and flat output. Similar techniques of control design is used to convert the input-flat output model into error space. The ESO is also fed with intermediate signals that helps to stable the closed-loop system. The case of inverted pendulum on a cart, inertia wheel pendulum and the convey crane systems are included in [7, 25]. In [26], the method is extended to 3 degrees-of-freedom torsional plant.

The increases of the dimension of the model potentially deteriorate the performance of ESO, hence two intermediate signals are introduced in observers to guide the high-order differentiation of chosen flat output. The overall idea of this framework is further summarized in [27]. Another observation for Lagrangian mechanical systems is that nearly all flat outputs are not a general function of all the states, i.e., generalized coordinates and their velocities, but are only functions of generalized coordinates, with some proper approximation or reduction on the model. We notice this feature can greatly simplifies composition of the flat output in terms of the states and the trajectory design in these cases could have fewer constraints.

1.3 Contributions

For the problem of identification of flat output without explicit models, we propose a flat output identification (FOID) algorithm . The algorithm is able to identify differentially flat output or r-degree linearizing output [5] when the flat output is not available. We should point out that the flatness identified from the output is valid in the region spanned by the data set, and hence is local. We demonstrate the algorithm with single-input-multiple output (SIMO) underactuated nonlinear systems. Some of these system may not be globally feedback linearizable, but can still be controllable via the tangent linearization in the region spanned by the data set, and are thus locally flat. FOID offers an efficient way to identify the flatness and flat outputs or r-degree linearizing outputs from the input-output data of underactuated mechanical system (UMS) when the system operates near its equilibrium. The flatness- and model-based control with ADRC has many successful examples on stabilization and tracking problems of UMS. The same result of flatness and flat outputs can still be obtained by applying FOID without the mathematical model. Results of experiments and various simulations are given to support the effectiveness and feasibility of FOID.

The FOID problem is further extended to a class of MIMO UMSs. We develop an modified version of FOID to find locally flat outputs for a class of multiple-input nonlinear UMSs. The main contributions include two aspects. First, the modified FOID(MFOID) algorithm can deal with flat output identification for both single-input UMSs and a class of MIMO UMSs with high efficiency. Due to the complexity of flatness in MIMO cases, the problem is therefore simplified to finding flat outputs of some specific form, and the relation between relative degree vector and MIMO flatness is researched to give the new condition for algorithm to find flat outputs. Second, we also prove that the reduced linearized model with damping neglected can have fewer number of states involved in the expression of flat outputs and induce simpler process of identification. This is a simple explanation why flat outputs are normally and mostly composed of few states in linearized mechanical systems. The reduction, as a result, allows fewer number of sensors and measurements used for construction of flat output, and finally the input-to flat output equation of motion of

MIMO nonlinear UMSs is derived with all neglected terms and external disturbances included in a time-varying term called total disturbance.

FOID-Net, a neural network framework of FOID problem, is first proposed to solve the same problem for SIMO mechanical systems, including UMSs. The idea of FOID-Net is inspired from the autoencoder network used extensively in machine learning and deep learning community. It works as a function approximator to find the mapping between system's original states and expected flat outputs. We also introduce the tracking differentiator into neural network to help taking derivatives of signals. Only data series in time domain is needed for training the FOID-Net. The results are supported by the simulation results of two underactuated mechanical systems, which can also be validated by FOID algorithm.

A new framework of flatness-based ADRC for nonlinear single-input UMSs is proposed without the need of detailed knowledge of their mathematical models. The main procedure to design a data-driven robust tracking control of UMSs is presented. We take advantage of the result from previous FOID algorithm, or FOID-Net and extend them to control applications where identified flat output is exploited. It is proved that the number of states or outputs needed for identification of locally flat output can be decreased if the nonlinear model of UMS is reduced to a special linear form. When using FOID algorithm, the relations between states and flat outputs needs to be found. The SINDy method [28, 29] is tailored to investigate a sparse regression of states of the system in terms of the identified flat output and its time derivatives. Example of trajectory planning based on this result is given. The algebraic method in [30,31] is adopted to formulate the sparse regression problem without the need of derivatives of the measured time series. The approach to obtain even-order derivatives of the flat output for ADRC of high-order UMSs is developed. We show that estimation of even-order derivatives of the flat output can be expressed as a function of measurable states in the reduced model and can be either identified by a new sparse regression or directly solved from the previous result of the state-oriented sparse regression.

1.4 Thesis Organization

The rest of the thesis is organized as follows:

In Chapter 2 "Identification of Differentially Flat Output of Underactuated Dynamic Systems", the FOID algorithm is fully discussed with results of experiments and simulations. This chapter is fundamental for understanding the problem of identification and flatness-based control for UMSs.

In Chapter 3 "Data-Driven Robust Tracking Control of Underactuated Mechanical Systems using FOID, Sparse Regression and Flatness-based ADRC", we introduce the framework of robust tracking control design for UMS without leveraging the details of mathematical models. We discuss how to integrate FOID algorithm with classic ADRC setup and trajectory planning for flatness-based ADRC. The

difficulty of applying ESO to high-order UMSs are solved as high-order derivatives of flat outputs can be identified and expressed by measurable outputs by sparse regression and algebraic method. Experiments are done to validate the theory.

In Chapter 4 "Identification of linear differentially flat output of a class of MIMO underactuated mechanical systems", modified-FOID algorithm is extended to deal with FOID problem for a class of MIMO UMSs.

In Chapter 5 "FOID-Net: A Neural Network Framework identifying Linear Differentially Flat Output using Measurements", we introduce the structure of FOID-Net and the training method. The neural network framework can have some great advantages when identifying the flat outputs. The identified result could be used in our data-driven robust tracking control framework as well. Result of numerical simulations are given.

Chapter 6 concludes the whole thesis and also briefly discuss the future work for current algorithms.

Chapter 2

IDENTIFICATION OF DIFFERENTIALLY FLAT OUTPUT OF UNDERACTUATED DYNAMIC SYSTEMS

Flatness-based control has been an active research topic for decades. However, data-driven algorithm for flatness and flat output identification has not been researched before. This chapter presents a novel procedure to identify the locally flat output of nonlinear systems based on the output data only without the need for the mathematical model. More specifically, two interesting questions are addressed in this chapter: Is it possible to characterize the flatness, even if locally, and identify the flat output only from the input-output data of the system? If the system is non-flat or flat output is not available due to the lack of states measurement, are there any other special outputs that transform the system into the normal form with the minimum number of states representing the internal dynamics? Since the existence of flat outputs implies the controllability of the system, determining the flatness by using the data only is also an interesting and emerging topics in the application of the data science to control studies.

The proposed flat output identification (FOID) algorithm In this chapter is able to identify differentially flat output or r-degree linearizing output automatically near arbitrary controllable equilibrium point of nonlinear UMSs. We will calculate the flat output from the given model to show that same result of flatness and flat outputs can be obtained by applying FOID without the mathematical model.

The rest of the chapter is organized as follows. In Section 2.1, we introduce the mathematical concepts of the flatness. In Section 2.2, a statement of the problem is given. In Section 2.3, an identification algorithm of optimal output with the highest relative degree is discussed. Sections 2.4 and 2.5 present numerical and experimental examples to validate the algorithm. The chapter is concluded in Section 2.6.

2.1 Mathematical Preliminaries

In this section, we discuss the mathematical background of the work. In particular, we introduce the notion of flatness for general nonlinear systems. Then we present a SIMO nonlinear underactuated mechanical system of interest and discuss its linearization around equilibrium point. We also discuss the relationship

between the local flatness and relative degree of this class of nonlinear systems. A disturbance-rejection-based control is used to show the advantage of using the flatness property.

A nonlinear dynamical system $\dot{\mathbf{x}} = \mathbf{f}(\mathbf{x}, \mathbf{u})$ with state vector $\mathbf{x} \in \mathbb{R}^{2n}$, and input vector $\mathbf{u} \in \mathbb{R}^m$ is said differentially flat or flat for short if it is equivalent to a linear controllable system with the same number of inputs via a proper change of coordinates. The coordinate transformation given in the form $\mathbf{y}_f(\mathbf{x}) = [y_{f_1}, \ldots, y_{f_1}^{(d_1)}, y_{f_2}, \ldots, y_{f_1}^{(d_2)}, \ldots, y_{f_m}, \ldots, y_{f_m}^{(d_m)}]$ is called a flat output (vector). The superscript d_i $(i = 1, 2, ..., m)$ represents the order of time derivatives of y_{f_i}. The corresponding transformation is endogenous, which implies that all the states of the original system are transformed without the aid of exogenous variables. There are several features of nonlinear system characterizing its flatness.

- All the states and inputs can be expressed by the flat output vector $\mathbf{y}_f(\mathbf{x})$, or equivalently, by its components y_{f_i} and their finite number of time derivatives.
- Conversely, the flat output vector $\mathbf{y}_f(\mathbf{x})$ is also expressible in terms of original states $\mathbf{x}$.
- All components y_{f_i} are differentially independent, which means that $\mathbf{y}_f(\mathbf{x})$ does not satisfy any differential equation of the form $g(\mathbf{y}_f, ..., \mathbf{y}_f^{(k)}) = 0$.

The flat coordinates thus realize a directly input-to-output description of the original system without any zero dynamics in which the new outputs are generally considered as the components y_{f_i}. These properties of flat systems turn out to be extremely useful in trajectory planning and design of tracking control. When $m = 1$, the flat output vector consists of only one component y_{f_1} and its finite number of time derivatives. We will stick to the discussion of single-input system in the rest of the chapter and denote it by y_f .

Consider the state-space representation of an n-degree-of-freedom SIMO nonlinear UMS with m outputs as:

$$\begin{aligned} \dot{\mathbf{x}} &= \mathbf{F}(\mathbf{x}) + \mathbf{G}(\mathbf{x})u(t), \\ \mathbf{y} &= \mathbf{H}(\mathbf{x}), \end{aligned} \tag{2.1}$$

where $\mathbf{x} \in \mathbb{R}^{2n}$ is state vector, $u(t) \in \mathbb{R}$ is the input scalar function, $\mathbf{F}(\mathbf{x}) \in \mathbb{R}^{2n}$ is a nonlinear function of the argument, $\mathbf{G}(\mathbf{x}) \in \mathbb{R}^{2n}$ is the input influence vector which has at least one nonzero entry and $\mathbf{H}(\mathbf{x}) \in \mathbb{R}^m$ is an output function. The system is assumed to be control-affine. The system represented by Equation (2.1) is said to be underactuated if $\text{rank}(\mathbf{G}) < n$, which implies that u is not capable of commanding instantaneous accelerations of the system in arbitrary directions.

Let $p = (\mathbf{x}_e, u_e)$ denote an operation or equilibrium point of the system. The tangent linearization of the system can be obtained as

$$\begin{aligned}\dot{\mathbf{x}}_\delta &= \left(\left.\frac{\partial \mathbf{F}}{\partial \mathbf{x}}\right|_p + \left.\frac{\partial \mathbf{G}}{\partial \mathbf{x}} u(t)\right|_p \right) \mathbf{x}_\delta + \left.\mathbf{G}\right|_p u_\delta \\ &\equiv \mathbf{A}\mathbf{x}_\delta + \mathbf{B}u_\delta,\end{aligned} \tag{2.2}$$

where $\mathbf{x}_\delta = \mathbf{x} - \mathbf{x}_e$, $u_\delta = u - u_e$ and $\mathbf{B}$ is a $2n \times 1$ control influence vector, $\mathbf{A}$ is a $2n \times 2n$ matrix of the linear state. The tangent or Jacobian linearized system (2.2) is flat if, and only if, it is controllable, which means there exists a function y_f of the output $\mathbf{y}_\delta$ such that all the states $\mathbf{x}_\delta$ are expressible in terms of y_f and its finite successive time derivatives [5, 32]. In this case, the original nonlinear system is called locally flat at the point p and the local flatness can be interpreted as local controllability. With the assumption of controllable linearization, it is always possible to find a nonsingular square matrix $\mathbf{T}$ that transforms the linearized system into the controllable canonical form. Let $\mathbf{z} = \mathbf{T}\mathbf{x}_\delta$ where $\mathbf{z} = [z_1, z_2, ..., z_{2n}]^T$. The transformed state satisfies the equation in the controllable canonical form as

$$\dot{\mathbf{z}} = \mathbf{A}_c\mathbf{z} + \mathbf{b}u_\delta, \tag{2.3}$$

where

$$\mathbf{A}_c = \begin{bmatrix} 0 & 1 & 0 & \cdots & 0 \\ 0 & 0 & 1 & \cdots & 0 \\ \vdots & \ddots & \ddots & \ddots & \vdots \\ 0 & 0 & 0 & \ddots & 1 \\ a_1 & a_2 & a_3 & \cdots & a_{2n} \end{bmatrix}, \quad \mathbf{b} = \begin{bmatrix} 0 \\ 0 \\ \vdots \\ 0 \\ 1 \end{bmatrix}, \tag{2.4}$$

and $a_i \in \mathbb{R}$ $(1 \leqslant i \leqslant 2n)$. Consider an output $y = z_1$ for the controllable system (2.3). The system is then observable. Hence, $y_f = z_1(\mathbf{x}_\delta)$ is a flat output. Another important observation is that the flat output $y = z_1$ has a relative degree equal to the system dimension $2n$. The following lemma and corollary restate the relationship between relative degree of linearization (2.2) and flatness.

Lemma 2.1.1. *A $2n^{th}$-order single-input linear system in the form of Equation (2.2) is controllable if there exists a scalar function $y = y_f(\mathbf{x}_\delta)$ such that when y is taken as an output of system (2.2), it has relative degree $2n$.*

Corollary 2.1.2. *A linear system in the form of Equation (2.2) with a scalar output function $y = y_f(\mathbf{x}_\delta)$ having relative degree $2n$ is flat. $y_f(\mathbf{x}_\delta)$ is one of the flat output functions.*

The proof of the lemma and corollary is straightforward. To save space, we omit the proof. It should be pointed out that the necessity part of Lemma 2.1.1 does not generally hold. The construction of transformation matrix $\mathbf{T}$ that transforms

system (2.2) to system (2.3) may need strong accessibility of its original states from its m measurable outputs. These outputs are used to reconstruct all the required state variables for flat output $y_f(\mathbf{x}_\delta)$. The desired flat output $y_f(\mathbf{x}_\delta)$ may not be physically measurable since the observability of the required states is not guaranteed by controllability of tangent linearization (2.2), although such output with relative degree $2n$ does theoretically exist. On the other hand, it immediately shows that system (2.2) fits into the form of system (2.3) by state redefinition if a scalar output function $y = y_f(\mathbf{x}_\delta)$ with relative degree $2n$ is found and measured, from which the controllability, hence flatness, is implied. Clearly, the observability of both system (2.2) and (2.3) is also asserted with measurable y as flat output.

We use $y_f(\mathbf{x}_\delta)$ to denote the flat output function. The flat output defined in [5] is a vector of functions given by $\mathbf{y}_f = \left[y_f, \dot{y}_f, ..., y_f^{(2n-1)}\right]$. Once the y_f is available, the calculation of derivatives of y_f for the vector $\mathbf{y}_f$ is trivial. For convenience, we shall refer to y_f as the flat output function in this chapter. Since the number of outputs m is less then $2n$, the existence of a flat output as a linear combination of the m outputs requires the system to be locally observable. When the system is not completely controllable and observable, we may find an output function y_l with relative degree $r < 2n$. The question is how to find the maximum relative degree r for a given system and its outputs.

Recall that when we take the flat output $y_f = z_1$ and define the states as $z_{i+1} = y_f^{(i)}$, we have Equation (2.3), the last line of which reads

$$y_f^{(2n)} = f(\mathbf{y}_f) + bu_\delta, \tag{2.5}$$

where $f(\mathbf{y}_f) : \mathbb{R}^{2n} \longrightarrow \mathbb{R}$ is a linear map, $b \in \mathbb{R}$. Equation (2.5) is the basis for the feedback linearization control in terms of the incremental input u_δ. Controls can be readily designed to track a given trajectory y_f^* or stabilize the equilibrium point. Note that the evolution of $y_f(\mathbf{x}_\delta)$ indirectly manipulates the original states $\mathbf{x}_\delta$ as the functional relationship implies.

To conclude, the flatness as defined in [5] refers to the characteristics that a flat output and its time derivatives can form a state transformation, leading to the controllability form of the system. The system in this form has no zero dynamics and is clearly feedback linearizable. The control design of the transformed systems benefits from great freedom of choices of mature linear controls. Flatness can also be viewed as an extension of the Kalman controllability for nonlinear systems due to the equivalence between the flat system and linear controllable system. We notice that the exact nonlinear system models are not always available. When the equations of the linearized system cannot be obtained accurately, the traditional flatness-based control method that relies on the precise model and transformation of the original system will not apply. Many nonlinear UMSs are not inherently or strictly flat on account of nonexistence of flat coordinates. The notion of flatness can be extended

to become a local property of a nonlinear system around an equilibrium point in the state space. It has been proven that a nonlinear system is locally flat at an equilibrium point if its tangent linearization at this point is controllable. Clearly, locally flat systems benefit from all properties of flatness around the equilibrium point.

2.2 Problem Statement

In this section, we will re-state the problem of finding locally flat output of nonlinear underactuated system in a more formal manner. Because the measurement of all the states is either expensive or unrealizable, it is worth exploring the optimally constructed outputs of linear model (2.2) that has the highest relative degree.

Definition 2.2.1. *Given n-degree-of-freedom (DOF) SIMO nonlinear underactuated control affine system (2.1), it is said to be differentially flat (or shortly flat) at the state p if its tangent linearized system (2.2) around the point p is controllable. An incremental flat output $y_f(\mathbf{x}_\delta)$ of the linearized system (2.2) is called locally flat output, or locally linearizing output, of system (2.1) around the point p.*

The definition of locally linearizing output is an extension of the differentially flat output discussed in [5] and [32] for SIMO nonlinear underactuated control affine system. We will stick to the term 'locally linearizing output' next with some modifications to distinguish the locally flat output in case the linearized system does not have full relative degree.

Definition 2.2.2. *Let $y_i(\mathbf{x}_\delta)$ $(i = 1, 2, ..., m)$ be m incremental outputs of the tangent linearized system (2.2) around the state $p = (\mathbf{x}_e, u_e)$. A linear combination $y_l = \sum_{i=1}^{m} c_i y_i(\mathbf{x}_\delta)$ with relative degree r is said to be r-degree locally linearizing output of $2n$-dimensional system (2.1) around the point p, denoted by y_l^r. y_l is a locally flat output, or full-degree locally linearizing output of system (2.1), if, and only if, it has a relative degree $r = 2n$, denoted as y_l^{2n} or simply y_f.*

The relative degree specifies the number of the states may be reconstructed from the outputs. In this work, we only consider linear combinations of the outputs. Nonlinear combinations are not considered. The idea of using a linear combination of the system outputs to form a so-called "redefined" output such that the internal dynamics of the system is stable has been studied before in the literature. However, most studies on the output redefinition are model-based.

Definition 2.2.3. *Define a set $S = \{(y_l, r_c) \mid y_l = \sum_{i=1}^{m} c_i y_i(\mathbf{x}_\delta),\ c_i \in \mathbb{R}\}$. The set S consists of all possible linear combinations y_l of the m outputs with relative degree*

r_c determined by m coefficients c_i. A r-degree locally linearizing output y_l^r of $2n$-dimensional system (2.1) around the point p is globally optimal if $r \geqslant r_c$ for any combination determined by $c_i \in \mathbb{R}$.

We should point out that the globally optimal linearizing output needs not to be unique. There possibly exists two or more elements in set S that share the same relative degree r and $r \geqslant r_c$. As shown in the next section, we will restrict the searching region in S for globally optimal linearizing output since S is an infinite set. Despite the restriction, locally flat output which has relative degree $2n$ is still clearly globally optimal over the whole set. Otherwise, the global optimality can only be concluded in a finite region.

With these definitions, we state the problem as follows:

Problem 1. *Find the r-degree locally linearizing output y_l of a given $2n$ dimensional SIMO nonlinear underactuated mechanical system defined by Equation (2.1) with m measurable outputs such that the relative degree r is maximum. When $r = 2n$, the output is locally flat denoted as y_f.*

2.3 Flat Output Identification (FOID)

The proposed FOID algorithm is based on the following assumptions.

2.3.1 Assumptions

Assumption 1. *The system state dimension $2n$ is known.*

We should point out that with sufficient input-output data, it is possible to estimate the dimension of the so-called "embedding state space" [33].

Assumption 2. $\mathbf{x}_e = 0$ *and* $u_e = 0$ *represent the equilibrium state p of the nonlinear system. The linearized system in the form of Equation (2.2) exists at the point p. Hence,* $\mathbf{x}_\delta = \mathbf{x}$ *and* $u_\delta = u$.

For this reason, we shall refer to $\mathbf{x}_\delta$ as $\mathbf{x}$, and u_δ as u in the rest of the chapter.

Assumption 3. *The time histories of m independent outputs and the control input $u(t)$ are available.*

The objective of the FOID algorithm is to find the maximum relative degree r among all the output functions $y_l \in S$ according to Definition 2.2.3. If an output function is found such that $r = 2n$, it is a flat output from the input-output data. If $r < 2n$, we can only conclude that the given data set of input and output does not support the flat output in the form of *linear combinations of the measurable outputs*. Finding the maximum relative degree r with respect to coefficients c_i is an optimization problem, which is the computational core of the FOID algorithm.

2.3.2 Frequency-domain Analysis

Recall that the relative degree of a SISO linear system is equal to the slope of the Bode amplitude plot in the log-log scale as the frequency $\omega \to \infty$. The first step of the FOID algorithm involves estimation of the transfer function from the control input u to the constructed output $y_l \in S$.

Estimation of transfer functions from input-output data is a well-studied topic [34, 35]. Several optimal unbiased estimates of the transfer function in the least-squares sense have been developed over the years. The transfer function of a SISO time-invariant system can be estimated from its input $u(t)$ and output $y(t)$ by taking ratio of their cross power spectral density (CPSD) denoted as P_{yu} to the power spectral density (PSD) of $u(t)$ denoted as P_{uu}. The estimated transfer function known as H_1 estimation is given by

$$H_1(\omega) = \frac{P_{yu}(\omega)}{P_{uu}(\omega)}. \tag{2.6}$$

It is noted that Equation (2.6) may underestimate the true transfer function if the noise exists in both input and output channels or the system is strongly nonlinear. Many numerical methods such as FFT, Welch's method and Bartlett's method have been developed for computing PSD and CPSD of signals. The computed spectrum is called periodogram.

Assume that the transfer function $H(s)$ of the linearized system (2.2) with a constructed output y_l is given by

$$H(s) = \frac{Y_l(s)}{U(s)} = \frac{b_k s^k + b_{k-1}s^{k-1} + \ldots + b_1 s + b_0}{s^{2n} + a_{2n-1}s^{2n-1} + \ldots + a_1 s + a_0}. \tag{2.7}$$

Note that in general, the order k of the polynomial in the numerator is unknown while the order of the polynomial in the denominator is $2n$ according to Assumption 1. The relative degree of the system is computed from the following limit,

$$s_l = \lim_{\omega \to +\infty} \frac{\log |H(j\omega)|}{\log \omega} = -(2n - k). \tag{2.8}$$

The absolute value of the slope s_l of the transfer function in the log-log plot as $\omega \to +\infty$ is the relative degree of the output y_l,

$$r_l = |s_l| . \tag{2.9}$$

The transfer function from $u(t)$ to $y_l \in S$ can be expressed in terms of PSD and CPSD as discussed earlier,

$$H(j\omega) = \frac{Y_l(j\omega)}{U(j\omega)} = \frac{\sum_{i=1}^{m} c_i Y_i(j\omega)}{U(j\omega)} = \sum_{i=1}^{m} c_i G_i(j\omega). \tag{2.10}$$

Each transfer function $G_i(j\omega)$ from input $u(t)$ to output $y_i(t)$ can be estimated by using Equation (2.6). The slope of $H(j\omega)$ as $\omega \to +\infty$ is given by

$$s_l = \lim_{\omega \to +\infty} \log \left| \frac{\sum_{i=1}^{m} c_i P_{y_i u}(\omega)}{P_{uu}(\omega)} \right| \div \log \omega. \tag{2.11}$$

In order to estimate s_l accurately, we must compute the slope of $H(j\omega)$ at high frequencies. This automatically implies the need for high sampling frequency of the measurements in this application. The high sampling frequency has a couple of undesirable consequences from the practical point of view. First, the measured outputs are more likely contaminated by the measurement noise, even when an anti-aliasing filter is used. Second, it is more likely to pick up resonant responses of high frequency unmodelled dynamics of the mechanical system. Both can cause difficulties in estimating the slope s_l of the transfer function. In general, the numerical estimate of $H(j\omega)$ near the Nyquist frequency ω_F is not accurate enough for estimation of s_l due to the effect of digitization.

In the following, we shall discuss how to effectively identify the slope s_l of the transfer function at high frequencies.

2.3.3 The Algorithm

The algorithm involves the following components.

1. **Selection of a Frequency Band**

   After $H(j\omega)$ is obtained numerically, a frequency range is to be selected to evaluate the slope of $H(j\omega)$ in the log-log plot. The lower bound of the band should be greater than the highest resonant frequency of the resonances picked up by the outputs and the upper bound of the band should be smaller than the Nyquist frequency. Sometimes, the selection has to be done manually from the Bode plot.

2. **Regression**

   The data in the selected range of frequencies is used to create a linear regression curve fitting. The slope of the fitted line is an estimate of the slope s_l. The least mean square (LMS) method is used for the regression problem. The norm of residuals R of the LMS is used to judge the quality of the regression. The slope estimated from the regression can either be truncated or rounded off to an integer.

3. **Segmentation**

Consider the data set W_b of $(H(j\omega), \omega)$ in the chosen frequency band denoted as b for an output y_l. Divide W_b into q nonconsecutive subsets denoted as w_{b_i} $(i = 1, 2, ..., q)$. Each subset should not contain too few sample points. The size of each subset is denoted as p_i. When the slope s_i of each subset is calculated and rounded denoted as $[s_i]$, we compare the rounded values. The maximum absolute value denoted as $r_l = \max_i |[s_i]|$ is taken as an estimate of the relative degree of the output y_l as is in Equation (2.9). The subset corresponding to r_l is denoted as w_b^*.

2.3.4 Optimization for Linearizing Output

Recall the set S in Definition 2.2.3. In the following study, we restrict the coefficients $c_i \in [-\tau_i, \nu_i]$ $(i = 1, 2, ..., m)$ in a finite region where τ_i and ν_i are positive real numbers. We consider the following optimization problem for all the subsets w_{b_i}.

$$\max_{c_i \in [-\tau_i, \nu_i]} r_l \quad (y_l, r_l) \in S. \tag{2.12}$$

We should point out that the real numbers τ_i and ν_i are selected on the trial and error basis. We denote the optimal coefficients as c_i^* and the corresponding relative degree as r_l^*. It turns out that the solution to the optimization problem (2.12) is usually not unique. In the following, we introduce a concept of relative data usage as a metric to select one optimal solution to use.

For high dimensional optimization problem (2.12), we can apply the cell mapping based search algorithm to find the optimal coefficients. The cell mapping method proposes to use a grid to discretize the search space and carry out the search over the grid points. A refinement strategy is also available to reduce the grid size gradually to improve the accuracy of the search results. The cell mapping method can be carried out in parallel computing with CPUs or GPUs. More details on the method can be found in the cited references. Furthermore, the computer programs of many examples are also available on-line as open source code.

Relative Data Usage (RDU)

Assume that there are d solutions to the optimization problem (2.12). Let p_i^* $(i = 1, 2, ..., d)$ be the size of the subset $w_{b_i}^*$ which is associated with the relative degree $r_{l_i}^*$ of the optimal output $y_{l_i}^*$. The relative data usage (RDU) of each optimal output is defined as a ratio given by,

$$\text{RDU}(y_{l_i}^*) = \frac{p_i^*}{\sum_{j=1}^{d} p_j^*}, \quad i = 1, 2, ..., d. \tag{2.13}$$

To some extend, the RDU ratio indicates the confidence of the i^{th} optimal output since the accuracy of regression is strongly coupled to the number of active data points in the regression.

2.4 Numerical Simulations

We present two numerical simulation examples to demonstrate the feasibility and efficiency of the proposed algorithm.

2.4.1 Furuta Pendulum

The rotary inverted pendulum, also known as the Furuta pendulum, is a popular UMS. A flatness-based active disturbance rejection control for tracking problem of the Furuta pendulum is proposed in [23]. The local differentially flat output of the nonlinear Furuta pendulum model is derived from its tangent linearization, which requires a full knowledge of the system dynamics beforehand. The undamped nonlinear model of the Furuta Pendulum is given by,

$$\begin{aligned}(J_r + m_p l_0^2 + m_p l_1^2 \sin^2(\phi))\ddot{\theta} - m_p l_1 l_0 \cos(\phi)\ddot{\phi} \\ +2m_1 l_1^2 \dot{\theta}\dot{\phi} \sin(\phi)\cos(\phi) + m_1 l_1 l_0 \dot{\phi}^2 \sin(\phi) = \tau, \end{aligned} \tag{2.14}$$

$$\begin{aligned}-m_p l_0 l_1 \cos(\phi)\ddot{\theta} + (J_p + m_p l_1^2)\ddot{\phi} \\ -m_p l_1^2 \dot{\phi}^2 \sin(\phi)\cos(\phi) - m_p g l_1 \sin(\phi) = 0, \end{aligned} \tag{2.15}$$

where θ is the angle of the horizontal rotary arm, ϕ is the angular displacement of the pendulum, J_r represents the moment of inertia of the rotary arm, J_p is the moment of inertia of the pendulum, m_p is the mass of pendulum, l_0 and l_1 are the length of rotary arm and the distance from the joint to center of the mass of the pendulum, respectively. τ is the torque generated by the DC motor. The tangent linearization of Equations (2.14) and (2.15) around the unstable equilibrium $\theta = 0$, $\dot{\theta} = 0$, $\phi = 0$, $\dot{\phi} = 0$ and $\tau = 0$ is obtained as,

$$(J_r + m_p l_0^2)\ddot{\theta}_\delta - m_p l_1 l_0 \ddot{\phi}_\delta = \tau_\delta, \tag{2.16}$$

$$-m_p l_0 l_1 \ddot{\theta}_\delta + (J_p + m_p l_1^2)\ddot{\phi}_\delta - m_p g l_1 \phi_\delta = 0, \tag{2.17}$$

where $\theta_\delta = \theta - 0$, $\phi_\delta = \phi - 0$, $\tau_\delta = \tau - 0$. A local differentially flat output y_f can be found analytically from Equations (2.16) and (2.17) as

$$y_f = -\frac{l_0}{l_1}\theta_\delta + (\frac{J_p}{m_p l_1^2} + 1)\phi_\delta. \tag{2.18}$$

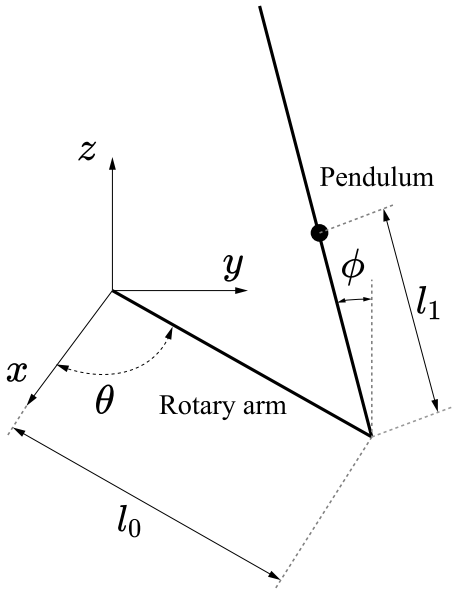

Figure 2.1: Schematic of the rotary inverted pendulum.

We can show that all the incremental states of the system can be expressible in terms of y_f and its time derivatives.

$$\begin{aligned}
\phi_\delta &= \frac{-m_p l_0 l_1 \ddot{\theta}_\delta + (J_p + m_p l_1^2)\ddot{\phi}_\delta}{m_p g l_1} = \frac{m_p l_1^2}{m_p g l_1}\ddot{y}_f = \frac{l_1}{g}\ddot{y}_f, \\
\dot{\phi}_\delta &= \frac{l_1}{g}\dddot{y}_f, \\
\theta &= \frac{l_1}{l_0}\left[(\frac{J_p}{m_p l_1^2}+1)\frac{l_1}{g}\ddot{y}_f - y_f\right], \\
\dot{\theta} &= \frac{l_1}{l_0}\left[(\frac{J_p}{m_p l_1^2}+1)\frac{l_1}{g}\dddot{y}_f - \dot{y}_f\right].
\end{aligned} \tag{2.19}$$

Equation (2.19) suggests that a nonsingular state transformation is generated by the flat output y_f. The system equations can be written in the norm form, the last line of which in the form of Equation (2.5) reads

$$\begin{aligned}
y_f^{(4)} = &\frac{(J_r + m_p l_0^2)\frac{l_1}{l_0}}{\left[(J_r + m_p l_0^2)\frac{l_1}{l_0}(\frac{J_p}{m_p l_1^2}+1)\frac{l_1}{g} - m_p l_1 l_0 \frac{l_1}{g}\right]}\ddot{y}_f \\
&+ \frac{1}{\left[(J_r + m_p l_0^2)\frac{l_1}{l_0}(\frac{J_p}{m_p l_1^2}+1)\frac{l_1}{g} - m_p l_1 l_0 \frac{l_1}{g}\right]}\tau_\delta.
\end{aligned} \tag{2.20}$$

We now assume that the complete knowledge of system (2.14) and (2.15) is not available. We apply the FOID algorithm to identify y_f from the incremental

input signal τ_δ and incremental outputs θ_δ and ϕ_δ. Since the equilibrium of the inverted pendulum is unstable, it is not possible to generate data of an open-loop system. We assume that a full-state feedback control, such as LQR control, has been applied to stabilize the system. Consider the following control τ_δ for Equation (2.16)

$$\tau_\delta = -k_1\theta_\delta - k_2\dot{\theta}_\delta - k_3\phi_\delta - k_4\dot{\phi}_\delta + r(t). \tag{2.21}$$

We have

$$(J_r + m_p l_0^2)\ddot{\theta}_\delta - m_p l_1 l_0 \ddot{\phi}_\delta + k_1\theta_\delta + k_2\dot{\theta}_\delta + k_3\phi_\delta + k_4\dot{\phi}_\delta = r(t), \tag{2.22}$$

where $r(t)$ is an reference input, typically a white noise signal, for identification purpose. Equation (2.17) still holds when the feedback control is applied. We should point out that in general, the feedback control may change the property of the output. The locally flat output y_f for this system remains the same after the control τ_δ is applied, which is the reason we chose this system as the first example to illustrate the proposed method. The resulting input-output model can be rewritten as

$$y_f^{(4)} = \alpha_1 y_f^{(3)} + \alpha_2 \ddot{y}_f + \alpha_3 \dot{y}_f + \alpha_4 y_f + \beta r(t), \tag{2.23}$$

where α_1, α_2, α_3, α_4 and β are coefficients to be determined.

The parameters of the Furuta pendulum are taken as $l_0 = 0.33m$, $l_1 = 0.275m$, $m_r = 1.64kg$, $m_p = 0.141kg$, $J_r = 0.0481kgm^2$ and $J_p = 0.0036kgm^2$. Let the four gains of the LQR control be $[18.7663\ 3.6997 - 1.0000 - 1.4614]$. $r(t)$ is a normally distributed random reference signal that follows $N(0, 0.01)$ distribution. The state-space representation of the closed-loop system is given by

$$\dot{\mathbf{x}} = \begin{bmatrix} 0 & 1 & 0 & 0 \\ -291.3562 & -63.8581 & 17.2605 & 25.2243 \\ 0 & 0 & 0 & 1 \\ -354.4923 & -71.1805 & 19.2397 & 28.1167 \end{bmatrix} \mathbf{x} + \begin{bmatrix} 0 \\ 17.2605 \\ 0 \\ 19.2397 \end{bmatrix} r(t), \tag{2.24}$$

$$\mathbf{y} = \begin{bmatrix} 1 & 0 & 0 & 0 \\ 0 & 0 & 1 & 0 \end{bmatrix} \mathbf{x}, \tag{2.25}$$

where $\mathbf{x} = \left[\theta_\delta, \dot{\theta}_\delta, \phi_\delta, \dot{\phi}_\delta\right]$. The outputs of the closed-loop system in the time interval $t = [0, t_f]$ are $\theta_\delta(t)$ and $\phi_\delta(t)$. The number of outputs is $m = 2$. The trial output $y_l \in S$ has two coefficients c_1 and c_2. Without loss of generality, we assume that $c_1 = 1$ and call c_2 as C_r. The trial output y_l is thus in the form

$$y_l = \phi_\delta + C_r\theta_\delta. \tag{2.26}$$

For the simulations, we have chosen the following parameters: sample frequency is $f_s = 1kHz$, time duration is $t_{span} = 20s$, the dimension of the state of the

original nonlinear system is known $2n = 4$, the frequency band selected for regression is from 0.5 to $250Hz$, the range of the coefficient is $C_r \in [-1, 0) \cup (0, 1]$ and the grid size is $h = 0.0001$. The 5000-point Kaiser window function with a shape factor $\beta = 35$ is applied to the estimation of periodogram [36]. The minimal eligible size for every subset w_b^* is 5% of the data points in the frequency band. The threshold for the residual of linear regression R is 5. 20000 trial outputs y_l are constructed in search for the optimal linear combination. The main results are discussed next.

Figure 2.2 shows the response of the closed-loop system. The initial conditions are small random numbers around the origin so that the system is considered linear during the simulation. The FOID will search for the largest relative degree of the output functions in terms of θ_δ and ϕ_δ as defined in Equation (2.26).

The relative degree of the output function as a function of C_r is shown in Figures 2.3 and 2.4. Each C_r corresponds to a distinctive output y_l. The identification algorithm finds the ratio that gives the output the highest relative degree. In the search range, we have found the optimal ratio as $C_r^* = -0.8971$ and the corresponding relative degree $r^* = 4$ is maximum. Furthermore, the RDU of that output function is also the highest. The optimal output y_l^* is therefore a full-degree linearizing output or locally differentially flat output. From extensive numerical searches, we can also confirm that C_r^* is not only be optimal in the range $[-1, 0) \cup (0, 1]$, but also optimal in $\mathbb{R}$.

Figures 2.5 through 2.8 show the estimated transfer functions from the input to different outputs y_l. Take Figure 2.7 as an example. A small portion of the Bode amplitude plot in the lower end of the chosen frequency band is curved and can be discarded, which amounts to about 5% of the data in the frequency range. The relative degree of the system can be estimated based on the slope of the remaining smooth curve. The subset used for the regression takes up nearly 95% points. The slope as defined by Equation (2.8) is found to be -2/decade after rounding off. The relative degree of the output $y_l^r = \theta_\delta + 0.35\phi_\delta$ is thus identified as 2.

If the amplitude graph in the chosen frequency range cannot be fitted by a straight line, we introduce break points at the resonant peaks and corners in order to form subsets. Only the subset with enough data points, say more than 10% of the data in the frequency range, is eligible to be used in identification of the relative degree. Figures 2.5 and 2.8 show the cases when one subset is eligible, while the other subset is not. More than one subset can be eligible, as shown in Figure 2.6. The one with higher RDU ratio is used to identify the relative degree. The estimated optimal coefficient C_r from the simulations can be verified by the output in Equation (2.18).

$$\begin{aligned} y_f &= \left(\frac{J_p}{m_p l_1^2} + 1\right)\left(\phi_\delta - \frac{l_0 m_p l_1}{J_p + m_p l_1^2}\theta_\delta\right) \\ &= 1.3376(\phi_\delta - 0.8971\theta_\delta). \end{aligned} \tag{2.27}$$

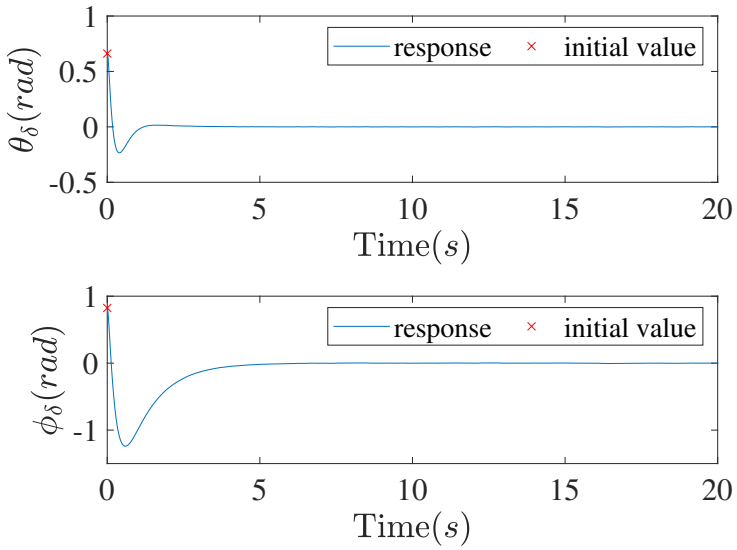

Figure 2.2: Response of the closed-loop system for simulation example of the Furuta pendulum.

The simulation results are in excellent agreement with the theoretical analysis of the locally flat output based on the mathematical model. FOID is promising in applications to flatness-based controls such as the ones proposed in [23] and [24].

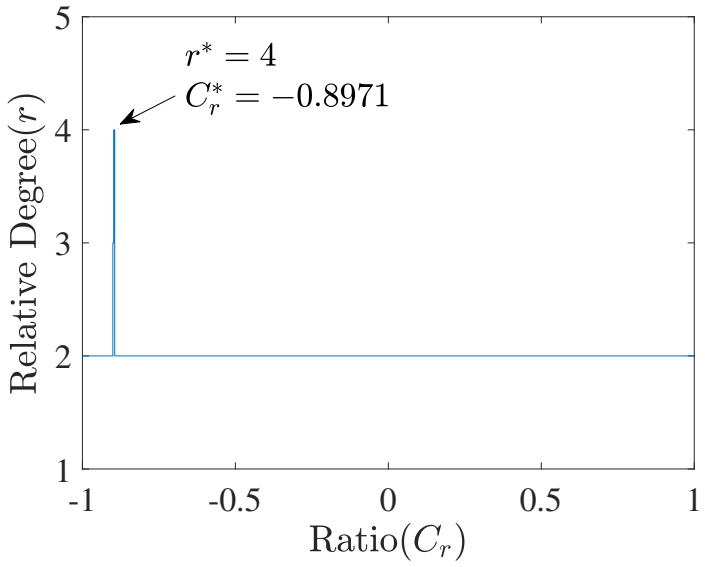

Figure 2.3: Relative degree of the output of the tangent linearized system in simulation example of the Furuta pendulum as a function of C_r.

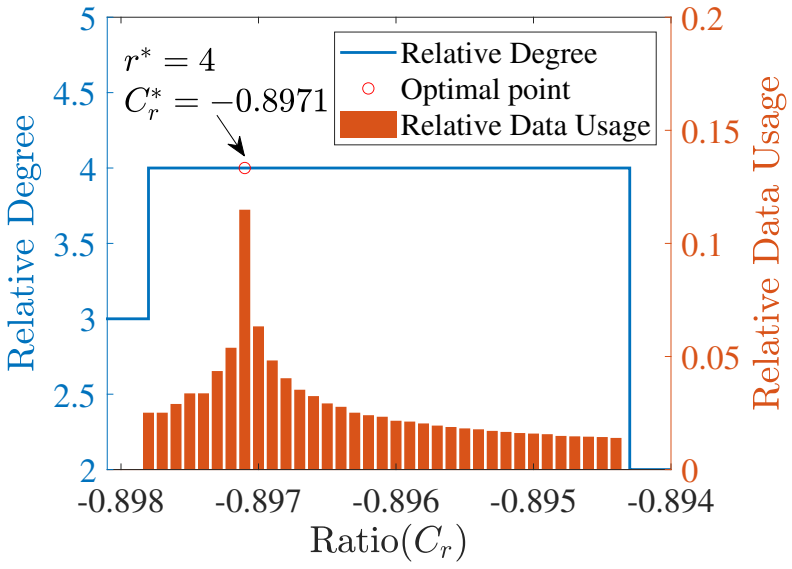

Figure 2.4: Zoomed view of Figure 2.3.

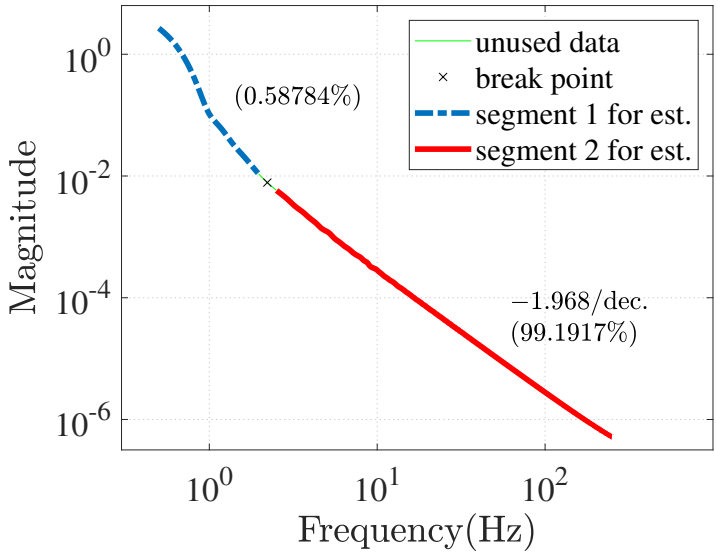

Figure 2.5: The estimated transfer function of the closed-loop system, $Cr = -0.95$. Segment of the Furuta pendulum is below the threshold of the residual of linear regression $R = 5$ and its size is less than.5% of the total data in the range. Segment 1 is discarded. Segment 2 is chosen as w_b^*.

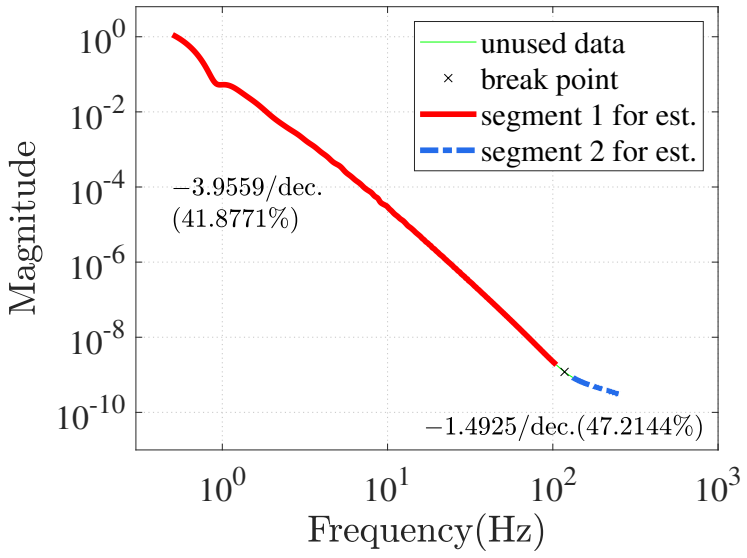

Figure 2.6: The estimated transfer function of the closed-loop system of the Furuta pendulum, $Cr = -0.8971$. Segment 1 has a larger slope (-3.9559/dec) than segment 2 (-1.1925/dec). Segment 1 is chosen as w_b^*.

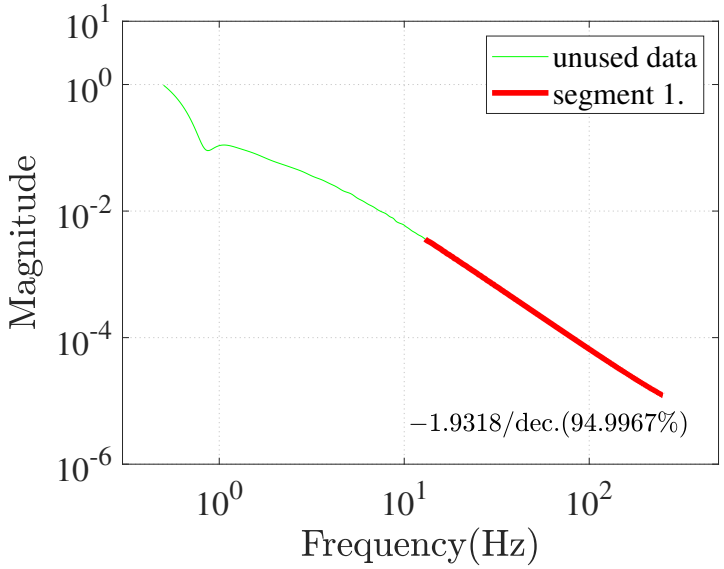

Figure 2.7: The estimated transfer function of the closed-loop system of the Furuta pendulum, $Cr = 0.35$. Segment 1 is chosen as w_b^*. The lower frequency portion has 5% data points and is discarded.

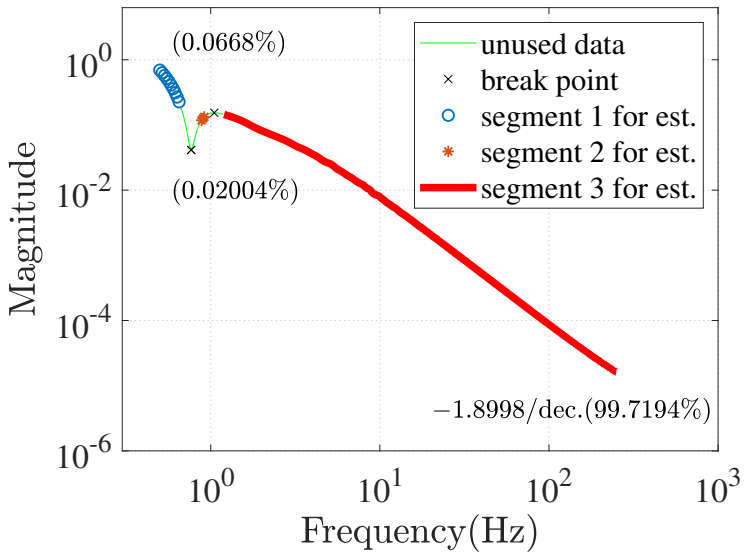

Figure 2.8: The estimated transfer function of the closed-loop system of the Furuta pendulum, $Cr = 0.75$. Less than 5% data around the resonance and antiresonance identified by the break points are unused. Segment 3 is selected as w_b^*.

2.4.2 A Nonlinear Underactuated System

Consider a 4^{th} order nonlinear underactuated system as follows:

$$\begin{aligned}
\dot{x}_1 &= x_2 + x_1^3, \\
\dot{x}_2 &= -105.6415x_1 - 94.1675x_2 - 72.7381x_3 - 54.1651x_4 - r(t), \\
\dot{x}_3 &= x_1 + 3x_2 + x_3 + x_4 + x_3^2, \\
\dot{x}_4 &= 165.9623x_1 + 143.2512x_2 + 113.6072x_3 + 84.2476x_4 + 1.5r(t).
\end{aligned} \tag{2.28}$$

The input $r(t)$ is a random signal following the normal distribution $N(0, 0.01)$. We apply the same steps as used in the previous example. Figures 2.9 and 2.10 show the simulated response of the system.

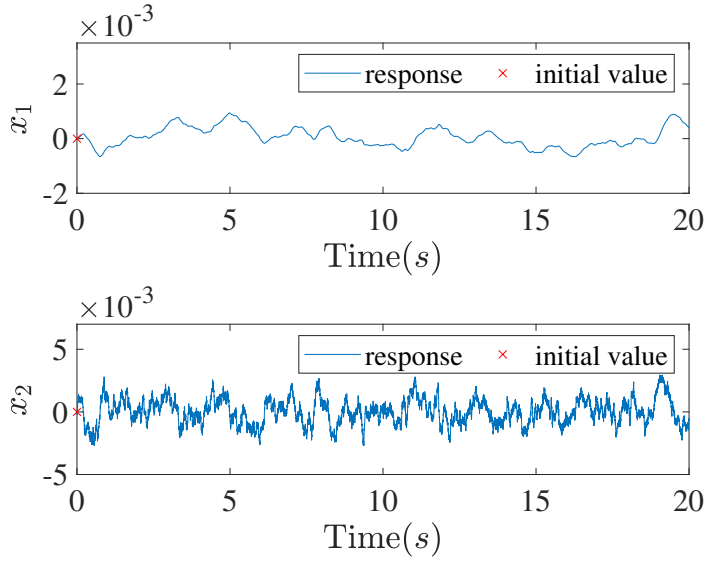

Figure 2.9: Responses $x_1(t)$ and $x_2(t)$ of the 4^{th} order nonlinear underactuated system.

Consider the tangent linearization of the nonlinear system around the origin. We consider two cases. In the first case, we assume that x_1 and x_2 are the outputs. The trial output y_{l_1} is a linear combination of the outputs x_1 and x_2 similar to Equation (2.26)

$$y_{l_1} = x_1 + C_r x_2. \tag{2.29}$$

Figures 2.11 and 2.12 show the variation of the relative degree of the output function y_{l_1} as C_r varies. The largest relative degree of y_{l_1} can be found is 2 when the linearizing output is $y_{l_1}^* = x_1 - 0.0015x_2$. The optimal coefficient is found to be $C_r^* = -0.0015$. Since the system is 4^{th} order $2n = 4$, $y_{l_1}^*$ is hence not a locally flat output. There will be internal dynamics of order two.

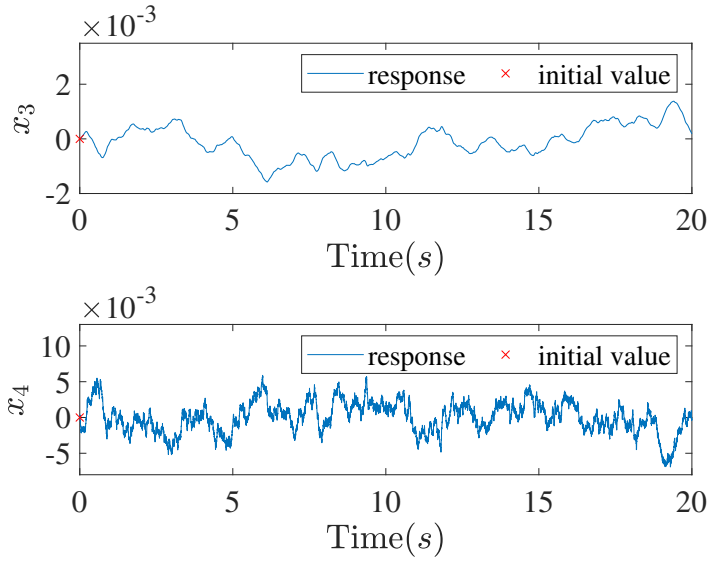

Figure 2.10: Responses $x_3(t)$ and $x_4(t)$ of the 4^{th} order nonlinear underactuated system.

Because the optimal coefficient C_r^* in this case is a small number, we can have an approximate output of relative degree 2 as $\hat{y}_{l_1}^* = x_1$. This approximate output with relative degree 2 can be verified from system (4.53) where the input $r(t)$ appears in the second equation for the derivative of x_2. However, the largest relative degree can only be 1 theoretically if C_r is nonzero, which is shown in the Figure 2.11 when values of C_r are larger so that x_2 can not be neglected.

In the second case, we consider the outputs x_1 and x_3. The trial output y_{l_2} reads,

$$y_{l_2} = x_1 + C_r x_3. \tag{2.30}$$

Figures 2.13 and 2.14 show the variation of the relative degree of the output function y_{l_2} as C_r varies. The largest relative degree of y_{l_2} is found to be 4 when $C_r^* = -0.6667$. Hence, we find a locally flat output or full-degree linearizing output.

The locally flat output can be verified with the original system. The tangent linearization of Equation (4.53) around the origin is given by

$$\begin{aligned}
\dot{x}_1 &= x_2, \\
\dot{x}_2 &= -105.6415x_1 - 94.1675x_2 - 72.7381x_3 - 54.1651x_4 - r(t), \\
\dot{x}_3 &= x_1 + 3x_2 + x_3 + x_4, \\
\dot{x}_4 &= 165.9623x_1 + 143.2512x_2 + 113.6072x_3 + 84.2476x_4 + 1.5r(t).
\end{aligned} \tag{2.31}$$

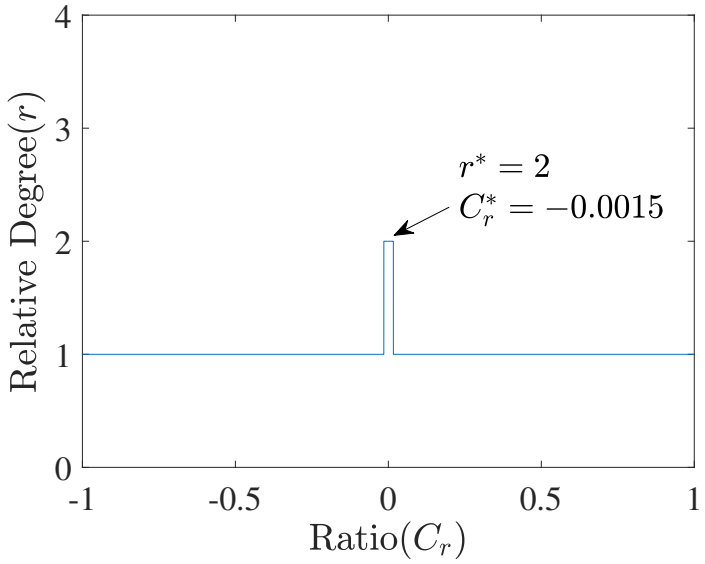

Figure 2.11: Variation of relative degree with C_r of the output y_{l_1} of the 4^{th} order nonlinear underactuated system.

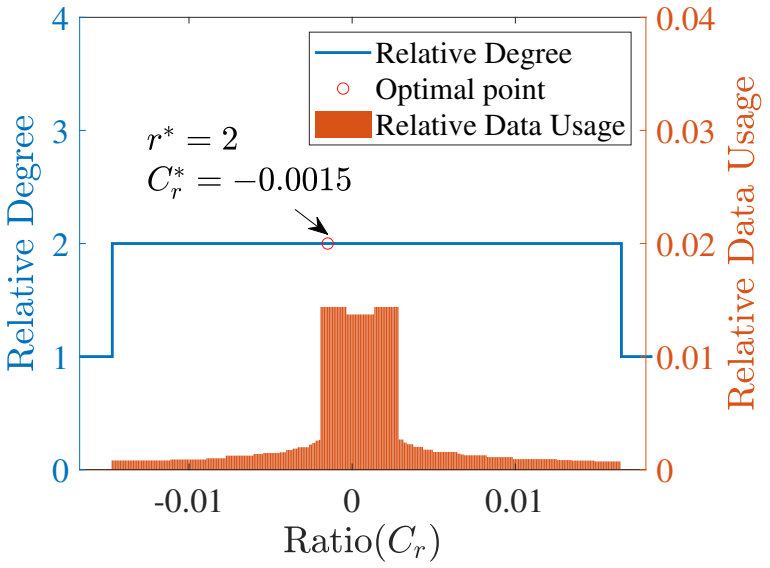

Figure 2.12: Variation of relative degree with C_r of the output y_{l_1} of the 4^{th} order nonlinear underactuated system. Zoomed view of Figure 2.11.

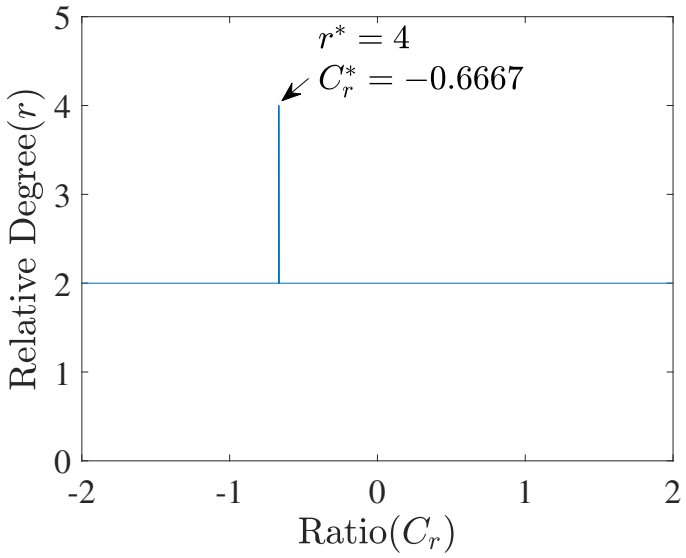

Figure 2.13: Variation of relative degree with C_r of the output y_{l_2} of the 4^{th} order nonlinear underactuated system.

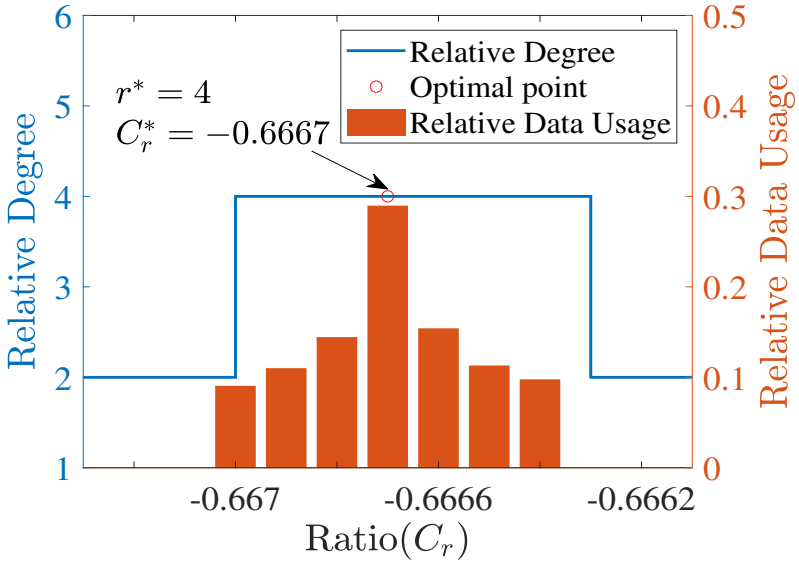

Figure 2.14: Variation of relative degree with C_r of the output y_{l_2} of the 4^{th} order nonlinear underactuated system. Zoomed view of Figure 2.13.

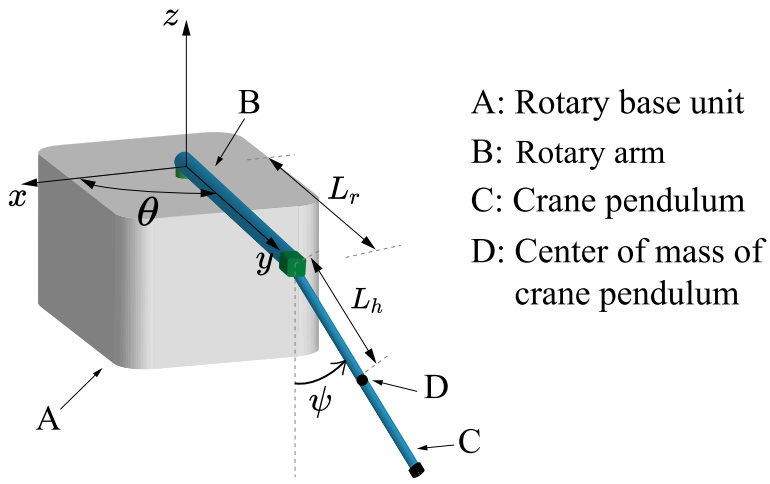

Figure 2.15: Schematic of the rotary crane system.

The output function $y_{l_2}^* = x_1 - \frac{2}{3}x_3$ has the relative degree 4, as is shown below.

$$\begin{aligned}
\dot{y} &= -\frac{2}{3}x_1 - x_2 - \frac{2}{3}x_3 - \frac{2}{3}x_4, \\
\ddot{y} &= -5.6667x_1 - 4x_2 - 3.6667x_3 - 2.6667x_4, \\
\dddot{y} &= -23.6724x_1 - 22.0048x_2 - 15.6706x_3 - 11.6694x_4, \\
y^{(4)} &= 372.2690x_1 + 329.7973x_2 + 259.1889x_3 + 193.1026x_4 + 4.5007r(t).
\end{aligned} \tag{2.32}$$

2.5 Experimental Validation

2.5.1 Rotary Crane

A rotary crane system is a typical example of nonlinear UMS. Experiments are done with this system to validate the proposed algorithm. The rotary crane system made by Quanser is driven by a DC servo motor system as shown in Figure 2.15. A control has been designed to let the rotary arm track a desired trajectory and keep the pendulum vertically downward during motion, as opposed to keeping it upright. The horizontal arm is attached to the output shaft of the gear system, which is actuated by the torque τ generated by the DC motor. The angular positions of the horizontal arm and pendulum are denoted as θ and ψ, respectively. The voltage applied to the DC motor is denoted as V.

We ignore the damping of the system. The equations of the linearized system around the origin of the state space ($\theta = 0$, $\psi = 0$, $\dot{\theta} = 0, \dot{\psi} = 0$, $\tau = 0$, $V = 0$) can

be obtained by applying the Euler-Lagrange method:

$$(J_r + m_p l_0^2)\ddot{\theta}_\delta + m_p l_1 l_0 \ddot{\psi}_\delta = \tau_\delta, \tag{2.33}$$

$$m_p l_0 l_1 \ddot{\theta}_\delta + (J_p + m_p l_1^2)\ddot{\psi}_\delta + m_p g l_1 \psi_\delta = 0, \tag{2.34}$$

$$\tau_\delta = \frac{\eta_g K_g \eta_m k_t (V_\delta - K_g k_m \dot{\theta})}{R_m}, \tag{2.35}$$

where $\tau_\delta = \tau - 0 = \tau$ is the incremental torque and $V_\delta = V - 0 = V$ is the incremental voltage. The system variables and their values are listed in Table 2.1. With the full knowledge of the system, we can find one locally flat output as

$$y_f = \theta_\delta + \frac{J_p + m_p l_1^2}{m_p l_1 l_0}\psi_\delta = \theta_\delta + 1.039\psi_{\delta.} \tag{2.36}$$

The original states can be expressed in terms of y_f and its derivatives as,

$$\psi_\delta = \frac{m_p l_0 l_1 \ddot{\theta}_\delta + (J_p + m_p l_1^2)\ddot{\psi}_\delta}{-m_p g l_1} = -\frac{l_0}{g}\ddot{y}_f, \tag{2.37}$$

$$\dot{\psi}_\delta = -\frac{l_0}{g}\dddot{y}_f, \tag{2.38}$$

$$\theta_\delta = y_f - \frac{J_p + m_p l_1^2}{m_p l_1 l_0}\psi_\delta = y_f + \frac{J_p + m_p l_1^2}{m_p l_1 g}\ddot{y}_f, \tag{2.39}$$

$$\dot{\theta}_\delta = \dot{y}_f + \frac{J_p + m_p l_1^2}{m_p l_1 g}\dddot{y}_f. \tag{2.40}$$

A block diagram for realization of the experimental identification of the flat output is shown in Figure 2.16. In the experiment, the angular positions θ_δ and ψ_δ are recorded. We consider the output given by $y_l = \theta_\delta + C_r\psi_\delta$. The parameters of the rotary pendulum are given in Table 2.1.

In the experiment, the angular positions θ_δ and ψ_δ are recorded. We consider the output given by $y_l = \theta_\delta + C_r\psi_\delta$.

The input voltage V is a normally distributed random signal following the distribution $N(0, 5)$ with sample time $t_s = 0.001$. The system is forced into random motions around the equilibrium. The execution time of the experiment is $t_{span} = 60$s. Two direct outputs θ and ψ will be measured and their incremental values are shown in Figure 2.17. The order of the original nonlinear system is known $2n = 4$. We shall search for the flat output in the domain $C_r \in [-2, 0) \cup (0, 2]$. The Welch's method is used to compute the frequency response function in order to obtain the H_1 estimate of the transfer function from V to y_l. The transfer functions from the input V to θ_δ and ψ_δ are shown in Figure 2.18.

The frequency band selected for regression is from 0.5Hz to 25Hz. The frequency increment is $h = 0.001$. A 5000-point Kaiser window function with a shape

Table 2.1: Parameters of the rotary crane system.

Symbol	Description	Value
J_r	Rotary arm moment of inertia about its center of mass	9.9829×10^{-4} kg·m^2
J_p	Pendulum moment of inertia about its center of mass	0.0012 kg·m^2
m_p	Mass of pendulum	0.1270 kg
L_h	Half length of pendulum	0.1683 m
L_r	Total length of rotary arm	0.2159 m
g	Gravitational acceleration	9.81 m·s^2
η_g	Gearbox efficiency	0.90
K_g	High-gear total gear ratio	70
η_m	Motor efficiency	0.69
k_t	Motor current-torque constant	7.68×10^{-3} N·m
k_m	Motor back-emf constant	7.68×10^{-3} V/(rad/s)
R_m	Motor armature resistance	2.6 Ω

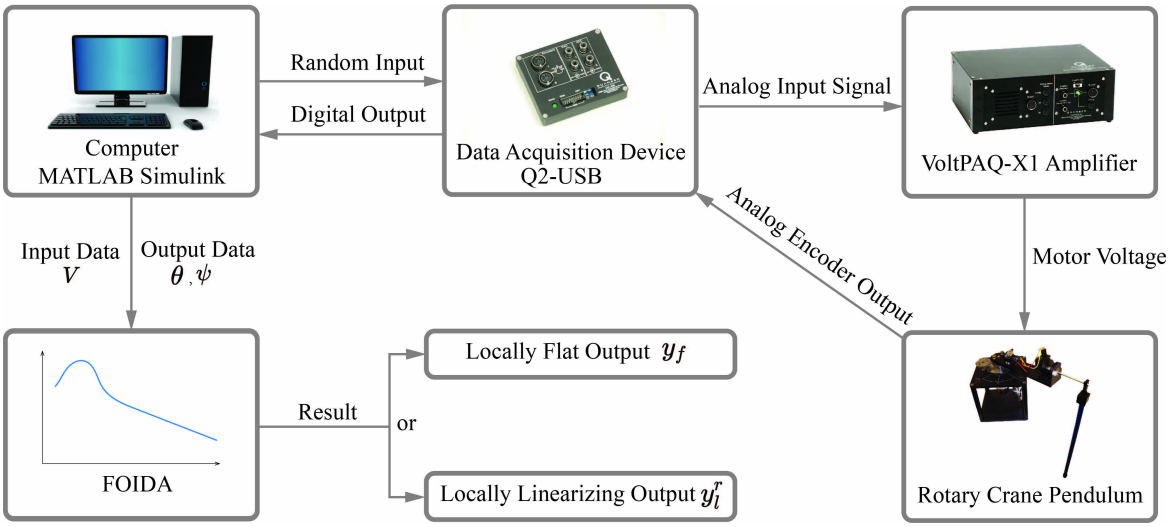

Figure 2.16: Block Diagram For Experiment

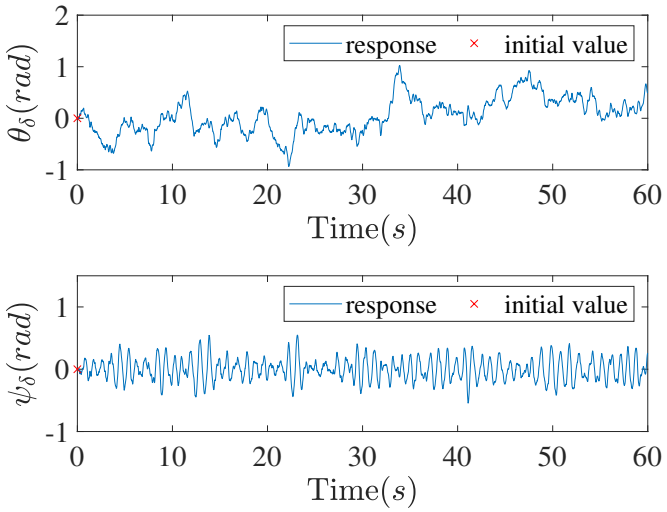

Figure 2.17: The open-loop response of the rotary crane system with normally distributed random input.

factor $\beta = 35$ is applied to the estimation of periodogram. The minimal eligible size for every subset w_b^* is 5%. The threshold for residual of linear regression R is 5. The passive range around the peaks is ±5% about the frequency of resonance and antiresonance. 5% points of lower frequency are dropped. 4000 trial outputs y_l are constructed during the search for the optimal linear combination. Figures 2.19 and 2.20 show the variation of relative degree of the output with C_r. A locally flat output is found from Figure 2.20 as

$$y_l^{r^*} = \theta_\delta + 1.037\psi_\delta, \tag{2.41}$$

where the largest relative degree is $r^* = 4$, which equals to the order of the system. The result is in a good agreement of the theoretical flat output in Equation (2.36).

2.6 Conclusions

A flat output identification (FOID) algorithm is presented in this chapter from experimental data of a dynamic system of known order. The system can be nonlinear, SIMO and underactuated. No detailed mathematical model of the system is needed. Trial output is written as a linear combination of measured outputs. An optimization problem is proposed to search for the linear combination that leads to the highest relative degree of the trial output. The identification is done in the frequency domain by taking advantage of the asymptotic behavior of transfer functions of linear systems. Various data handling strategies have been developed to achieve the best estimate of the relative degree in the presence of measurement noise, high frequency dynamics and Nyquist digitization effect. The FOID algorithm

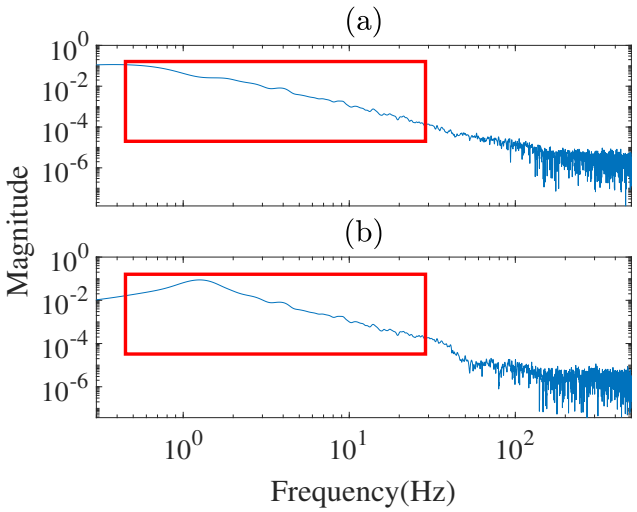

Figure 2.18: The estimated transfer functions from input V to measurable outputs (a) θ_δ and (b) ψ_δ. The red boxes indicate the area selected for relative degree estimation in the chosen frequency band.

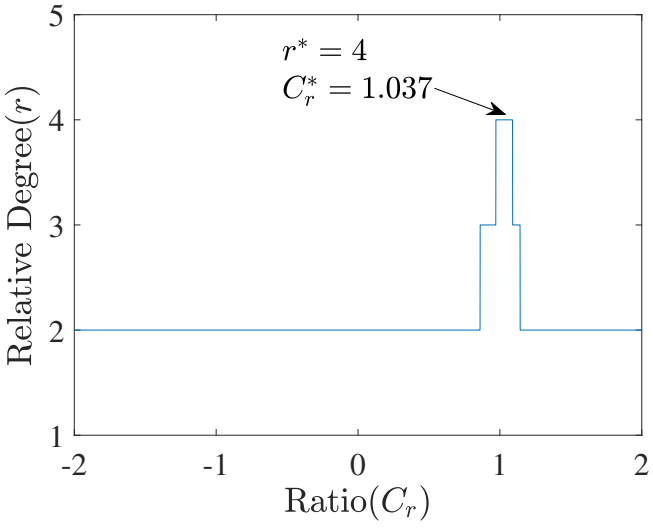

Figure 2.19: The relative degree of the output y_l as a function of C_r for the rotary crane system around the origin.

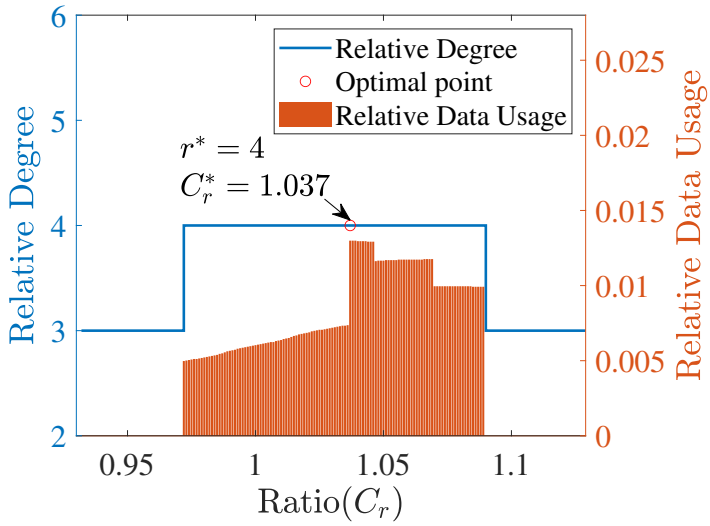

Figure 2.20: The relative degree of the output y_l as a function of C_r for the rotary crane system around the origin. Zoomed view of Figure 2.19.

has been tested with two numerical examples of nonlinear dynamic systems and also validated with an experimental study of a rotary crane system.

Chapter 3

DATA-DRIVEN ROBUST TRACKING CONTROL OF UNDERACTUATED MECHANICAL SYSTEMS USING FOID, SPARSE REGRESSION AND FLATNESS-BASED ADRC

When UMSs are known to be differentially non-flat, and the control design cannot make use of the flatness property. In this case, the well-known ADRC can be introduced to resolve this issue [37, 38]. The paradigm of ADRC assumes that the nonlinear system of interest is in a canonical form and lumps all disturbances including, for instance, uncertainties, unmodeled dynamics and external excitations, into one time-varying term called the total disturbance. The total disturbance can be estimated online and be canceled in real time. This allows us to modify the model of non-flat nonlinear systems to render flatness, such as linearization, and use control to compensate such modification, viewed as one of endogenous disturbances. Flatness indicates that there is a direct input-output model in terms of flat outputs and control input existing without internal dynamics, which is naturally in accordance with the premise of using ADRC. Many examples have shown the success in control design of UMSs by combining flatness and ADRC in Chapter 1.

This chapter we adopt previously proposed data-driven approach FOID to identify the flat output and applies the flatness-based ADRC to UMSs. This work also includes a sparse representation of differential relationships of state variables in order to overcome the deficiency of the ADRC for higher order systems. Several issues about implementing data-driven robust tracking control using ADRC and flat output are proposed as follows and the potential solutions are addressed and given:

(I1) It seems necessary to characterize flatness first and find flat output for nonlinear systems, or at least locally flat output for its linearization. A data-driven method of finding flat output is needed.

(I2) The reference trajectory planning for the output of UMSs may need the mathematical expression of states and flat outputs, which is not a problem in model-based setting. The relationship between them should be identified in data-driven environment for the purpose of planning and understanding of the system behavior.

(I3) Many UMSs have high degrees of freedom, which means a large number of states and high-order ESOs may be involved in the ADRC design. The increase

of the order of linear or nonlinear ESOs can intensely deteriorate the performance of estimation of the total disturbance and derivatives of the tracking error due to noises. It also causes large phase lag of the estimates so that the closed-loop system may become unstable.

The rest of the chapter is organized as follows. In Section 3.1, we present the single-input-multiple-output (SIMO) nonlinear UMS of interest in this chapter. The basic concepts of the flatness, flat output and ADRC design are discussed. In Section 3.2, the control objectives for the SIMO UMS including the special requirements and principles are stated. In Section 3.3, a data-driven framework of ADRC design is proposed that integrates FOID, state-oriented sparse identification, trajectory planning and a cascade of low-order ESOs or Leunberger observers. Experiments of a rotary crane pendulum are carried out to validate the effectiveness of the control design. Conclusion of the chapter is included in Section 3.5.

3.1 Preliminaries

3.1.1 Single-input-multiple-output UMS

Although we have introduced the general form of UMS in last chapter, we would like to restrict the system of interest to a class of single-input-multiple-output(SIMO) nonlinear UMS in this section. There are many underactuated systems naturally fitting into this category, such as acrobot, inverted pendulum and cart-pole system. The dynamical equations of n-degree-of-freedom ($n > 1$) SIMO nonlinear UMS can be given as [39]:

$$m_{11}(\mathbf{q})\ddot{q}_a + \mathbf{m}_{12}(\mathbf{q})\ddot{\mathbf{q}}_u + h_1(\mathbf{q}, \dot{\mathbf{q}}) = u \tag{3.1}$$

$$\mathbf{m}_{21}(\mathbf{q})\ddot{q}_a + \mathbf{m}_{22}(\mathbf{q})\ddot{\mathbf{q}}_u + \mathbf{h}_2(\mathbf{q}, \dot{\mathbf{q}}) = \mathbf{0}, \tag{3.2}$$

where $q_1 \in \mathbb{R}$ and $\mathbf{q}_u \in \mathbb{R}^{(n-1)\times 1}$ are the generalized coordinates $\mathbf{q} = [q_a, \mathbf{q}_u^T]^T \in \mathbb{R}^{n\times 1}$, the scalar function $h_1(\mathbf{q}, \dot{\mathbf{q}})$ and vector function $\mathbf{h}_2(\mathbf{q}, \dot{\mathbf{q}}) \in \mathbb{R}^{(n-1)\times 1}$ contain Coriolis, centrifugal and gravitational terms, and $u \in \mathbb{R}$ is the generalized force applied to the system produced by a single actuator. The terms $m_{11} \in \mathbb{R}$, $\mathbf{m}_{12} \in \mathbb{R}^{1\times(n-1)}$, $\mathbf{m}_{21} \in \mathbb{R}^{(n-1)\times 1}$ and $\mathbf{m}_{22} \in \mathbb{R}^{(n-1)\times(n-1)}$ form the mass matrix given by

$$\mathbf{M}(\mathbf{q}) = \begin{bmatrix} m_{11} & \mathbf{m}_{12} \\ \mathbf{m}_{21} & \mathbf{m}_{22} \end{bmatrix}_{n\times n}, \tag{3.3}$$

$\mathbf{M}(\mathbf{q})$ is symmetric and positive definite. Equations (4.1) and (4.2) can be written in the state-space form. The state vector consists of generalized coordinates and velocities. Due to the fewer number of actuators than degrees of freedom, the input of a single actuator is not capable of driving the UMS arbitrarily in any direction along the generalized coordinates. The nature of nonlinearity and underactuation makes the stabilization and trajectory tracking problem of the UMS intractable in general.

3.1.2 Flatness-based Active Disturbance Rejection Control

To distinguish the flat output from MIMO system cases, we now denote the flat output of SIMO by y_{f_1}. The input-output model, as a result of parameterization of input in terms of states, naturally lends itself to the paradigm of ADRC design. Active disturbance rejection control, or shortly ADRC, is an observer-based control approach that estimates unknown total disturbances online, including endogenous system dynamics and exogenous disturbances, and cancels them by feedfoward compensation. By finding the flat output, a flat nonlinear control-affine system of order n in the state space, with a single input u for example, can be transformed into the form

$$y_{f_1}^{(n)} = g(\mathbf{y}_{f_1}) + b(\mathbf{y}_{f_1})u. \tag{3.4}$$

$\mathbf{y}_{f_1}$ is the vector of the flat output and its time derivatives. $g(\cdot)$ and $b(\cdot)$ are scalar functions. ADRC treats $g(\mathbf{y}_{f_1})$, all its variations due to parametric uncertainties and unmodeled dynamics as endogenous perturbation, and inteprets any external disturbance to the system, regardless of its type and origin, as exogenous perturbation. The basic idea of disturbance rejection is to estimates both types of perturbations together on-line, called the total disturbance, and compensate them by the feedforward control. After the compensation, a variety of linear and nonlinear control schemes can be applied to the resulting trivial system of pure integrators. When $b(\mathbf{y}_{f_1})$ is not known exactly in advance, a common technique is to incorporate the state-dependent part of $b(\mathbf{y}_{f_1})$ into the total disturbance and retains a constant b_0 or known function of $\mathbf{y}_{f_1}$ as a nominal input gain. The input-output model in ADRC is therefore rewritten as

$$y_{f_1}^{(n)} = \xi(t) + b_0 u, \tag{3.5}$$

where $\xi(t)$ is a time-varying term representing the total disturbance. The control law is in the following form

$$u = \frac{1}{b_0}(-\widetilde{\xi}(t) + v) \tag{3.6}$$

where $\widetilde{\xi}(t)$ is an estimate of $\xi(t)$ and v is the control designed for the trivial integral system $y_{f_1}^{(n)} = v$. Consequently, the influence of unknown disturbances could be suppressed adaptively, and the robustness of the closed-loop system with respect to disturbances is significantly improved.

The performance of ADRC is highly relied on accurate on-line estimation of the flat output vector $\mathbf{y}_{f_1}$ and the total disturbance, which requires an effective algorithm for state and disturbance estimation with low latency. The core component udertaking this task in ADRC is the extended state observer (ESO). Although a

large number of variants of ESOs have been developed over past decades, the main structure of them for system (4.14) can be summarized as,

$$\begin{aligned} e_1 &= z_1 - y_{f_1} \\ \dot{z}_1 &= z_2 - \beta_1 \varphi_1(e_1) \\ \dot{z}_2 &= z_3 - \beta_2 \varphi_2(e_1) \\ &\vdots \\ \dot{z}_n &= z_{n+1} + b_0 u - \beta_n \varphi_n(e_1) \\ \dot{z}_{n+1} &= -\beta_{n+1} \varphi_{n+1}(e_1), \end{aligned} \tag{3.7}$$

where $\mathbf{z} = [z_1, z_2, \ldots, z_{n+1}]^T$ is the estimate of the extended vector

$$\overline{\mathbf{y}}_{f_1} = [y_{f_1}, \ldots, y_{f_1}^{(n-1)}, \xi(t)]^T,$$

$\varphi_i(e_1)$ and β_i $(i = 1, 2, \ldots n+1)$ are the gain functions of tracking error e_1 and tuning parameters, respectively. The ESO with nonlinear gain functions are called the nonlinear ESO (NLESO) and can produce better transient behavior and faster convergence than the linear ESO (LESO), which is a special class of ESO with linear gain functions. However, the LESO has shown its advantages of simple tuning process and clear physical interpretation in applications, whereas the design of gain functions and tuning parameters in NLESO are overall more difficult and may vary from one specific system to another.

3.2 Problem Formulation

We first address the solutions for the issues proposed at the beginning of this chapter.

A potential solution for issue (I1), i.e., finding flat output of UMS from input-output data, has been addressed in Chapter 2. The study assumed that the linearized UMS around its equilibrium point is controllable and hence is flat. The locally flat output of the linearized system is then identified offline from the measured input and output data. The flat output identification algorithm (FOID) searches for an optimal linear combination of measurable outputs that grants the system highest relative degree, which can be interpreted as the flat output of the linearized system.

Once the flat output is available, issue (I2) can be solved by identifying linear regression representation of all the states and input in terms of the base functions consisting of the flat output and its finite number of time derivatives. For high dimensional UMSs, there can be many coefficients to be determined in the regression. Furthermore, not all the base functions may contribute the regression. The method of sparse identification of nonlinear dynamics (SINDy) in [28] or the

least absolute shrinkage and selection operator in [40] are good solutions to remove unnecessary terms.

For issue (I3), the idea of dividing the whole system into several subsystems works well to reduce the need for computing higher order derivatives of the flat output in [23, 26]. The second-order ESOs and Leunberger observers can handle the estimation efficiently with very small phase lag. To this end, we have found that the even-order derivatives of flat output are necessarily needed and can be expressed in terms of the measured output so that the order of ESOs can be kept low. The estimates of even-order derivatives of the flat output can be obtained with a linear regression with the base functions that are measurable states of the linearized system. The method of SINDy can be used here also to reduced the number of needed states.

Given the SIMO nonlinear UMS in the form of Equations (4.1) and (4.2), one challenging task of control design is to derive a robust feedback control law that forces one of its outputs to track prescribed smooth trajectory. Only one generalized coordinate, by reason of underactuation, is capable of following designated motion, and the difficulty of off-line motion planning differs from system to system, also depending on the trajectory of which output of the system, denoted by y_p, is being planned. Without loss of generality, we do not restrict our discussion to any specific UMS here, but assume the choice of y_p is known. Several requirements are proposed for designing tracking control in order to achieve disturbance rejection, robustness and noise attenuation.

A1. The output y_p should asymptotically track preplanned smooth trajectory y_p^* for y_p, while satisfying the given initial and final conditions.

A2. The desired controller can deal with unmodeled dynamics, parameter variations and external disturbances to a relatively large extent. These features are extremely valuable in engineering practice and yet often elusive.

A3. Need for high-order derivatives of measured signals should be avoided. Tracking control often involves computations of high-order derivatives of both states and reference signals, which tends to amplify the measurement noise and then leads to bad performance or instability of the closed-loop system.

For many engineering systems, a detailed mathematical model may not be readily available. We are interested in meeting the above control design requirements without such a model. We particularly focus on two aspects:

B1. Only the general structure of the model, such as the form of Equations (4.1) and (4.2), is known. No prior knowledge of system dynamics and control input specified in mathematical expressions is needed.

B2. The least number of sensors are available to lower the cost of building the system and to simplify its architecture. The actual number of sensors needed can be determined from the input-output data of the system without knowing the mathematical model.

The control problem studied in this article, as summarized in the previous discussions, is formalized as follows:

Problem 2. *Design a robust tracking controller for SIMO nonlinear UMS in Equations (4.1) and (4.2) subject to requirements A1-A3 based on principles B1 and B2.*

3.3 Data-Driven Robust Tracking Control Design

In this section, a data-driven framework of robust tracking control design for SIMO nonlinear UMS in Equations (4.1) and (4.2) is presented. The flat output identification (FOID) and sparse identification with the algebraic method are applied to explore the least number of terms in the representation of information from input-output data in order to develop a flatness-based ADRC without knowing the detailed mathematical expressions in Equations (4.1) and (4.2). The proposed framework for control design can be applied to different types of UMSs.

3.3.1 Trajectory Planning for Flat System

The trajectory planning problem for flat system can be solved with the help of the parametrization of the states with respect to a flat output. Consider a nonlinear single-input flat system with the flat output y_{f_1}. Let y_p be a prescribed motion over a time interval $t \in [t_0, t_f]$ such that it satisfies the following initial and final conditions [41].

$$y_p(t_0) = y_{p0}, \tag{3.8}$$

$$y_p(t_f) = y_{pf}. \tag{3.9}$$

Making use of the properties of flatness, we express $y_p(t)$ as a function of y_{f_1} and its time derivatives as

$$y_p(t) = \gamma_1(y_{f_1}, \dot{y}_{f_1}, \ldots, y_{f_1}^{(r)}), \tag{3.10}$$

From conditions (3.8) and (3.9), the initial and final conditions of $(y_{f_1}, \dot{y}_{f_1}, \ldots, y_{f_1}^{(r)})$ can be specified to satisfy Equation (3.10). The design of trajectory $y_p(t)$ becomes equivalent to the design of a desired trajectory $y_{f_1}^*$ for y_{f_1}. $y_{f_1}^*$ can be expressed as a polynomial of time with the order at least r. Normally, Equation (3.10) should be known to obtain all initial and final conditions $y_{f_1}^{(k)}(t_0)$ and $y_{f_1}^{(k)}(t_f)$, $k = 0, 1, \ldots, r$. A special trajectory is a rest-to-rest path where y_{p0} and y_{pf} are taken as the equilibrium points of the system. In this case, all derivatives of y_{f_1} at the initial and final time are zero resulting in

$$y_{p0} = \gamma_1(y_{f_1}(t_0), 0, \ldots, 0). \tag{3.11}$$

$$y_{pf} = \gamma_1(y_{f_1}(t_f), 0, \ldots, 0). \tag{3.12}$$

The initial and final values of output y_p are fully determined by the values of $y_{f_1}(t_0)$ and $y_{f_1}(t_f)$. One can add more zero conditions to Equation (3.11) and (3.12) such that $y_{f_1}^*$ can be sufficiently smooth at the beginning and end of the planned path.

3.3.2 Reduced Nominal Model with Linear Flat Output

Even though many nonlinear UMSs are non-flat, their linearized system around the equilibrium, as long as controllable, can be flat to take advantage of the simplified process of trajectory planning. Consider a state-space linearized form of Equations (4.1) and (4.2) around an equilibrium point $p = (\mathbf{x}_e, u_e)$ given by,

$$\dot{\mathbf{x}}_\delta = \mathbf{A}\mathbf{x}_\delta + \mathbf{b}u_\delta, \tag{3.13}$$

where $\mathbf{x}_\delta = \mathbf{x} - \mathbf{x}_e$ and $\mathbf{x} = [\mathbf{q}^T, \dot{\mathbf{q}}^T]^T \in \mathbb{R}^{2n}$. $\mathbf{x}_\delta$ is the incremental state vector, $u_\delta = u - u_e$ is the incremental scalar input variable. $\mathbf{A} \in \mathbb{R}^{2n\times 2n}$ is the linearized system matrix and $\mathbf{b} \in \mathbb{R}^{2n}$ is the input vector. Assume that $(\mathbf{A}, \mathbf{b})$ is controllable. The flat output of the linearized system can be given by

$$y_f = \begin{bmatrix} 0 & 0 & \dots & 1 \end{bmatrix} \mathbf{C}^{-1}\mathbf{x}_\delta, \tag{3.14}$$

where $\mathbf{C} = \begin{bmatrix} \mathbf{A} & \mathbf{A}\mathbf{b} & \mathbf{A}^2\mathbf{b} & \dots & \mathbf{A}^{n-1}\mathbf{b} \end{bmatrix}$ is the controllability matrix. The flat output y_f, in general, is a linear function of all the components of incremental state vector $\mathbf{x}_\delta$, which implies that the construction of y_f, as a physical and measurable output, must require full access of the original states **x.** Additional sensors or state estimators are needed for flatness-based control as a result. Moreover, this increases the burden of trajectory planning as more initial and final conditions of the states are involved.

A simplified model which neglects the effect of damping can be adopted so as to minimize the number of the needed states to construct flat output y_f. Such simplification is feasible in the framework of flatness-based ADRC, given that the unmodeled dynamics is in the scope of estimation. Consider a linearized system of Equations (4.1) and (4.2) around the origin without the damping term $\dot{\mathbf{q}}$

$$\mathbf{M}_c\ddot{\mathbf{q}} + \mathbf{K}_c\mathbf{q} = \mathbf{u}, \tag{3.15}$$

where $\mathbf{M}_c$ and $\mathbf{K}_c$ are constant mass and stiffness matrices, $\mathbf{u} = \begin{bmatrix} u & 0 & \dots & 0 \end{bmatrix}^T_{1\times n}$. Flat outputs can be found as linear functions of the generalized coordinates, or at most half of the states in state space, as the following theorem states.

Theorem 3.3.1. *If the simplified linearized model (3.15) of a SIMO nonlinear UMS is controllable, there exists a scalar linear function $y_c(\mathbf{q})$ such that $y_c(\mathbf{q})$ is the flat output of the system (3.15).*

Proof. A trivial state-space realization of (3.15) is carried out by choosing state as $\mathbf{x} = [x_1, x_2, \cdots, x_{2n}] = [\mathbf{q}^T, \dot{\mathbf{q}}^T]^T$,

$$\dot{\mathbf{x}} = \mathbf{A}_c\mathbf{x} + \mathbf{b}_c u, \tag{3.16}$$

where input variable $u = \tau$ and controllable pair $(\mathbf{A}_c, \mathbf{b}_c)$ are of the form:

$$\mathbf{A}_c = \left[\begin{array}{c|c} \mathbf{0} & \mathbf{I}_n \\ \hline \mathbf{H} & \mathbf{0} \end{array}\right], \mathbf{b}_c = \left[\begin{array}{c} \mathbf{0} \\ \hline \mathbf{v} \end{array}\right]_{2\times n}, \tag{3.17}$$

$$\mathbf{H}_{n\times n} = \begin{bmatrix} a_{11} & a_{12} & \cdots & a_{1n} \\ a_{21} & a_{22} & \cdots & a_{2n} \\ \vdots & \vdots & \ddots & \vdots \\ a_{n1} & a_{n2} & \cdots & a_{nn} \end{bmatrix}, \mathbf{v} = \begin{bmatrix} b_1 \\ b_2 \\ \vdots \\ b_n \end{bmatrix}, \tag{3.18}$$

$\mathbf{I}_n$ is $n \times n$ identity matrix. At least one of $b_i, i = 1, 2, \cdots, n$, is not zero. In the following discussions, we shall use the following symbols interchangeably.

$$\mathbf{x} = [\mathbf{x}_1^T, \mathbf{x}_2^T] = [\mathbf{q}^T, \dot{\mathbf{q}}^T]^T \in \mathbb{R}^{2n} \tag{3.19}$$

where $\mathbf{x}_1 = \mathbf{q} = [x_1, x_2, \cdots, x_n]^T$. Consider scalar function $y_c(x_1, x_2, \cdots x_n) = c_1x_1 + c_2x_2 + \cdots + c_nx_n = \mathbf{c}^T\mathbf{x}_1$. Taking derivative of y_c $2n$ times gives,

$$\ddot{y}_c = \mathbf{c}^T\ddot{\mathbf{x}}_1 = \mathbf{c}^T(\mathbf{H}\mathbf{x}_1 + \mathbf{v}u), \tag{3.20}$$

$$y_c^{(4)} = \mathbf{c}^T\mathbf{x}_1^{(4)} = \mathbf{c}^T(\mathbf{H}^2\mathbf{x}_1 + \mathbf{H}\mathbf{v}u + \mathbf{v}\ddot{u}), \tag{3.21}$$

$$y_c^{(6)} = \mathbf{c}^T\mathbf{x}_1^{(6)} = \mathbf{c}^T(\mathbf{H}^3\mathbf{x}_1 + \mathbf{H}^2\mathbf{v}u + \mathbf{H}\mathbf{v}\ddot{u} + \mathbf{v}u^{(4)}), \tag{3.22}$$

$$\vdots$$

$$\begin{aligned} y_c^{(2n)} &= \mathbf{c}^T\mathbf{x}_1^{(2n)} = \mathbf{c}^T\mathbf{H}^n\mathbf{x}_1 + \mathbf{c}^T(\mathbf{H}^{n-1}\mathbf{v}u + \\ &\quad \cdots + \mathbf{H}^2\mathbf{v}u^{(2n-6)} + \mathbf{H}\mathbf{v}u^{(2n-4)} + \mathbf{G}u^{(2n-2)}). \end{aligned} \tag{3.23}$$

Let $\mathbf{c}^T\mathbf{H}^i\mathbf{v} = \mathbf{0}$, we have

$$(\mathbf{H}^i\mathbf{v})^T\mathbf{c} = \mathbf{0}, \tag{3.24}$$

where $i = 0, 1, \cdots, n-2$. Equation (3.24) forms at most $n-1$ independent linear equations of $\mathbf{c}$ having infinitely many solutions $\{\mathbf{c}^k\} = \{[c_1^k, c_2^k, \cdots, c_n^k]^T\}$, $k = 1, 2, \cdots$, in general. Taking any nonzero solution $\mathbf{c}^*$ from set $\{\mathbf{c}^k\}$, $(\mathbf{v}, \mathbf{H}\mathbf{v}, \cdots \mathbf{H}^{n-1}\mathbf{v})$ are linearly independent since $(\mathbf{A}_c, \mathbf{b}_c)$ is controllable, which implies,

$$[\mathbf{v}, \mathbf{H}\mathbf{v}, \cdots, \mathbf{H}^{n-1}\mathbf{v}]_{n\times n}^T\mathbf{c}^* \neq \mathbf{0}. \tag{3.25}$$

Therefore, $(\mathbf{H}^{n-1}\mathbf{v})^T\mathbf{c}^* \neq 0$, and equivalently, $(\mathbf{c}^*)^T\mathbf{H}^{n-1}\mathbf{v} \neq 0$. The scalar function $y_c(\mathbf{q}) \equiv y_c(x_1, x_2, \cdots x_n) = (\mathbf{c}^*)^T\mathbf{x}_1$, having $(2n)^{th}$ order derivatives in the form of

$$y_c^{(2n)} = (\mathbf{c}^*)^T\mathbf{x}_1^{(2n)} = (\mathbf{c}^*)^T\mathbf{H}^n\mathbf{x}_1 + (\mathbf{c}^*)^T\mathbf{H}^{n-1}\mathbf{v}u, \tag{3.26}$$

is hence the flat output according to Corollary 2.2 in [52]. □

Theorem 3.3.1 implies that the flat output of system (3.15) or (3.16) can be constructed, as a combination of the generalized coordinates, or the corresponding states, through limited number of sensors. When the states are not directly measurable, the flat output can be a linear function of the measured outputs as long as the required states can be reconstructed from them. Although less knowledge is needed to derive the flat output from the reduced model, one must know $\mathbf{M}_c$ and $\mathbf{K}_c$ in advance from a proper modelling process. By treating (3.15) as a nominal model, however, it is possible to identify the desired flat output from enough measured data, simply assuming the controllability holds, as shown in the following subsection.

3.3.3 Flat Output Identification (FOID)

FOID from last chapter automatically searches the flat output as a linear combination of measured outputs and identify the flatness of the mechanical system operating around its equilibrium. Consider a reduced linear model around origin, for simplicity, as given by Equation (3.15). According to the statement of Theorem 3.3.1, at most n sensors that measure the signals of generalized coordinates are required, while the minimum number of measurements of output needed for building flat output, which depends on system dynamics, is unknown. A possible candidate of flat output of system (3.15) is given by

$$y_l(t) = c_1 y_1(t) + c_2 y_2(t) + \dots c_j y_j(t), \tag{3.27}$$

where $y_1(t), \dots, y_j(t)$ are measured outputs. It has been shown that the flat output of system (3.15) is the one having full relative degree, that is, the order of differentiation of the output function until the input variable $u(t)$ explicitly appears. The optimal output $y_{opt}(t)$ with highest relative degree r_{opt} will be chosen, and the system described by the nominal model can be transformed into an input-output model without zero dynamics, if $r_{opt} = 2n$, as

$$y_{opt}^{(2n)}(t) = g(\mathbf{y}_{opt}) + b(\mathbf{y}_{opt})u(t), \tag{3.28}$$

where $\mathbf{y}_{opt} = \left[\dot{y}_{opt}, \ddot{y}_{opt}, \dots, y_{opt}^{(2n-1)}\right]^T$ is the flat output vector. Taking all uncertainties and unmodeled dynamics into account, Equation (3.28) can be furthermore extended to

$$y_{f_1}^{(n)}(t) = \xi(t) + b_0 u(t), \tag{3.29}$$

where $y_{opt}(t)$ is replaced with $y_{f_1}(t)$.

The dimension of system (3.16), $2n$, is assumed to be known, which is the assumption of FOID. The derivation of dimension is sometimes straightforward for simple mechanical systems by knowledge of physics and mechanics. A determination of principal dimension in a data-driven method can be found in [33].

3.3.4 Sparse Identification for States and Derivatives of Flat Output

It is common to measure the generalized coordinates $\mathbf{q}$ as outputs of UMS. For instance, the motion of Acrobot can be described by the joint angle at shoulder and relative joint angle at elbow which are measurable by two rotary encoders. In the state-space model shown before, the generalized coordinates, as well as their first derivatives, constitute the state vector. Suppose there are enough sensors directly measuring $\mathbf{q}$, the first n states in (3.16), for control design, the flatness and linearity of (3.15) indicates that all these states x_i can be expressed as a linear function of flat output and its time derivatives up to the order of $2n-1$. Consider a general case when flat output y_{f_1} of (3.15) consists of linear combination of all generalized coordinates,

$$y_{f_1}(t) = c_1 x_1(t) + c_2 x_2(t) + \ldots + c_n x_n(t) = \mathbf{c}^T \mathbf{x}_1, \tag{3.30}$$

To configure the motion of certain output $y_p(t) = x_i(t)$, $i \in \{1, 2, \ldots, n\}$, and design the reference trajectory $y^*_{f_1}$ for flat output, the relationship given as equation (3.10) are necessary. Moreover, one may need to know what trajectories the rest of the states will have when $y_p(t)$ follows desired reference.

Sparse regression has manifested the versatility and effectiveness in identification of nonlinear systems recently, where the basic assumption is that the governing equations are sparse in high-dimensional function space, which is reasonable for many systems in action. The library of nonlinear functions in sparse regression comprises the candidate functions, such as constant, polynomial, trigonometric functions and discontinuous terms, that are chosen based on the understanding of the system of interest, and hence the building of the library has become a challenge in application of this technique. When it comes to discovering the relationship between original states and flat output as equation (3.10), the collection of candidates is constrained with a limit number of members which are only flat output y_{f_1} and its successively finite time derivatives. Interestingly, assumption of simplified model (3.15) also allows us to have even fewer terms of candidates, as shown by the next theorem.

Theorem 3.3.2. *All generalized coordinates* $\mathbf{q}$ *in model (3.15) are functions of linear flat output (3.26) and its finite number of even-order derivatives.*

Proof. From Theorem 3.3.1, any linear flat output y_{f_1} is a function of all generalized coordinates $y_{f_1}(\mathbf{q}) \equiv y_c(x_1, x_2, \cdots, x_n) = (\mathbf{c}^*)^T \mathbf{x}_1$ in which $c_1^*, c_2^*, \cdots, c_n^*$ have at least one nonzero coefficient. Differentiating y_{f_1} $2(i-1)$ times gives $n-1$ equations as

$$y_{f_1}^{(2i-2)}(\mathbf{x}_1) = (\mathbf{c}^*)^T \mathbf{H}^{i-1} \mathbf{x}_1, i = 2, \cdots, n. \tag{3.31}$$

Due to feature of flat output, Equation (3.31) along with $y_{f_1}(\mathbf{x}_1) = (\mathbf{c}^*)^T \mathbf{x}_1$ forms n linearly independent equations, for which the solution $\mathbf{x}_1$, equivalently $\mathbf{q}$, are all linear functions of even-order derivatives. □

Corollary 3.3.3. *All generalized velocities* $\dot{\mathbf{q}}$ *in model (3.15) are functions of linear flat outputs' finite number of odd-order derivatives.*

To figure out how generalized coordinates are represented in terms of locally flat output without relying on prior mathematical model, one can now perform sparse regression with the library comprising $y_{f_1}, \ddot{y}_{f_1}, \ldots, y_{f_1}^{(2n-2)}$ to identify their relationship. The rest of the states, generalized velocities $\dot{\mathbf{q}}$, can be obtained by the direct differentiation of $\mathbf{q}(y_{f_1}, \ddot{y}_{f_1}, \ldots, y_{f_1}^{(2n-2)})$ by corollary. Consider i-th component of $\mathbf{q}$ is written by

$$q_i = \chi_{i1} y_{f_1} + \chi_{i2} \ddot{y}_{f_1} + \ldots + \chi_{in} y_{f_1}^{(2n-2)} = \boldsymbol{\chi}_i^T \mathbf{y}_{f_1}, \tag{3.32}$$

where $\chi_{ij}, j = 1, 2, \ldots, n$, are the scalar coefficients. Differentiation of signals, especially when it comes to computing high-order derivatives, is usually confronted with unexpected disturbance caused by random noise from environment, which hinders the result of sparse regression to be useful. In order to tackle this issue, the algebraic operation in [30] is applied. Applying Laplace transformation to equation (3.32) gives

$$\begin{aligned} Q_i(s) = \chi_{i1} Y_{f_1}(s) + \chi_{i2} \left[s^2 Y_{f_1}(s) - s y_{f_1}(0) - \dot{y}_{f_1}(0) \right] + \ldots \\ + \chi_{in} \left[s^{2n-2} Y_{f_1}(s) - (s^{2n-1} y_{f_1}(0) + s^{2n-2} \dot{y}_{f_1}(0) \ldots + y_{f_1}^{(2n-1)}(0)) \right], \end{aligned} \tag{3.33}$$

where $Q_i(s)$ and $Y_{f_1}(s)$ are the Laplace transform q_i and y_{f_1} respectively. Taking derivatives $2n-2$ times with respect to s can eliminate the dependence of all initial conditions. To show this method but keep procedures compact, case of $n = 2$ are shown below.

$$\frac{d^2 Q_i(s)}{ds^2} = \chi_{i1} \frac{d^2 Y_{f_1}(s)}{ds^2} + \chi_{i2} \left[2 Y_{f_1}(s) + 4s \frac{d Y_{f_1}(s)}{ds} + s^2 \frac{d^2 Y_{f_1}(s)}{ds^2} \right]. \tag{3.34}$$

The next step is dividing s^{2n-2} on both side of the preceding result to avoid differentiation with respect to time. When $n = 2$, it gives

$$\frac{1}{s^2} \frac{d^2 Q_i(s)}{ds^2} = \chi_{i1} \frac{1}{s^2} \frac{d^2 Y_{f_1}(s)}{ds^2} + \chi_{i2} \left[\frac{2}{s^2} Y_{f_1}(s) + \frac{4}{s} \frac{d Y_{f_1}(s)}{ds} + \frac{d^2 Y_{f_1}(s)}{ds^2} \right]. \tag{3.35}$$

Equation (3.35) can be transformed back to time domain as

$$P_{q_i}(t) = \chi_{i1} P_{i1}(t) + \chi_{i2} P_{i2}(t), \tag{3.36}$$

where

$$P_q(t) = \int_0^t \int_0^{\tau_2} \tau_1^2 q_i(\tau_1) d\tau_1 d\tau_2, \tag{3.37}$$

$$P_{i1}(t) = \int_0^t \int_0^{\tau_2} \tau_1^2 y_{f_1}(\tau_1) d\tau_1 d\tau_2, \tag{3.38}$$

$$P_{i2}(t) = 2 \int_0^t \int_0^{\tau_2} y_{f_1}(\tau_1) d\tau_1 d\tau_2 - 4 \int_0^t \tau_1 y_{f_1}(t) d\tau_1 + t^2 y_{f_1}(t). \tag{3.39}$$

This result (3.36) can be easily extendable when $n > 2$ such that

$$P_{q_i}(t) = \chi_{i1}P_{i1}(t) + \chi_{i2}P_{i2}(t) + \ldots + \chi_{in}P_{in}(t) \tag{3.40}$$

in which all P_j, $j = 1, 2, \ldots, n$ can be defined similarly according to previous steps.

In implementation of sparse identification, all signals involved are considered discrete. Assuming only few terms dominate equation (3.40), we employ the least absolute shrinkage and selection operator (LASSO) [40] to estimate the coefficients vector χ_i of sparse terms through minimizing the cost function J_λ in (3.41) and defining error $e_i(t_k)$ at time t_k:

$$J_\lambda(\boldsymbol{\chi}_i) = \sum_{t_k} e_i^2(t_k) + \lambda \left\|\boldsymbol{\chi}_i\right\|_1, \tag{3.41}$$

$$e_i(t_k) = \chi_{i1}P_1(t_k) + \chi_{i2}P_2(t_k) + \ldots + \chi_{in}P_n(t_k) - P_{q_i}(t_k). \tag{3.42}$$

$\lambda > 0$ is a preselected positive number known as the sparse regulator. It is common to use K-fold cross-validation techniques from machine learning to determine the sparse regulation parameter λ. Consider signals $P_1(t_k), P_2(t_k), \ldots, P_n(t_k)$ and $P_{q_i}(t_k)$, $k = 1, 2, \ldots, N_t$, form the whole data set S_t. N_t is the total number of samples of each signal. The K-fold cross-validation divides all data points in S_t into roughly K equal parts and each time take one of the part to validate the performance of model while using the $K-1$ parts for training. When z-th part is selected as validation set, let S_v^z and S_k^z denote the selected validation set and k-th training set among the rest folds. The sum of square error for given λ on validation sets is defined by

$$\mathrm{SSE}_z(\lambda) = \sum_{k=1}^{K-1} \left\|\mathbf{P}_i^z c_k - \mathbf{P}_{q_i}^z\right\|_2^2,$$

where $c_k = \begin{bmatrix} \widetilde{\chi}_{i1}^k & \widetilde{\chi}_{i2}^k & \ldots & \widetilde{\chi}_{in}^k \end{bmatrix}^T$ is the k-th vector of coefficients in equation (3.40) that estimated by data from S_k^z, , $\mathbf{P}_i^z$ are the n-by-n_v matrix of signals $P_j^z(t_1), P_j^z(t_2) \ldots, P_j^z(t_{n_v})$, $j = 1, 2, \ldots, n$, n_v is the number of samples in S_v^z, and $\mathbf{P}_{q_i}^z$ is the vector of signals $P_j^z(t_1), P_j^z(t_2) \ldots, P_j^z(t_{n_v})$ from S_v^z. $\mathbf{P}_i^z$ and $\mathbf{P}_{q_i}^z$ are given by

$$\mathbf{P}_i^z = \begin{bmatrix} P_1^z(t_1) & P_2^z(t_1) & \ldots & P_n^z(t_1) \\ P_1^z(t_2) & P_2^z(t_2) & \ldots & P_n^z(t_1) \\ \vdots & \vdots & \ddots & \vdots \\ P_1^z(t_{n_v}) & P_2^z(t_{n_v}) & \ldots & P_n^z(t_{n_v}) \end{bmatrix}, \mathbf{P}_{q_i}^z = \begin{bmatrix} P_{q_i}^z(t_1) \\ P_{q_i}^z(t_2) \\ \vdots \\ P_{q_i}^z(t_{n_v}) \end{bmatrix}.$$

The mean square cross validation error MSEcv of model (3.40) for given λ on validation sets is defined by

$$\mathrm{MSEcv}(\lambda) = \frac{1}{n_v K} \sum_{z=1}^{K} \mathrm{SSE}_z(\lambda),$$

in which we assume n_v is equal in each validation set. The λ value which minimizes the cross-validation error is selected so that the resulting estimate $\widetilde{\boldsymbol{\chi}}_i$ is a set of optimal coefficients with a proper balance between complexity and accuracy. For the purpose of improving the robustness of sparse regression, the algorithm could be implemented with bootstrapping. It is always possible to add odd-derivatives of flat output to library of sparse regression of generalized coordinates. But by the assumption of reduced nominal model and framework of ADRC followed, we attribute the neglect into internal disturbances.

Another important observation from theorem 3.3.2 is that even-order derivatives of locally flat output $y_{f_1}(t)$, up to the order $2n-2$, are solely functions of generalized coordinates, which in turn allows one to construct high– and even-order derivatives of $y_{f_1}(t)$ without using extra sensors or estimation in flatness-based feedback control design. Given enough identified equation of generalized coordinates as (3.32), it is always possible to solve for a set of coefficients such that

$$y_{f_1}^{(2j-2)} = \boldsymbol{\eta}_j^T \mathbf{q}, \tag{3.43}$$

where $j = 2, 3, \ldots, n$ and $\boldsymbol{\eta}_j \in \mathbb{R}^n$ is the coefficient vector, of which some elements may be zero. $\boldsymbol{\eta}_j$ can be either estimated by sparse identification with time sequences of $y_{f_1}^{(2j-2)}(t)$ and all generalized coordinates $\mathbf{q}(t)$, or obtained by solving some linear equations based on sparse identification of $\mathbf{q}$. In fact, the elements of $\boldsymbol{\eta}_j$ could be trivially solved if any generalized coordinate is identified as $q_k = \chi_{kj} y_{f_1}^{(2j-2)}$. Otherwise, since $\mathbf{q}(y_{f_1}, \ddot{y}_{f_1}, \ldots, y_{f_1}^{(2n-2)})$ can be estimated, there are $l+1$ equations as (3.32) that contain $y_{f_1}^{(2j-2)}$ and have totally $l+1$ number of nonzero terms of flat output and its derivatives on right hand side of them:

$$q_k = \chi_{kj} y_{f_1}^{(2j-2)} + w_{k_1} y_{d_1} + w_{k_2} y_{d_2} + \ldots + w_{k_l} y_{d_l} \tag{3.44}$$

where $y_{d_1}, \ldots, y_{d_l}$ can represent the flat output y_{f_1} and some derivatives of y_{f_1} of certain even-order that is less or equal than $2n-2$ except $y_{f_1}^{(2j-2)}, 1 \leqslant l \leqslant n-1$. $w_{k1}, \ldots, w_{kl}$ are coefficients from sparse regression of q_k, where $k \in [1, 2, \ldots, n]$. A coefficient vector $\overline{\boldsymbol{\eta}}_j = \begin{bmatrix} \overline{\eta}_{j1} & \overline{\eta}_{j2} & \ldots & \overline{\eta}_{jl} \end{bmatrix}^T$ can be defined such that

$$\begin{aligned} y_{f_1}^{(2j-2)} &= \overline{\boldsymbol{\eta}}_j^T \mathbf{q}_l \\ &= \sum_k \overline{\eta}_{jk} \left(\chi_{kj} y_{f_1}^{(2j-2)} + w_{k_1} y_{d_1} + w_{k_2} y_{d_2} + \ldots + w_{k_l} y_{d_l} \right) \\ &= \sum_k \overline{\eta}_{jk} \chi_{kj} y_{f_1}^{(2j-2)} + \sum_k \overline{\eta}_{jk} \left(w_{k_1} y_{d_1} + w_{k_2} y_{d_2} + \ldots + w_{k_l} y_{d_l} \right), \end{aligned} \tag{3.45}$$

where $\mathbf{q}_l$ is the vector of l generalized coordinates that are relevant to $y_{f_1}^{(2j-2)}$. Matching coefficients on both sides of the equations gives a set of linear equations of $\overline{\boldsymbol{\eta}}_j$ to solve

$$\sum_k \overline{\eta}_{jk}\chi_{kj} = 1, \tag{3.46}$$

$$\sum_k \overline{\eta}_{jk}\left(w_{k_1}y_{d_1} + w_{k_2}y_{d_2} + \ldots + w_{k_l}y_{d_l}\right) = 0 \tag{3.47}$$

By filling up zeros for irrelevant $n-l$ generalized coordinates, $\overline{\boldsymbol{\eta}}_j$ can be extended to $\boldsymbol{\eta}_j$ with n dimensions. Construction of high-order derivatives of y_{f_1} extremely reduce the noise effect and phase lag in feedback signal. These good properties make the extended-state observer, illustrated in next subsection, available to high-order flat system. For example, the second-order derivative $\ddot{y}_{f_1}$, when $2n = 4$, is generally involved in

$$\begin{aligned} q_1 &= \chi_{12}\ddot{y}_{f_1} + w_{_{11}}y_{d_1} = \chi_{12}\ddot{y}_{f_1} + \chi_{11}y_{f_1}, \\ q_2 &= \chi_{22}\ddot{y}_{f_1} + w_{_{21}}y_{d_1} = \chi_{22}\ddot{y}_{f_1} + \chi_{21}y_{f_1}. \end{aligned}$$

$\overline{\boldsymbol{\eta}}_2$ is the solution of

$$\begin{bmatrix} \chi_{12} & \chi_{22} \\ \chi_{11} & \chi_{21} \end{bmatrix} \begin{bmatrix} \overline{\eta}_{21} \\ \overline{\eta}_{22} \end{bmatrix} = \begin{bmatrix} 1 \\ 0 \end{bmatrix},$$

where $\overline{\boldsymbol{\eta}}_2$ is also $\boldsymbol{\eta}_2$. Equation (3.31) has shown $\eta_j^T = (\mathbf{c}^*)^T\mathbf{H}^{j-1}$ so solving for $y_{f_1}^{(2j-2)}$ from (3.46) and (3.47) is always possible under the setting of reduced model. The calculation result of η_j should be consistent with the one from applying sparse regression to equation (3.43).

3.3.5 Error-space Representation and Extend-state Observer Design

Tangent linearized model (3.29) has limitation because it only approximates nonlinear system within a small range around certain equilibrium point. The idea of linearization works in many applications but can be invalid when large range operations are required and non-negligible hard nonlinearities are detected. To compensate the unmodeled dynamics neglected by tangent linearization and extend the range of operation as large as possible, the input-to-flat output representation (3.29) is considered in the framework of ADRC, where the term $\zeta(t)$ represents the total disturbance and b_0 is a constant nominal gain. Many different types of extended-state observer have been studied in past decade [42–46], however, their role in ADRC design and basic structure remain almost unchanged. We will illustrate flatness-based ADRC with classic LESO due to its simple tuning process and light computational burden. Note that any NLESO can be adopted to replace LESO in this framework if it fulfills basic requirements, like stability and fast enough convergence.

Conventional flatness-based ADRC for tracking control would estimate and filter the flat output y_{f_1} and its time derivatives $\dot{y}_{f_1}, \ldots, y_{f_1}^{(2n-1)}$ by ESO, and reference signals for $y_{f_1}, \dot{y}_{f_1}, \ldots, y_{f_1}^{(2n)}$ are introduced for feedback purpose. While this scheme needs all high-order time derivatives of reference signals, another approach is introduced to transform system (3.29) into error space and treat reference signals as part of the external disturbance, hence part of the total disturbance. We assume that a particular output $y_p = x_p$ is to be planned. The prescribed trajectory designed for y_p, y_p^* , leads to a reference of flat output $y_{f_1}^*$ according to (3.10). The tracking error is defined as $e(t) = y_{f_1}(t) - y_{f_1}^*(t)$. Therefore error dynamics reads

$$e^{(2n)} = y_{f_1}^{(2n)} - y_{f_1}^{*(2n)} = \zeta_1(t) + b_0 u(t), \tag{3.48}$$

where $\zeta_1(t)$ is the new total disturbance term, which lumps $\zeta(t)$ defined in (3.29) and desired trajectories of $y_{f_1}, \dot{y}_{f_1}, \ldots, y_{f_1}^{(2n)}$. The series of low-order Leunberger observers and LESO are used to generate feedback signal in design of control law. Because even-order derivatives of y_{f_1} are accessible from linear combination of generalized coordinates, system (3.48) can be divided into several subsystems

$$\dot{e}_i = e_{i+1}, \tag{3.49}$$

$$\dot{e}_{i+1} = e_{i+2}, \tag{3.50}$$

$$e_i = e^{(i)} = y_{f_1}^{(i)} - y_{f_1}^{*(i)}, i = 0, 2, \ldots, 2n-4, \tag{3.51}$$

and

$$\dot{e}_{2n-2} = e_{2n-1}, \tag{3.52}$$

$$\dot{e}_{2n-1} = \zeta_1(t) + b_0 u(t). \tag{3.53}$$

The subsystems in the form of equation (3.49)(3.50) are purely second-order differential equations of error and its even-order derivatives. To derive the estimate of $e_1, e_3, \ldots e_{2n-3}$, $n-1$ Leunberger observers can be built as

$$\dot{z}_i = z_{i+1} - \beta_i(z_i - e_i), \tag{3.54}$$

$$\dot{z}_{i+1} = z_{i+2} - \beta_{i+1}(z_i - e_i), i = 0, 2, \ldots, 2n-4, \tag{3.55}$$

where z_i, z_{i+1} is the estimate of e_i and e_{i+1}, β_i are the gains of observers to be selected. Note that z_i are redundant because the relationship between e_i and generalized coordinate $\mathbf{q}$ are assumed known from sparse identification. The LESO for subsystem (3.52)(3.53) is given by

$$\dot{z}_{2n-2} = z_{2n-1} - \beta_{2n-2}(z_{2n-2} - e_{2n-2}), \tag{3.56}$$

$$\dot{z}_{2n-1} = z_{2n} + b_0 u(t) - \beta_{2n-1}(z_{2n-2} - e_{2n-2}), \tag{3.57}$$

$$\dot{z}_{2n} = -\beta_{2n}(z_{2n-2} - e_{2n-2}), \tag{3.58}$$

where z_{2n-1}, z_{2n-2} and z_{2n} are estimate of e_{2n-2}, e_{2n-1} and $\zeta_1(t)$ respectively, $\beta_{2n-2}, \beta_{2n-1}$ and β_{2n} are gains of ESO to be determined.

The reason that dividing (3.48) into subsystems is that estimates of higher order derivatives from high-order Leunberger Observer or ESO are easily polluted and distorted by noise. The more times the derivatives of $e(t)$ has been taken, the worse accuracy of their estimates will have. Some other work about building cascaded ESO to avoid this issue can be found in [47] and [48].

The convergence of observation error of Leunberger observers requires to choose appropriate β_i and β_{i+1} such that

$$\ddot{\widetilde{e}}_i + \beta_i \dot{\widetilde{e}}_i + \beta_{i+1} \widetilde{e}_i = 0, i = 0, 2, \ldots, 2n-4, \tag{3.59}$$

has asymptotically stable solution $\widetilde{e}_i$, defined as observation error $\widetilde{e}_i = z_i - e_i$. A pair of straightforward choice is $\beta_i = 2\omega_i, \beta_{i+1} = \omega_i^2$, where ω_i can be interpreted as bandwidth of observers in frequency domain. The observation error of ESO $\widetilde{e}_{2n-2} = z_{2n-1} - e_{2n-2}$ provides the error dynamics:

$$\dddot{\widetilde{e}}_{2n-2} + \beta_{2n-2} \ddot{\widetilde{e}}_{2n-2} + \beta_{2n-1} \dot{\widetilde{e}}_{2n-2} + \beta_{2n} \widetilde{e}_{2n-2} = -\dot{\zeta}_1(t). \tag{3.60}$$

Selecting $\beta_{2n-2}, \beta_{2n-1}, \beta_{2n}$ such that its characteristic polynomial

$$s^3 + \beta_{2n-2} s^2 + \beta_{2n-1} s + \beta_{2n} = 0 \tag{3.61}$$

has negative roots in which $\beta_{2n-2} = 3\omega_{2n-2}, \beta_{2n-1} = 3\omega_{2n-2}^2, \beta_{2n} = \omega_{2n-2}^3$ is a common choice. Define estimation error of total disturbance as $\widetilde{e}_\zeta = z_{2n} - \zeta_1(t)$.Assuming the total disturbance $\zeta_1(t)$ and its first time derivative $\dot{\zeta}_1(t)$ is uniformly absolutely bounded, it can be proved the estimation errors $\widetilde{e}_i, \widetilde{e}_{2n-2}$ and $\widetilde{e}_\zeta$, based on the selection of gains $\beta_i, \beta_{i+1}, \beta_{2n-2}, \beta_{2n-1}, \beta_{2n}$, can become as small in magnitude as desired and uniformly approach a neighborhood of the origin in error space [37].

The control law for flatness-based ADRC can be designed as

$$u(t) = \frac{1}{b_0}(-\widetilde{\zeta}_1(t) - \alpha_1 z_{2n-1} - \alpha_2 z_{2n-2} \ldots - a_{2n-1} z_1 - \alpha_{2n} z_0), \tag{3.62}$$

which leads to

$$e^{(2n)} + \alpha_1 e^{(2n-1)} + \alpha_2 e^{(2n-2)} \ldots \alpha_{2n} e = \widetilde{e}_\zeta - \sum_{j=1}^{2n} \alpha_j \widetilde{e}_{(2n-j)}, \tag{3.63}$$

where $\alpha_1, \alpha_2, \ldots, \alpha_{2n-1}$ coefficients chosen such that characteristic equation of differential equation (3.63) has negative roots. The flat output tracking error $e(t)$ and its time derivatives asymptotically converge to a small neighborhood of the origin in error space, with proper high gains in ESO and Leunberger observers, as

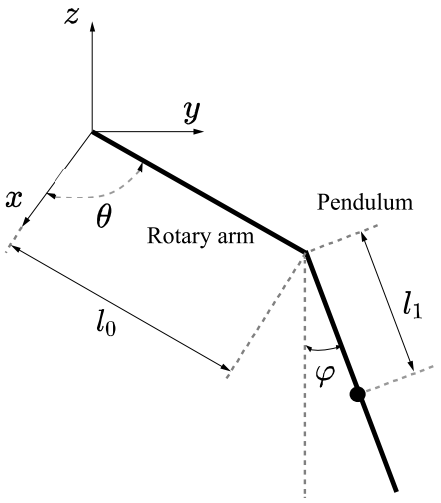

Figure 3.1: Schematic of Rotary Crane Pendulum

$\mu(t) = \widetilde{e}_\zeta - \sum_{j=1}^{2n} \alpha_j \widetilde{e}_{(2n-j)}$ does [37]. Stability analysis of the closed-loop system, when $\zeta_1(t)$ and $\dot{\zeta}_1(t)$ is bounded or uniformly bounded, can be found in [26, 49, 50].

The burden of keeping track of good performance and closed-loop stability is shifted to Leunberger observer and LESO. The upper bound of the estimation error of LESO is decreased monotonically with its bandwidth increased [51]. Setting up proper bandwidth for closed-loop system and these observers is crucial to keep ADRC working on the right track. There are other variants of ESO with time-varying gain [50], or generalized proportional integral observer(GPIO) [37] that can be used in this framework. As previously stated, these versions of ESO can freely replace classic linear ESO. For simplicity, however, the details are not in the scope of research in this chapter.

3.4 Experimental Validation: Rotary Crane Pendulum

In this section, we illustrate the data-driven tracking control design and experiment by an example of rotary crane pendulum. Model information of rotary crane pendulum will be briefly introduced, however, details of which are not used in following control design. FOID and sparse identification are carried out with enough data collected from device, after which trajectory planning and design of ADRC follow.

3.4.1 Introduction of Rotary Crane Pendulum

The rotary crane pendulum (RCP) is 2-degree-of-freemdom SIMO nonlinear UMS shown in Figure 3.1 and 3.2. Its main structure consists of two components: rotary arm and crane pendulum. The DC motor and gear system, providing torque

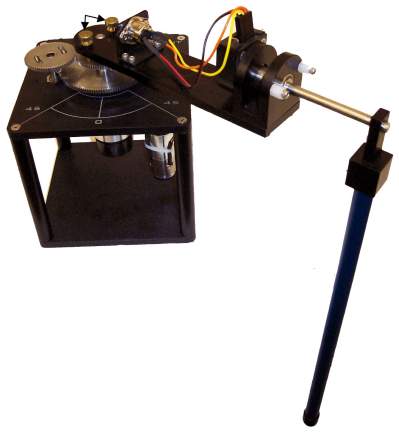

Figure 3.2: Rotary Crane Pendulum

τ, drive the arm to rotate in a horizontal plane, while the pendulum tied to the end of the arm can swing back and forth along the motion. Assume two rotary encoders mounted to measure θ, the angular position of arm, and φ, the angle of swing, are all incremental. Two generalized coordinates, as well as measurable outputs, θ and φ are chosen for modelling process, that is $\mathbf{q} = [\theta, \varphi]^T$. The mathematical model of the linearized system around the origin of the state space ($\theta = 0$,$\varphi = 0$, $\dot{\theta} = 0$, $\dot{\varphi} = 0$, $\tau = 0$) can be obtained by applying the Euler-Lagrange method:

$$\mathbf{M}_c\ddot{\mathbf{q}} + \mathbf{K}_c\mathbf{q} = \boldsymbol{\tau}, \tag{3.64}$$

$$\begin{bmatrix} J_r + m_p l_0^2 & m_p l_1 l_0 \\ m_p l_0 l_1 & J_p + m_p l_1^2 \end{bmatrix} \begin{bmatrix} \ddot{\theta} \\ \ddot{\varphi} \end{bmatrix} + \begin{bmatrix} 0 & 0 \\ 0 & m_p g l_1 \end{bmatrix} \begin{bmatrix} \theta \\ \varphi \end{bmatrix} = \begin{bmatrix} \tau \\ 0 \end{bmatrix}, \tag{3.65}$$

where we neglect the terms related to equivalent viscous damping involving $\dot{\theta}$ and $\dot{\varphi}$. All other notations are: rotary arm moment of inertia about its center of mass J_r, pendulum moment of inertia about its center of mass J_p, mass of pendulum m_p, half length of pendulum l_1, full length of rotary arm l_0 and gravitational acceleration g. The device of rotary crane system in the experiment is made by Quanser as shown in Figure . The voltage applied to the DC motor is denoted as V. The relation between voltage V and torque τ is given by

$$\tau = \frac{\eta_g K_g \eta_m k_t}{R_m}(V - K_g k_m \dot{\theta}) \approx \frac{\eta_g K_g \eta_m k_t}{R_m} V, \tag{3.66}$$

where term $\frac{\eta_g K_g \eta_m k_t K_g k_m}{R_m}\dot{\theta}$ is also neglected in our 'no damping' reduced model.

Simplified model (3.65) can be easily verified as differentially flat system since it is controllable. The details can be found in chapter 2. One possible but not unique flat output can be found as

$$y_{f_1} = \theta + \frac{J_p + m_p l_1^2}{m_p l_1 l_0}\varphi. \tag{3.67}$$

The value of all parameters from RCP's manual are shown in Table 2.1.

3.4.2 Locally Flat Output Identification of RCP

Without the knowledge of equation (3.65), we assume the degree of freedom $n = 2$ is known and the RCP around its equilibrium point is controllable, that is, locally flat. Such equilibrium point can be reached at any static position of rotary arm and crane pendulum since all encoders have incremental data from the starting point of motion. For simplicity, the angular position of arm and swing angle of pendulum are denoted by θ and φ without extra notation indicating increment. The flat output y_{f_1} should be a function of θ and φ. Let us define y_{f_1} as

$$y_{f_1} = \theta + C_f\varphi, \tag{3.68}$$

where C_f is a constant. (3.68) is always available because any other flat output $\overline{y}_{f_1}$ of the form

$$\begin{aligned} \overline{y}_{f_1} &= \lambda_1\theta + \lambda_2\varphi \\ &= \lambda_1(\theta + \frac{\lambda_1}{\lambda_2}\varphi) \\ &= \lambda_1(\theta + C_f\varphi) \\ &= \lambda_1 y_{f_1} \end{aligned} \tag{3.69}$$

indicate y_{f_1} is also a flat output of the same system, where C_f is predetermined by the system dynamics in linear flat output, λ_1 and λ_2 are scalars. FOID algorithm is capable of finding C_f in proper range for RCP with measured input and output data. The best approximate coefficient of C_f in FOID is denoted by C_r^*.

To create input-output data, voltage V is designed as a random input sequence $u[k]$ that has Gaussian distribution that has zero mean and variance 5, and corresponding open-loop responses of $\theta(t)$ and $\varphi(t)$, as time sequences $\theta[k]$ and $\varphi[k]$, are measured. The RCP hence has random motion around the equilibrium. The transfer function between a $u(t)$ and a candidate function $y_l = \theta(t) + C_r\varphi(t)$ is estimated by H_1 method within frequency band from 0.5Hz to 25Hz, where C_r is incrementally selected from predetermined range $[-2, 0) \cup (0, 2]$. With 1 kHz sample rate and 60-second measurements, the FOID gives the optimal C_r, denoted by

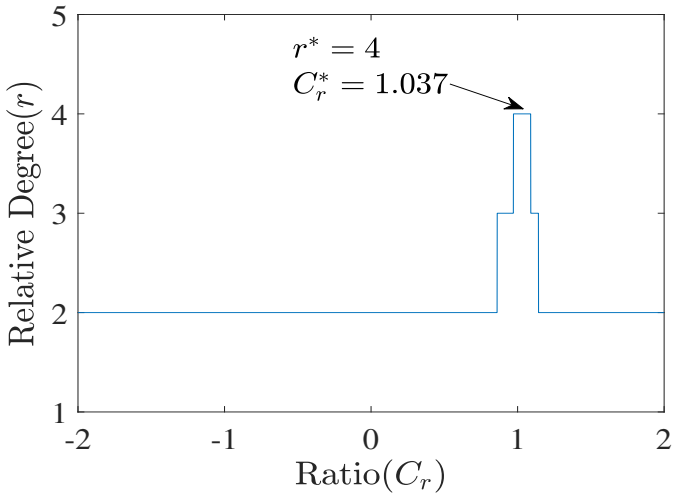

Figure 3.3: The relative degree of the candidate output y_l as a function of Cr for the rotary

C_r^*, that maximizes the relative degree of y_l as result shown in Figure 3.3 and 3.4. Several values of C_r are eligible for deriving flat output, however, only one optimal $C_r^* = 1.037$ is chosen based both on relative degree r and relative data usage that calculates relative ratio of data used in identification over other candidate functions will full relative degree. The optimal candidate, or identified flat output, with maximum relative degree r_{opt} is $2n = 4$ and highest relative data usage, is given by

$$y_l^* \equiv y_{f_1} = \theta(t) + 1.037\varphi(t). \tag{3.70}$$

The estimated transfer function for optimal candidate y_l^* is shown in Figure 3.5. The segmentation by FOID results in three segments of the estimated function: unused data and two subsets to be analyzed. The break point of curve is automatically found and the data points around the break points are considered distorted and will not be used in estimation of relative degree. The segment 1 takes up approximately 26% data out of total data within the chosen bandwidth of estimated transfer function, and segment 2 contains around 67% data points. The linear regression by feeding data from two segments gives the estimates of relative degree in which segment 2 does not generate a valid result because it almost leads to negative relative degree. The derivation of optimal relative degree $r_{opt} = 4$ is hence based on the segment 1.

Remark 3.4.1. *One can verify the result is in a good agreement of the theoretical flat output in Equation (3.65). It is also necessary to check if $y_{f_1} = \varphi$ is the flat output to complete the identification. More details about FOID can be found in [52].*

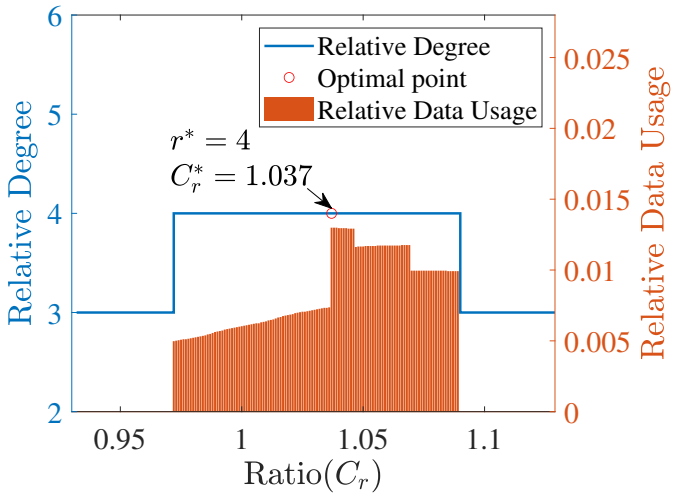

Figure 3.4: The relative degree of the candidate output y_l as a function of Cr for RCP around the origin. Zoomed view of Figure 3.3.

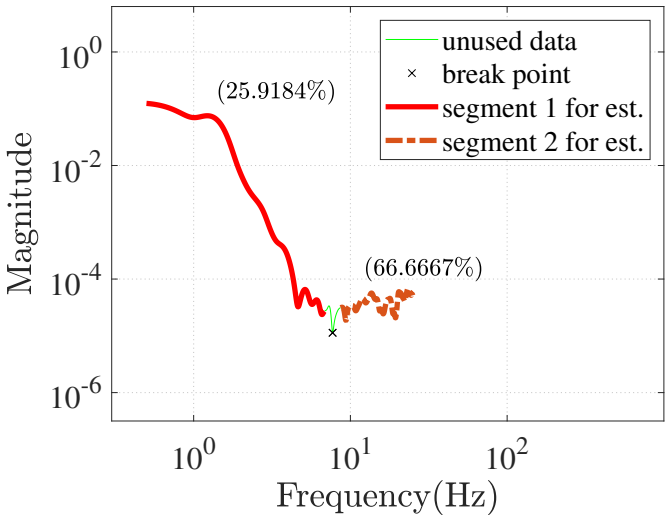

Figure 3.5: The estimated transfer function between input and optimal candidate output y_l^*, or flat output y_{f_1} when $C_r^* = 1.037$

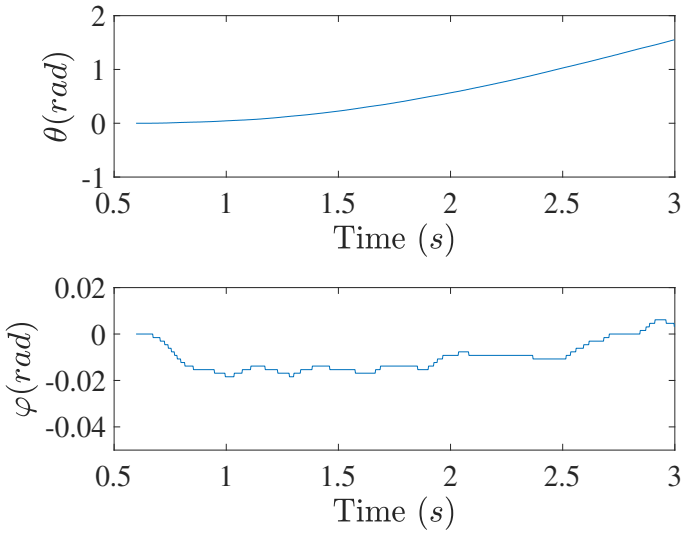

Figure 3.6: Open loop response collected for Sparse Identification of generalized coordinates

3.4.3 Sparse identification of states θ and φ

θ and φ are assumed to be two of the states in state-space model of RCP. Since flat output y_{f_1} is found, they can be expressed in terms of y_{f_1} and its even-order derivatives up to order 2 as

$$\theta = \chi_{11} y_{f_1} + \chi_{12} \ddot{y}_{f_1}, \tag{3.71}$$

$$\varphi = \chi_{21} y_{f_1} + \chi_{22} \ddot{y}_{f_1}. \tag{3.72}$$

Equation (3.71) leads to the following regression problem:

$$J_\lambda(\chi_1) = \sum_{t_k} \mathbf{e}_1^2(t_k) + \lambda \left\| \boldsymbol{\chi}_1 \right\|_1, \tag{3.73}$$

$$P_\theta(t_k) = \chi_{11} P_{11}(t_k) + \chi_{12} P_{12}(t_k), \tag{3.74}$$

$$\mathbf{e}_1(t_k) = \chi_{11} P_{11}(t_k) + \chi_{12} P_{12}(t_k) - P_\theta(t_k), k = 1, 2, \ldots, n_s. \tag{3.75}$$

where $J_\lambda(\chi_1)$ is the cost function that needs to be minimized, $\mathbf{e}_1$ is residual at time t_k, n_s is the number of elements in sequence, $P_\theta(t), P_{11}(t)$ and $P_{12}(t)$ are defined as equation (3.37) (3.38) (3.39). A sinusoidal input signal is set as input voltage $V = 0.1sin(0.25t)$. The sequence of $\theta[k]$ and $\varphi[k]$ used for sparse identification sparse regression is truncated within $0.6s$ and $3s$, shown in Figure 3.6. All other related settings from flat output identification remain the same . The best sparse regulator λ is automatically selected by cross-validation from 100 numbers within logarithmically spaced vector $[10^{-2}, 10^2]$. Figure 3.7 shows that least mean square

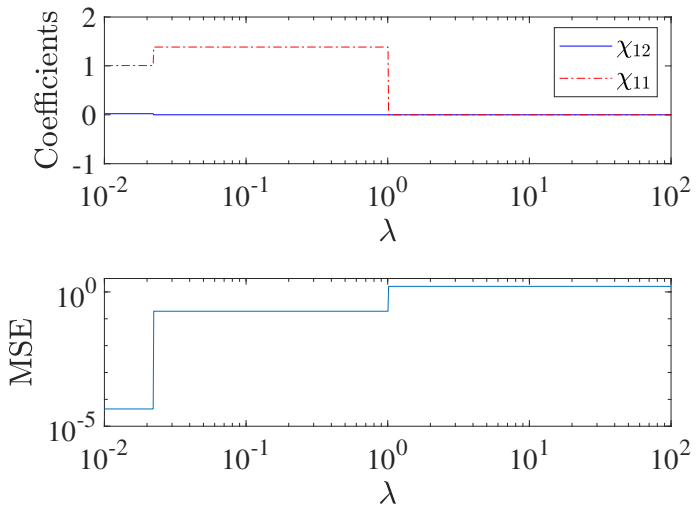

Figure 3.7: The estimated χ_{11}, χ_{12} from sparse identification and variation of corresponding MSE versus regression regulator λ

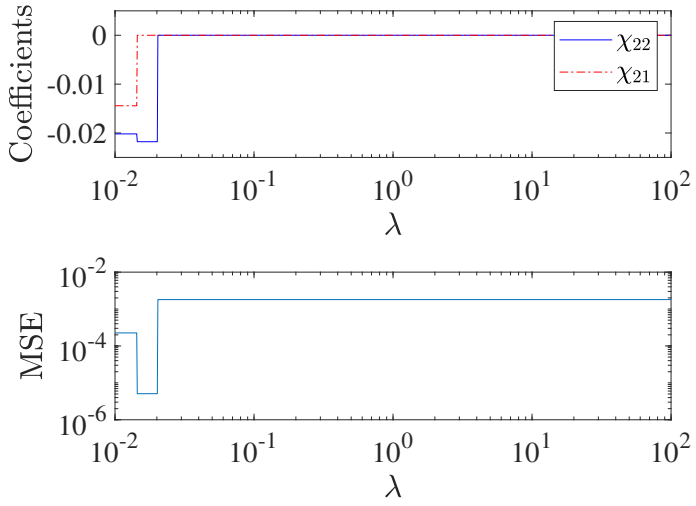

Figure 3.8: The estimated χ_{21}, χ_{22} from sparse identification and variation of corresponding MSE versus regression regulator λ

error (MSE) is attained when $\lambda = 0.00221$ or less, the best result of sparse regression for state θ is given by

$$\theta = 1.0077 y_{f_1} + 0.0223 \ddot{y}_{f_1}. \tag{3.76}$$

Applying same settings for φ, the result of sparse regression is shown in Figure 3.8. Equation (3.72) is identified as

$$\varphi = 0 \cdot y_{f_1} - 0.0219 \ddot{y}_{f_1}. \tag{3.77}$$

Note that the coefficient χ_{21} for y_{f_1} in equation (3.72) is 0 due to the effect of regularization term $\lambda \left\| \boldsymbol{\chi}_1 \right\|_1$. We are able to verify the result by simply adding (3.76) and (3.77) up with weight C_r^*, which gives

$$\theta + C_r^* \varphi = 1.0077 y_{f_1} - 0.0004 \ddot{y}_{f_1} \approx y_{f_1}. \tag{3.78}$$

The rest of the states, induced by generalized coordinates naturally, would be $\dot{\theta}$ and $\dot{\varphi}$, which are known as generalized velocities despite the lack of model information. Therefore the following identification for these two states is redundant. Instead, they can be given directly as

$$\dot{\theta} = 1.0077 \dot{y}_{f_1} + 0.0223 \, \dddot{y}_{f_1}. \tag{3.79}$$

$$\dot{\varphi} = 0 \cdot \dot{y}_{f_1} - 0.0219 \, \dddot{y}_{f_1}. \tag{3.80}$$

The even-order derivatives of y_{f_1}, solely $\ddot{y}_{f_1}$ in this case, can be estimated through generalized coordinates $q_1 = \theta$ and $q_2 = \varphi$ by weighting them properly

$$\ddot{y}_{f_1} = z_{21} q_1 + z_{22} q_2, \tag{3.81}$$

where clearly the solution is straightforward

$$z_{21} = 0, z_{22} = -\frac{1}{\chi_{21}} = -45.6621. \tag{3.82}$$

Therefore we conclude that $\ddot{y}_{f_1}$ is identified as

$$\ddot{y}_{f_1} = -45.6621 \varphi. \tag{3.83}$$

Remark 3.4.2. *The result of equation (3.76), (3.77) and (3.83) can be also verified approximately close to the ones derived from reduced model (3.65).*

Remark 3.4.3. *If there is nonzero coefficient associated with $\dot{y}_{f_1}$ in (3.77), $\ddot{y}_{f_1}$ can be found by solving a set of linear equations in the form of equation (3.46) and (3.47).*

3.4.4 Trajectory Planning for angular position θ and swing angle φ

We will show an example of rest-to-rest trajectory planning for RCP. The goal is maneuvering the rotary arm of RCP from one position to another in a time interval $[t_0, t_f]$ while forcing the swing angle of pendulum $\varphi(t)$ to be zero at time t_f and keeping it vertically downward thereafter. The starting and end position of the arm and the pendulum can be two equilibrium points of the systems. We assume the starting point is $(\theta(t_0), \varphi(t_0), \dot{\theta}(t_0), \dot{\varphi}(t_0)) = (0, 0, 0, 0)$ and ending point is $(\theta(t_f), \varphi(t_f), \dot{\theta}(t_f), \dot{\varphi}(t_f)) = (\Theta, 0, 0, 0)$, which is feasible with incremental encoders. The initial condition of $\theta(t), \varphi(t)$ and their first derivatives up to order 3 are all zeros, which forces the flat output y_{f_1} and its derivatives should satisfy

$$y_{f_1}(t_0) = \theta(t_0) + 1.037\varphi(t_0) = 0 \tag{3.84}$$

$$\dot{y}_{f_1}(t_0) = \ddot{y}_{f_1}(t_0) = \ddot{y}_{f_1}(t_0) = \dddot{y}_{f_1}(t_0) = 0 \tag{3.85}$$

Higher order derivatives of y_{f_1} can also be set 0 to smooth the trajectory at time $t = t_0$. Similarly, the final condition of y_{f_1} and its derivatives satisfies

$$y_{f_1}(t_f) = \theta(t_f) + 1.037\varphi(t_f) = \Theta \tag{3.86}$$

$$\dot{y}_{f_1}(t_f) = \ddot{y}_{f_1}(t_f) = \ddot{y}_{f_1}(t_f) = \dddot{y}_{f_1}(t_f) = 0 \tag{3.87}$$

The reference trajectory $y^*_{f_1}$ can be generated according to these conditions. From equation (3.76) , the actual trajectory of angular position θ will be affected by flat output y_{f_1} and its acceleration $\ddot{y}_{f_1}$ to different extents. One is able to modify the $y^*_{f_1}$ to have specific shape for intermediate motion between starting and end point but remain the initial and final conditions unchanged. The swing angle φ, based on equation (3.77), is always going to follow the acceleration $\ddot{y}_{f_1}$ weighted by a small number (-0.0219) from the beginning to the end. With this information, the motions for θ and φ are fully understandable and configurable even if the model is not elaborate. One practical example of $y^*_{f_1}$ is given when $t_0 = 2, t_f = 4$ and $\Theta = 1$ as

$$y^*_{f_1} = \begin{cases} 0, & 0 < t < 2 \\ -\frac{5}{32}(t-2)^7 + \frac{35}{32}(t-2)^6 - \frac{21}{8}(t-2)^5 + \frac{35}{16}(t-2)^4, & 2 \leqslant t \leqslant 4 \\ 1, & t > 4 \end{cases} . \tag{3.88}$$

3.4.5 LESO/Luenberger observer Design

The tracking error for control is defined as $e(t) = y_{f_1}(t) - y^*_{f_1}(t)$. The error dynamics in terms of equation (3.48) is then

$$e^{(4)} = \zeta_1(t) + b_0 u(t), \tag{3.89}$$

which can be divided into two subsystems:

$$\dot{e}_0 = e_1, \tag{3.90}$$
$$\dot{e}_1 = e_2, \tag{3.91}$$
$$e_2 = \ddot{e} = \ddot{y}_{f_1} - \ddot{y}^*_{f_1}, \tag{3.92}$$

and

$$\dot{e}_2 = e_3, \tag{3.93}$$
$$\dot{e}_3 = \zeta_1(t) + b_0 u(t). \tag{3.94}$$

The second derivative of tracking error, e_2, is directly accessible from $\ddot{y}_{f_1}$ and $\ddot{y}^*_{f_1}$. Therefore a low-order Leunberger observer and an LESO can be designed as,

$$\dot{z}_0 = z_1 - \beta_0(z_0 - e_0), \tag{3.95}$$
$$\dot{z}_1 = z_2 - \beta_1(z_0 - e_0) \tag{3.96}$$

$$\dot{z}_2 = z_3 - \beta_2(z_2 - e_2), \tag{3.97}$$
$$\dot{z}_3 = z_4 + b_0 u(t) - \beta_3(z_2 - e_2), \tag{3.98}$$
$$\dot{z}_4 = -\beta_4(z_2 - e_2), \tag{3.99}$$

where $\beta_0 = 2\omega_{lo}$ and $\beta_1 = \omega_{lo}^2$ can be chosen based on design one parameter ω_{lo}, the bandwidth of this Leunberger observer. The gains β_2, β_3 and β_4 are also tunable through the bandwidth method, and are conveniently given as $\beta_2 = 3\omega_{eso}, \beta_2 = 3\omega_{eso}^2$ and $\beta_3 = \omega_{eso}^3$. Assuming b_0 is known here, the feedback control law is hence given by,

$$u(t) = \frac{1}{b_0}(-\widetilde{\zeta_1}(t) - \alpha_1 z_3 - \alpha_2 z_2 - a_3 z_1 - \alpha_4 z_0), \tag{3.100}$$

3.4.6 Demonstration Experiment

We demonstrate an experiment on RCP to prove the feasibility and effectiveness of above data-driven design of flatness-based ADRC. The bandwidths of Leunberger observer and LESO are chosen with the same value ω_o and are open to multiple choices for performance comparison. The approximate range of the value of nominal control input variable b_0 is determined from result of several tests in which b_0 is first set as a large number and decreased until the controller reacts effectively. The sign of b_0 can be determined by inspecting the open-loop response

of RCP and analyze the relationship of variation between input $u(t)$, the voltage, and fourth-order derivative of y_{f_1}. A square wave signal is added to input voltage during the experiments to see its robustness in the presence of unknown external disturbances. We also implement the same experiments after tying a block of mass to the body of rotary arm and tip of rotary pendulum to test the robustness of control to variations of system parameters. The linear feedback control gains are $\alpha_1 = 60, \alpha_2 = 1350, a_3 = 13500, \alpha_4 = 50625$.

Figure 3.9, 3.10 and 3.11 show the responses of flat output, angular position of arm θ and swing angle φ when b_0 is fixed as 2000 and bandwidth ω has three different values. A short square wave is inserted at $t = 11$s and canceled at $t = 12$s with amplitude of 3 and frequency of 1 rad/s as shown in Figure 3.12. The flat output tracks the planned trajectory as desired at two equilibria. θ and φ accordingly overall satisfy the prescribed initial value and final value with small tracking error before the square wave is applied. The error is mainly caused by the damping existing in the bearing of pendulum so that the steady-state error of swing angle φ is not always eliminated but randomly distributed around origin in each experiment. The responses also show that relatively higher bandwidth ω results in better tracking performance during the transition between $t = 2s$ and $t = 4s$ and reduce the deviation of amplitude from reference when external disturbances applied to the control signal. The tracking error remains small after the disturbing voltage is cancelled, which manifests a good robustness with regards to disturbances from input channel.

Figure 3.13, 3.15 and 3.15 presents the responses of flat output, angular position of arm θ and swing angle φ when bandwidth of observer ω is fixed and nominal control input gain b_0 changes. It can be found that the steady-state error has a little bit increased if b_0 changes from $b_0 = 2000$ to 1500 and 2500 when LESOs have the same capability to estimate the error signals and their derivatives. It shows $b_0 = 2000$ may be closer to the real control input, which is unknown without explicit modelling of RCP, than $b_0 = 1500$ and $b_0 = 2500$. The large mismatched nominal gain may also increases the overshooting of tracking as one can observe in Figure 3.13. Although the nominal input gain b_0 might not chosen perfectly, we can still see its strong robustness against external disturbing signal.

The estimate of total disturbance by designed LESO is given in Figure 3.16 where the result is obtained when $b_0 = 1500$ and $\omega = 50$ rad/s. The total input voltage to RCP is also shown in Figure 3.17.

Responses in Figure 3.18, 3.19, 3.20 and 3.21 further prove the good robustness of proposed control to parametric variations. In these experiments, the mass or moment of inertia of both rotary arm and pendulum are subject to large variations, whereas the performance of proposed controller are still as good as the one before block of mass is placed.

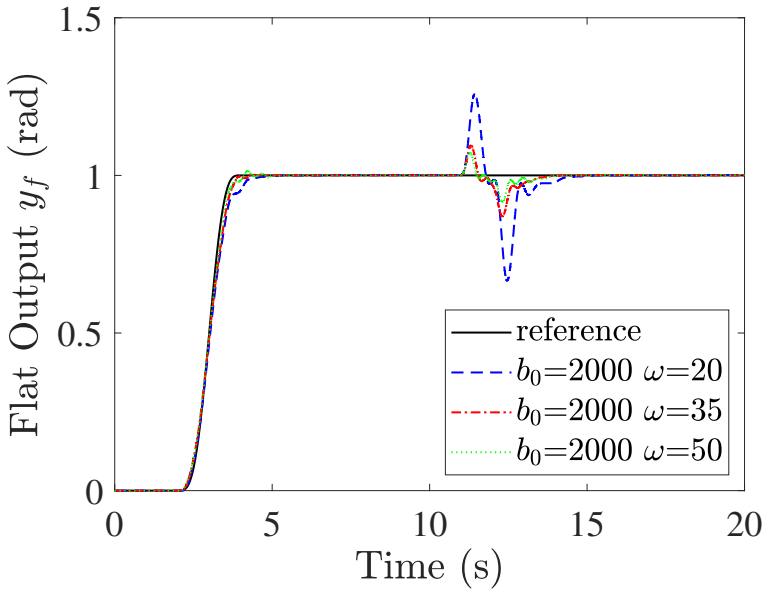

Figure 3.9: Response of flat output y_f in experiments when $b_0 = 2000, \omega = 20, 35$ and 50 rad/s

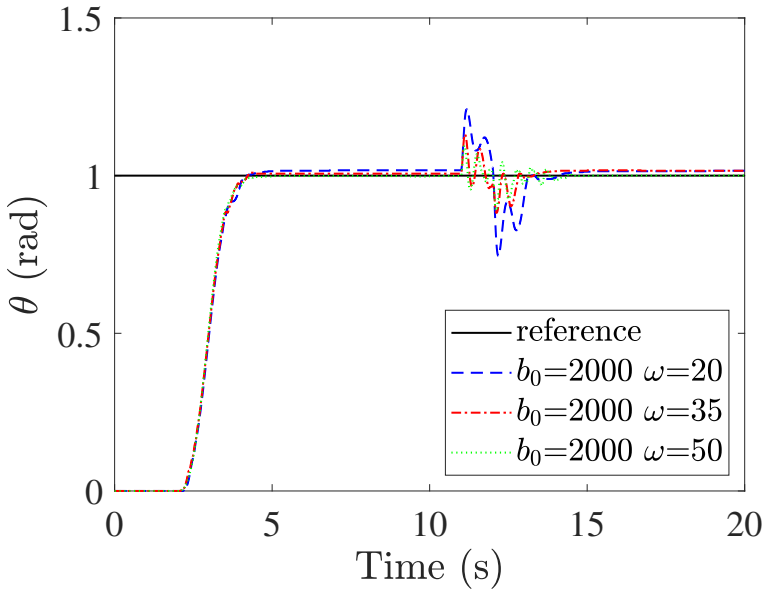

Figure 3.10: The angular position of rotary arm θ in experiments when $b_0 = 2000$ and $\omega = 20, 35$ and 40 rad/s

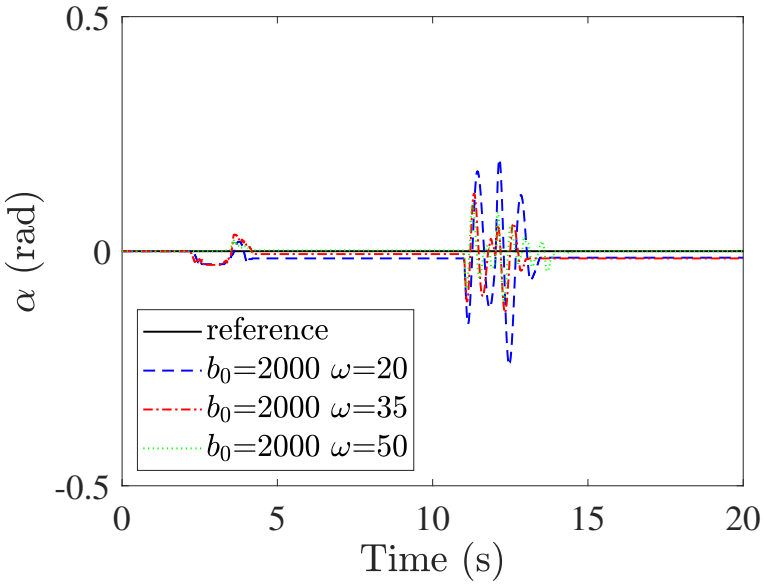

Figure 3.11: The swing angle of pendulum φ in experiments when $b_0 = 2000$ and $\omega = 20, 35$ and 40 rad/s

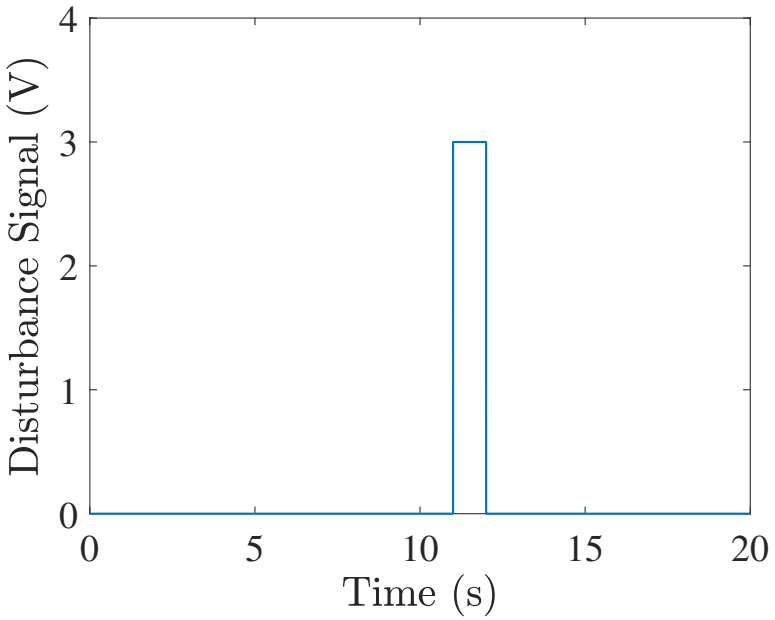

Figure 3.12: Disturbance voltage added between $11s$ and $12s$

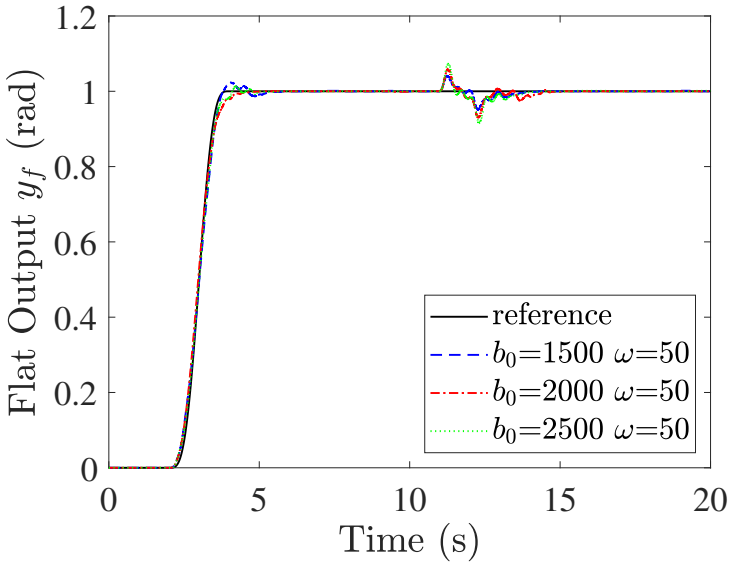

Figure 3.13: Response of flat output y_f in experiments when $\omega = 50, b_0 = 1500, 2000$ and 2500.

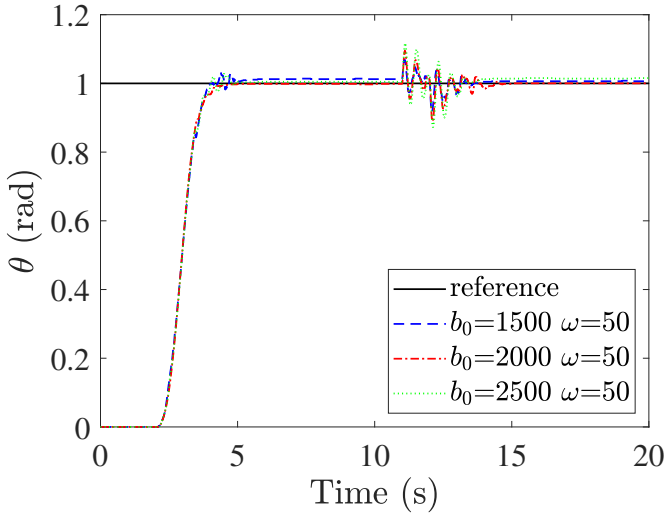

Figure 3.14: The angular position of rotary arm θ in experiments when $\omega = 50$ rad/s and $b_0 = 1500, 2000$ and 2500

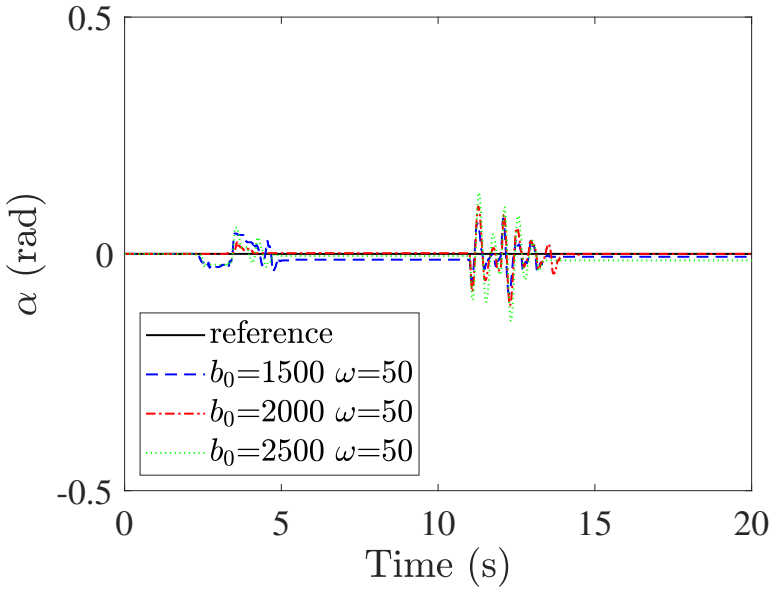

Figure 3.15: The swing angle of pendulum φ in experiments when $\omega = 50$ rad/s and $b_0 = 1500, 2000$ and 2500

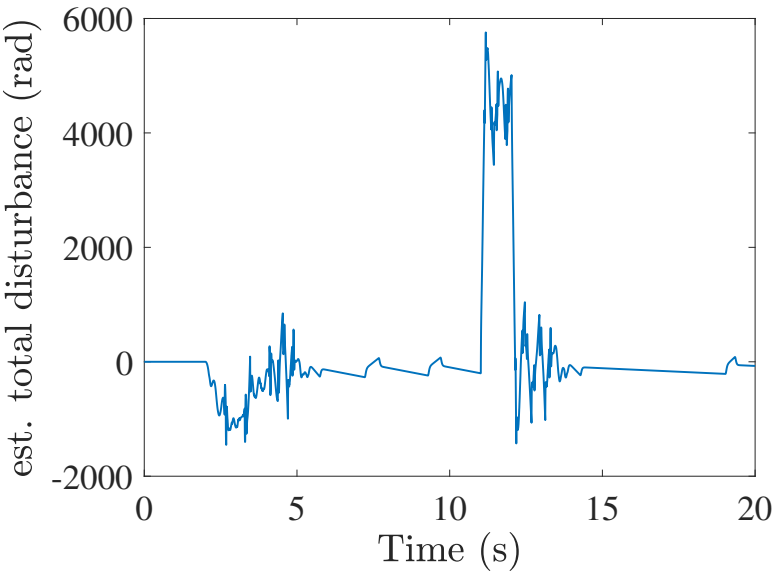

Figure 3.16: Estimated total disturbance from LESO when $b_0 = 1500$ and $\omega = 50$ rad/s.

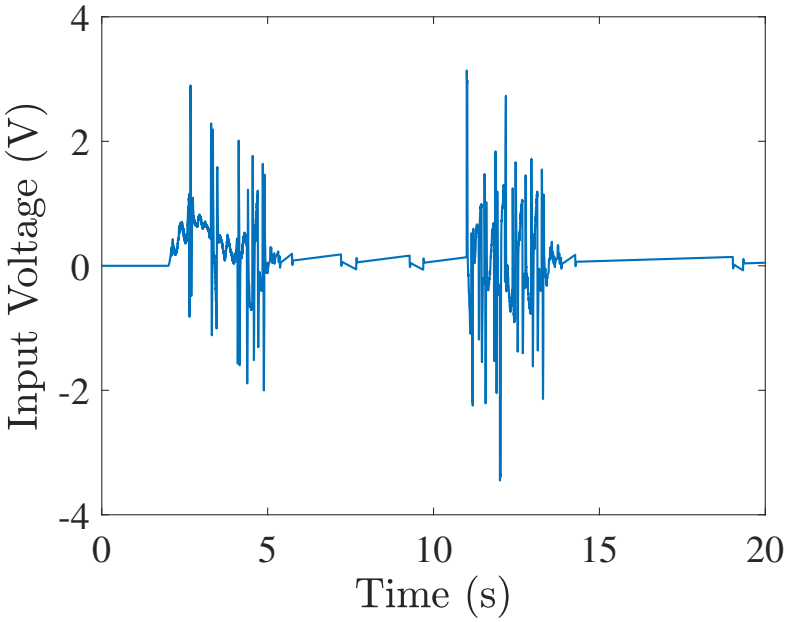

Figure 3.17: The input voltage to RCP when $b_0 = 1500$ and $\omega = 50$ rad/s.

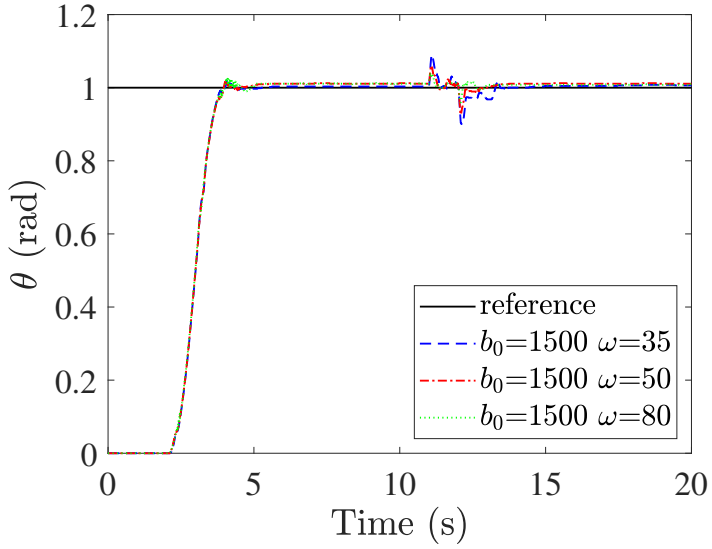

Figure 3.18: The angular position of rotary arm θ with 200g block of mass tying to end of the pendulum in experiments

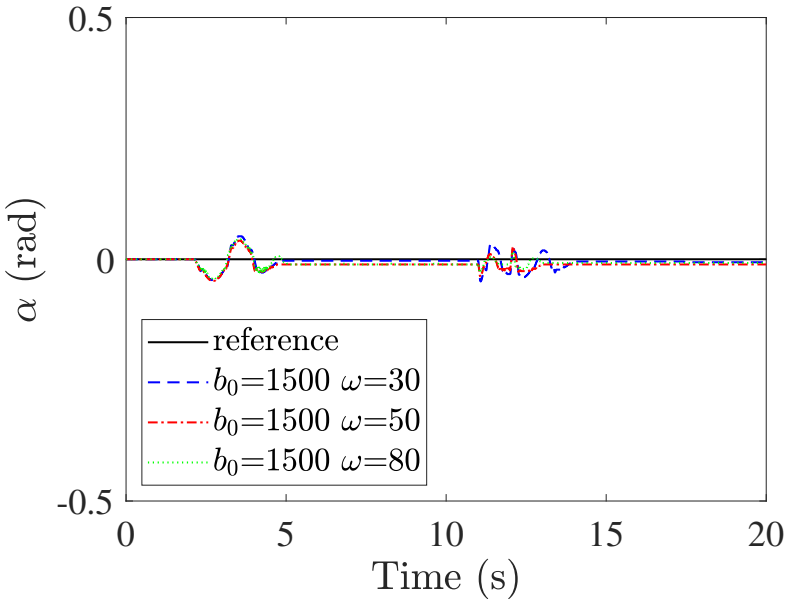

Figure 3.19: The swing angle of pendulum φ with 200g block of mass tying to end of the pendulum in experiments

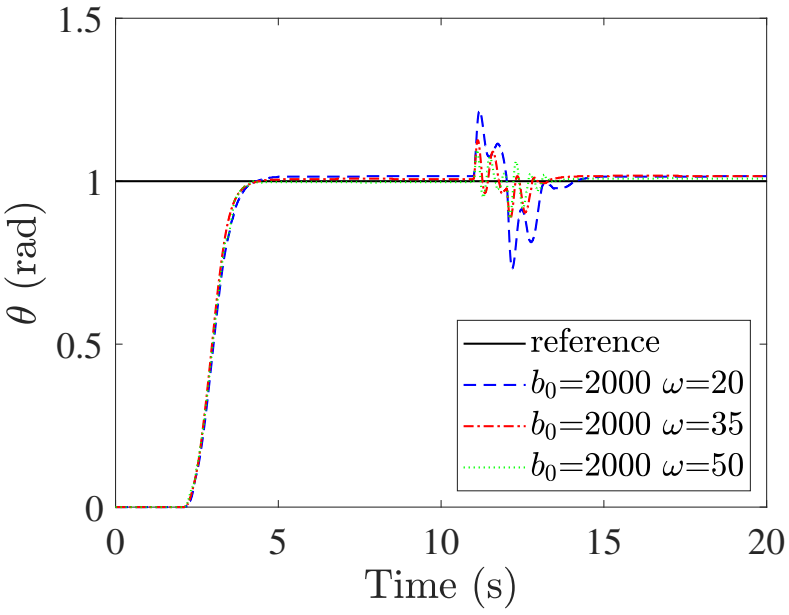

Figure 3.20: The angular position of rotary arm θ with 200g block of mass tying to body of rotary arm in experiments.

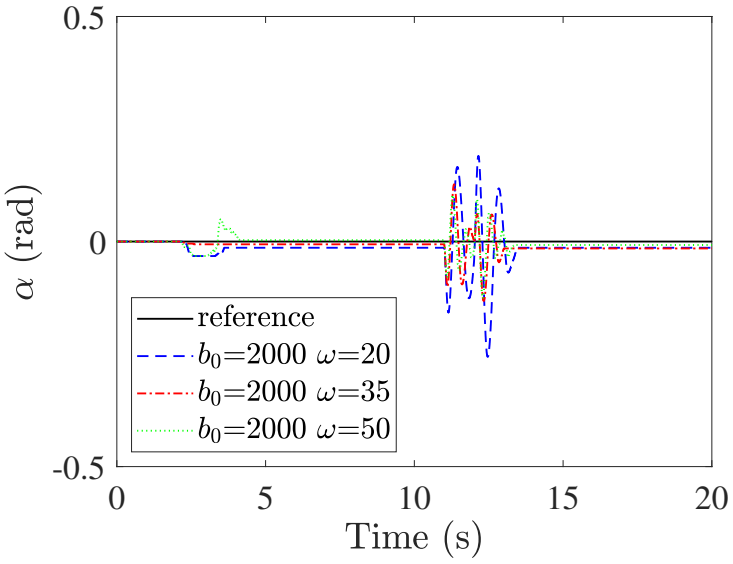

Figure 3.21: The swing angle of pendulum φ with 200g block of mass tying to body of rotary arm in experiments.

3.5 Conclusions

The advantages of flatness-based control and ADRC are attractive in designing control for UMS. While most of the research has been fully relying on the mathematical model of the system, we are interested in exploring the possibilities of doing the same work with less or without details of the models. In this chapter, a framework of designing robust tracking control for SIMO UMS is proposed based on flat output identification, sparse regression with algebraic method, and flatness-based ADRC without knowing details of its mathematical model. The locally flat output are identified and computed by applying FOID algorithm to input-output data sequence of UMS. It shows the locally flat output can convert the nominal model of UMS to a equation of input-output relation between control signal and flat output, which is naturally the system of interest in the realm of ADRC. The trajectory planning is convenient to be carried out with the aid of flat output and its relationship between system states, thanks to sparse regression and algebraic method. Ideas of reduced nominal model, error space and simple construction of high-order derivatives of flat output through measurable outputs are adopted to avoid directly using high-order ESO and make data-driven flatness-based ADRC feasible. The experiment of rotary crane pendulum strongly supports the effectiveness and robustness of provided control design.

Chapter 4

IDENTIFICATION OF LINEAR DIFFERENTIALLY FLAT OUTPUT OF A CLASS OF MIMO UNDERACTUATED MECHANICAL SYSTEMS

In this chapter, we introduce a data-driven algorithm that automatically identifies the locally flat output of a class of nonlinear MIMO underactuated mechanical systems (UMS) from input-output measurements to address these issues. Without the aid of a precise model, the concentration on local flatness not only simplifies the composition of flat outputs such that the simple mathematical relations between states, inputs and flat outputs can be obtained, but also allows non-flat nonlinear systems to have approximate flatness around their equilibria and potentially extend the use of flatness-based control to larger range of applications. We extend the FOID algorithm proposed in Chapterr 2 which focuses on the identification of locally flat outputs of single-input nonlinear UMSs and develop an modified version of FOID to find locally flat outputs for a class of multiple-input nonlinear UMSs.

The rest of the chapter is organized as follows. In Section 4.1, we introduce the MIMO nonlinear UMS of interest in this chapter and the mathematical concepts of the flatness and flat outputs. In Section 4.2, the flat output of specific form for linear reduced model is discussed. In Section 4.3, a statement of the problem is given. Section 4.4 is devoted to the proposal of modified algorithm of FOID that identifies locally flat outputs for MIMO nonlinear UMSs. In Section 4.5 two numerical examples are presented to validate the feasibility and efficiency of the modified algorithm. The chapter is concluded in Section 4.6.

4.1 Mathematical Preliminaries

4.1.1 Model of MIMO Nonlinear UMS

Given that the cases in which general MIMO nonlinear systems involve are mostly complicated to discuss, for sake of simplicity, the system of interest in the rest of chapter is proposed as a class of nonlinear UMSs with degrees of freedom $n = 3$ and two independent input channels. Applying Lagrange's equations to these UMSs typically gives the equation of motion as [39],

$$\mathbf{m}_{11}(\mathbf{q})\ddot{\mathbf{q}}_a + \mathbf{m}_{12}(\mathbf{q})\ddot{q}_u + \mathbf{h}_1(\mathbf{q}, \dot{\mathbf{q}}) = \mathbf{g}(\mathbf{q})\tau \tag{4.1}$$

$$\mathbf{m}_{21}(\mathbf{q})\ddot{\mathbf{q}}_a + m_{22}(\mathbf{q})\ddot{q}_u + h_2(\mathbf{q}, \dot{\mathbf{q}}) = 0, \tag{4.2}$$

where $\mathbf{q}_a \in \mathbb{R}^{2\times 1}$ and $q_u \in \mathbb{R}$ are the generalized coordinates $\mathbf{q} = [\mathbf{q}_a^{\mathrm{T}}, q_u]^{\mathrm{T}} \in \mathbb{R}^{3\times 1}$, the vector function $\mathbf{h}_1(\mathbf{q}, \dot{\mathbf{q}}) \in \mathbb{R}^{2\times 1}$ and scalar function $h_2(\mathbf{q}, \dot{\mathbf{q}}) \in \mathbb{R}$ contain Coriolis, centrifugal terms and the terms derived from potential energy, $\tau \in \mathbb{R}^{2\times 1}$ is the vector of generalized forces applied to the system, and $\mathbf{g}(\mathbf{q})$ is assumed to be a 2×2 invertible square matrix for all $\mathbf{q}$ in the configuration space. The terms $\mathbf{m}_{11} \in \mathbb{R}^{2\times 2}$, $\mathbf{m}_{21} \in \mathbb{R}^{1\times 2}$, $\mathbf{m}_{12} \in \mathbb{R}^{2\times 1}$ and $m_{22} \in \mathbb{R}$ form the mass matrix $\mathbf{M}(\mathbf{q})$ of the system, given by

$$\mathbf{M}(\mathbf{q}) = \begin{bmatrix} \mathbf{m}_{11} & \mathbf{m}_{12} \\ \mathbf{m}_{21} & m_{22} \end{bmatrix}_{n\times n}. \tag{4.3}$$

The systems are supposed to have three independent outputs in terms of the generalized coordinates $\mathbf{q}$,

$$\mathbf{y} = \mathbf{I}_{3\times 3}\mathbf{q}, \tag{4.4}$$

where $\mathbf{y} \in \mathbb{R}^{3\times 1}$ is the output vector and $\mathbf{I}$ is identity matrix. Equations (4.1) and (4.2) can also be rewritten in the state-space form. Let $\mathbf{x} = [\mathbf{q}_a^T, q_u, \dot{\mathbf{q}}_a^T, \dot{q}_u]^T \equiv [x_1, x_2, \cdots, x_6]^T$ be the state vector, and $\mathbf{u} = [u_1, u_2]^T \equiv \tau$. The state equations are given by,

$$\dot{\mathbf{x}} = \mathbf{F}(\mathbf{x}) + \mathbf{G}(\mathbf{x})\mathbf{u} \tag{4.5}$$

$$\mathbf{y} = \mathbf{I}_{3\times 3}[x_1, x_2, x_3]^T \tag{4.6}$$

or in the scalar form,

$$\begin{aligned} &\dot{x}_1 = x_4,\ \dot{x}_2 = x_5,\ \dot{x}_3 = x_6, \\ &\dot{x}_4 = f_1(\mathbf{x}) + g_{11}(\mathbf{x})u_1 + g_{12}(\mathbf{x})u_2, \\ &\dot{x}_5 = f_2(\mathbf{x}) + g_{21}(\mathbf{x})u_1 + g_{22}(\mathbf{x})u_2, \\ &\dot{x}_6 = f_3(\mathbf{x}) + g_{31}(\mathbf{x})u_1 + g_{32}(\mathbf{x})u_2, \\ &y_1 = x_1, y_2 = x_2, y_3 = x_3, \end{aligned} \tag{4.7}$$

where $\mathbf{F}(\mathbf{x}) \in \mathbb{R}^{6\times 1}$ and $\mathbf{G}(\mathbf{x}) \in \mathbb{R}^{6\times 2}$ are smooth vector fields defined through Equations (4.1) and (4.2). f_i, g_{i1} and g_{i2}, $i = 1, 2, 3$, are the components of $\mathbf{F}(\mathbf{x})$ and $\mathbf{G}(\mathbf{x})$. $\mathbf{G}(\mathbf{x})$ is assumed to have full rank, i.e., 2, for all $\mathbf{x}$, and $g_{i1}(\mathbf{x})$ and $g_{i2}(\mathbf{x})$ are nonzero for $i = 1, 2, 3$. Since the rank of $\mathbf{G}(\mathbf{x})$ equal to 2 is less than the number of degrees of freedom $n = 3$, the two independent inputs u_1 and u_2 cannot fully actuate the system along arbitrary directions in its configuration space, which normally makes the stabilization and tracking problem of the system intractable.

4.1.2 Flat Output for MIMO system

If there exists, a flat output of a MIMO nonlinear system with state vector $\mathbf{x} \in \mathbb{R}^{2n\times 1}$ and 2 independent inputs $\mathbf{u} = [u_1, u_2]^T$, it must be composed of two distinct components y_{f_1} and y_{f_2}. Thus it can be shown that there exists endogenous dynamic

feedback that makes the closed-loop system equivalent to the linear controllable system in the canonical form as

$$\begin{aligned} y_{f_1}^{(r_1+1)} &= v_1, \\ y_{f_2}^{(r_2+1)} &= v_2, \end{aligned} \tag{4.8}$$

where v_1 and v_2 are the new controls to be designed, r_1 and r_2 are integers such that $r_1 + r_2 \geq 2n$. $\mathbf{x}$ and $\mathbf{u}$ can be expressed as [41]

$$\mathbf{x} = \phi_1(y_{f_1}, \ldots, y_{f_1}^{(r_1)}, y_{f_2}, \ldots, y_{f_2}^{(r_2)}) \tag{4.9}$$

$$\mathbf{u} = \phi_0(y_{f_1}, \ldots, y_{f_1}^{(r_1+1)}, y_{f_2}, \ldots, y_{f_2}^{(r_2+1)}) \tag{4.10}$$

Equation (4.8) is an input-to-flat output description of the original system without any internal dynamics, which allows one to design new controls to directly shape the trajectories of flat outputs and hence achieve the prescribed trajectories of the state $\mathbf{x}$ in tracking control as Equations (4.9) and (4.10) suggest.

Although flat systems have good properties for simplifying tracking control design, a lot of nonlinear UMSs are not considered flat as they are not fully feedback linearizable. In other words, it is impossible to transform them into equivalent linear controllable systems through a feedback control law regardless of static or dynamic one. To extend the application of flatness on various systems, the flatness can be viewed as a local property of a nonlinear system around certain equilibrium in the state space. A well-known theorem [32] about flatness states that a nonlinear system is locally flat around an equilibrium point if the tangent linearized system around that point is controllable. The linearized controllable system therefore takes the advantage of flatness around its equilibrium point, and it is usually easier to find flat outputs, though not all of them, for linear systems than for general nonlinear ones. It can be transformed into controllable canonical form with the same inputs via a static state feedback. In addition, these locally defined flat outputs can be linear functions of states of the linearized system, which defines a diffeomorphism transformation and preserves the dimension of the original linearized system. This is usually not true for a nonlinear system whose flat outputs have nonlinear relations with the original system states.

4.1.3 Flatness and Flat Output of MIMO Linear System

Linear controllable systems are always flat. It requires relatively less effort to find flat outputs of linear systems as linear functions of states than that for nonlinear systems. We can show that finding a transformation matrix $\mathbf{T}$ that converts the original system to a controllable canonical form leads to the problem of finding the flat output for linear controllable systems.

Consider the transformed new state in the controllable canonical form is $\mathbf{z}$ and the original linear state vector satisfies $\mathbf{x} = \mathbf{T}^{-1}\mathbf{z}$. For $2n$-dimension single-input-single output linear system with controllable pair $(\mathbf{A}, \mathbf{b})$, the controllability matrix $\mathbf{C}_s = [\mathbf{b}, \mathbf{Ab}, \cdots, \mathbf{A}^{2n-1}\mathbf{b}]$ can be uniquely determined, and thus the flat output can be derived as the first state variable of transformed vector $\mathbf{z}$ given by

$$y_f = \mathbf{t}_1\mathbf{z} = [0, 0, \cdots, 1]\mathbf{C}_s^{-1}\mathbf{z}. \tag{4.11}$$

The transformation matrix $\mathbf{T}$ is then defined as $\mathbf{T} = [\mathbf{t}_1, \mathbf{t}_1\mathbf{A}, \cdots, \mathbf{t}_1\mathbf{A}^{2n-1}]^T$. The flat output y_f here is a linear combination of the state variables in $\mathbf{x}$ despite that some flat output with nonlinear relations may exist. One can immediately verify that all variables in $\mathbf{x}$ can be expressed by y_f and its finite number of time derivatives. Indeed, $\mathbf{x}$ is a linear function of the variables in new vector $\mathbf{z} = [y_f, \dot{y}_f, \cdots, y_f^{2n-1}]^T$ where the function relation is determined by $\mathbf{T}$. Note that y_f is not the unique linear flat output of the system since any variable $\bar{y} = ay_f$, where $a \in [-\infty, 0) \cup (0, \infty]$, can also be verified as flat output.

For MIMO controllable systems, the controllability matrix of $2n$-dimension MIMO system with m inputs $\mathbf{C}_m = [\mathbf{B}, \mathbf{AB}, \cdots, \mathbf{A}^{2n-1}\mathbf{B}]$ has $2n \times m$ columns, and there are many choices to pick out $2n$ linearly independent columns from $\mathbf{C}_m$ to form the transformation matrix $\mathbf{T}$. The Luenberger second controllable canonical form requires a special order for selecting $2n$ linearly independent columns which constitute a matrix $\mathbf{P}$ given by

$$\mathbf{P} = [\mathbf{b}_1, \mathbf{Ab}_1, \cdots, \mathbf{A}^{n_1-1}\mathbf{b}_1, \mathbf{b}_2, \mathbf{Ab}_2, \cdots, \mathbf{A}^{n_2-1}\mathbf{b}_1, \mathbf{b}_3, \cdots, \mathbf{A}^{n_m-1}\mathbf{b}_m]_{2n\times 2n}, \tag{4.12}$$

where $\{n_1, n_2, \ldots, n_m\}$ is the set of controllability indices and $\sum_{i=1}^{m} n_i = 2n$. The transformation matrix $\mathbf{T}$ can be further derived from $\mathbf{P}$. The resulting transformed system is given by

$$\begin{aligned}
z_1^{(n_1)} &= \bar{f}_1(\mathbf{z}) + u_1 + \bar{b}_{12}u_2 + \ldots + \bar{b}_{1m}u_m, \\
z_2^{(n_2)} &= \bar{f}_2(\mathbf{z}) + u_2 + \bar{b}_{23}u_3 + \ldots + \bar{b}_{2m}u_m, \\
z_3^{(n_3)} &= \bar{f}_3(\mathbf{z}) + u_3 + \bar{b}_{34}u_4 \ldots + \bar{b}_{3m}u_m, \\
&\vdots \\
z_m^{(n_m)} &= \bar{f}_m(\mathbf{z}) + u_m,
\end{aligned} \tag{4.13}$$

where z_1 is the first state of $\mathbf{z}$, $z_i, i = 2, 3, \cdots, m$, is the $(1 + n_1 + n_2 + \cdots n_{i-1})^{th}$ state of $\mathbf{z}$, $\bar{f}_j(\mathbf{z})$, $j = 1, 2, \cdots, m$, is a linear function of $\mathbf{z}$, and $\bar{b}_{kl}$ with proper subscript is a scalar coefficient for u_l. Since $\sum_{i=1}^{m} n_i = 2n$, the new state vector $\mathbf{z}$ consists of $z_i, i = 1, 2, \ldots, m$, and their finite number of time derivatives, the orders of which is determined by n_i. Therefore, it is straightforward to show that all the original states in $\mathbf{x}$ can be expressed by linear functions of states in $\mathbf{z}$, which indicates

$\mathbf{y}_f = [z_1, z_2, \dots z_m]^T$ is a (linear) flat output of MIMO system. Accordingly, we can calculate $\mathbf{y}_f$ from $\mathbf{z} = \mathbf{T}\mathbf{x}$, and component z_i is also a linear function of all the states in $\mathbf{x}$. The controllable canonical form derived in Equation (4.13) is extremely powerful in feedback control design as it allows to decouple the control design for each output z_i. It can be shown that the Brunosky canonical form can be obtained based on the controllable canonical form.

4.1.4 Flatness-based Active Disturbance Rejection Control

The input-output model, as a result of parameterization of input in terms of states, naturally lends itself to the paradigm of ADRC design. Active disturbance rejection control, or shortly ADRC, is an observer-based control approach that estimates unknown total disturbances online, including endogenous system dynamics and exogenous disturbances, and cancels them by feedforward compensation. ADRC treats all its variations due to parametric uncertainties and unmodeled dynamics as endogenous perturbation, and interprets any external disturbance to the system, regardless of its type and origin, as exogenous perturbation. The basic idea of disturbance rejection is to estimates both types of perturbations together on-line, called the total disturbance, and compensate them by the feedforward control. After the compensation, a variety of linear and nonlinear control schemes can be applied to the resulting trivial system of pure integrators. When $b(\mathbf{y}_{f_1})$ is not known exactly in advance, a common technique is to incorporate the state-dependent part of $b(\mathbf{y}_{f_1})$ into the total disturbance and retains a constant b_0 or known function of $\mathbf{y}_{f_1}$ as a nominal input gain. The input-output model in ADRC is therefore rewritten as

$$y_{f_1}^{(2n)} = \xi(t) + b_0 u, \tag{4.14}$$

where $\xi(t)$ is a time-varying term representing the total disturbance. The control law is in the following form

$$u = \frac{1}{b_0}(-\widetilde{\xi}(t) + v) \tag{4.15}$$

where $\widetilde{\xi}(t)$ is an estimate of $\xi(t)$ and v is the control designed for the trivial integral system $y_{f_1}^{(2n)} = v$. Consequently, the influence of unknown disturbances could be suppressed adaptively, and the robustness of the closed-loop system with respect to disturbances is significantly improved. The performance of ADRC is highly relied on accurate on-line estimation of the flat output vector $\mathbf{y}_{f_1}$ and the total disturbance, which requires an effective algorithm for state and disturbance estimation with low latency. The core component undertaking this task in ADRC is the extended state observer (ESO). The ESO with nonlinear gain functions are called the nonlinear ESO (NLESO) and can produce better transient behavior and faster convergence than the linear ESO (LESO), which is a special class of ESO with linear gain functions. However, the LESO has shown its advantages of simple tuning process and

clear physical interpretation in applications, whereas the design of gain functions and tuning parameters in NLESO are overall more difficult and may vary from one specific system to another. It should be pointed out that the performance of estimation generally deteriorates when n becomes large because the noise and the phase lag of signals will be amplified

4.2 Flat Output of Linear Reduced Model

Although many nonlinear UMSs are not inherently flat, their tangent linearization around certain equilibrium can be flat. Let $p = (\mathbf{x}_e, \mathbf{u}_e)$ denote an operation point or equilibrium of MIMO UMS (4.5). The tangent linearization around p is given by

$$\dot{\mathbf{x}}_\delta = \mathbf{A}\mathbf{x}_\delta + \mathbf{B}\mathbf{u}_\delta, \tag{4.16}$$

where $\mathbf{x}_\delta = \mathbf{x} - \mathbf{x}_e$, $\mathbf{u}_\delta = \mathbf{u} - \mathbf{u}_e$, $\mathbf{A}$ is a 6×6 system matrix and $\mathbf{B}$ is a 6×2 control influence matrix. The linearized system (4.16) is flat if pair ($\mathbf{A}$,$\mathbf{B}$) is controllable, which is an assumption that generally holds when the terms from potential energy, such as gravitational and elastic forces, are included in Equations (4.1) and (4.2). From the previous discussion, the linear flat output for system (4.16) exists and can be calculated by finding the transformation matrix $\mathbf{T}$ such that the system is in the form of Equation (4.13). It is worth noting that the derivation of vector $\mathbf{z}$ may need information of the full state vector $\mathbf{x}$, which is a strong condition that is occasionally not satisfied in practice. The linear flat output shown in Equation (4.13) may not be physically realizable if some states are not accessible. It is always desirable to have fewer number of states involved in the construction of vector $\mathbf{z}$, the flat output vector, and hence include the full dynamics of the original system within the components of flat output. Actually, the linearized system (4.16) can be further simplified by neglecting the terms related to the generalized velocities $\dot{\mathbf{q}}$ because they mostly affect the Coriolis forces, centrifugal forces and viscous damping which usually have minor contribution to system dynamics when the system is operated within a small range, to satisfy linear assumption in action. Consider the reduced model of system (4.16) given by

$$\dot{\mathbf{x}} = \mathbf{A}_r\mathbf{x} + \mathbf{B}\mathbf{u}, \tag{4.17}$$

where we redefine $\mathbf{x} = [x_1, x_2, \cdots, x_6]^T \equiv \mathbf{x}_\delta$ for simplicity,

$$\mathbf{A}_r = \begin{bmatrix} 0 & 0 & 0 & 1 & 0 & 0 \\ 0 & 0 & 0 & 0 & 1 & 0 \\ 0 & 0 & 0 & 0 & 0 & 1 \\ a_{11} & a_{12} & a_{13} & 0 & 0 & 0 \\ a_{21} & a_{22} & a_{23} & 0 & 0 & 0 \\ a_{31} & a_{32} & a_{33} & 0 & 0 & 0 \end{bmatrix}, \quad \mathbf{B} = \begin{bmatrix} 0 & 0 \\ 0 & 0 \\ 0 & 0 \\ b_{11} & b_{12} \\ b_{21} & b_{22} \\ b_{31} & b_{33} \end{bmatrix}, \tag{4.18}$$

The following theorem shows that the flat output is only linear functions of first three states in $\mathbf{x}_\delta$.

Theorem 4.2.1. *Given reduced linearized system of MIMO nonlinear UMS in the form of Equation (4.17), if the following matrices*

$$\mathbf{K} = \begin{bmatrix} b_{21} & b_{31} \\ b_{22} & b_{33} \end{bmatrix}, \quad \mathbf{Q} = \begin{bmatrix} c_2^* & c_3^* \\ a_{12} + c_2^* a_{22} + c_3 a_{32} & a_{13} + c_2^* a_{23} + c_3^* a_{33} \end{bmatrix}, \tag{4.19}$$

are non-singular, where c_2^* and c_3^* are the solution of equations

$$b_{11} + c_2 b_{21} + c_3 b_{31} = 0, \tag{4.20}$$

$$b_{12} + c_2 b_{22} + c_3 b_{33} = 0, \tag{4.21}$$

then the vector $\mathbf{y}_f = [y_{f_1}, y_{f_2}]^T$ is a flat output where

$$y_{f_1} = x_1, \tag{4.22}$$

$$y_{f_2} = x_1 + c_2^* x_2 + c_3^* x_3. \tag{4.23}$$

Proof. To prove that $\mathbf{y}_f$ is a flat output, we need to show that all the states of $\mathbf{x}$ can be expressed by the components $y_{f_1}, \dot{y}_{f_1}, \cdots, y_{f_1}^{(n_1)}, y_{f_2}, \ldots, y_{f_2}^{(n_2)}$, with n_1 and n_2 being some finite positive numbers. Apparently, $x_1 = y_1$ and $x_4 = \dot{x}_1 = \dot{y}_1$. Differentiating y_2 twice with respect to time gives,

$$y_{f_2} = x_1 + c_2 x_2 + c_3 x_3, \tag{4.24}$$

$$\begin{aligned} \ddot{y}_{f_2} &= (a_{11} + c_2 a_{21} + c_3 a_{31}) x_1 + (a_{12} + c_2 a_{22} + c_3 a_{32}) x_2 \\ &\quad + (a_{13} + c_2 a_{23} + c_3 a_{33}) x_3 + (b_{11} + c_2 b_{21} + c_3 b_{31}) u_1 + (b_{12} + c_2 b_{22} + c_3 b_{33}) u_2. \end{aligned} \tag{4.25}$$

By choosing $c_2 = c_2^*$, $c_3 = c_3^*$, it gives

$$\begin{aligned} \ddot{y}_{f_2} &= (a_{11} + c_2^* a_{21} + c_3^* a_{31}) x_1 + (a_{12} + c_2^* a_{22} + c_3^* a_{32}) x_2 \\ &\quad + (a_{13} + c_2^* a_{23} + c_3^* a_{33}) x_3. \end{aligned} \tag{4.26}$$

Substituting x_1 with y_1, x_2 and x_3 can be the linear functions of y_1, y_2 and $\ddot{y}_2$ by solving the following system of equations

$$\begin{aligned} &\begin{bmatrix} c_2^* & c_3^* \\ a_{12} + c_2^* a_{22} + c_3^* a_{32} & a_{13} + c_2^* a_{23} + c_3^* a_{33} \end{bmatrix} \begin{bmatrix} x_2 \\ x_3 \end{bmatrix} \\ &= \begin{bmatrix} -1 \\ -a_{11} - c_2^* a_{21} - c_3^* a_{31} \end{bmatrix} y_{f_1} + \begin{bmatrix} 1 \\ 0 \end{bmatrix} y_{f_2} + \begin{bmatrix} 0 \\ 1 \end{bmatrix} \ddot{y}_{f_2}. \end{aligned} \tag{4.27}$$

Denote the solution by $x_2 = \chi_2(y_{f_1}, y_{f_2}, \ddot{y}_{f_2})$ and $x_3 = \chi_3(y_{f_1}, y_{f_2}, \ddot{y}_{f_2})$. Since $\mathbf{Q}$ is invertible, the solution is given by

$$\begin{bmatrix} \chi_2(y_1, y_2, \ddot{y}_2) \\ \chi_3(y_1, y_2, \ddot{y}_2) \end{bmatrix} = \mathbf{Q}^{-1} \left(\begin{bmatrix} -1 \\ -a_{11} - c_2 a_{21} - c_3 a_{31} \end{bmatrix} y_1 + \begin{bmatrix} 1 \\ 0 \end{bmatrix} y_2 + \begin{bmatrix} 0 \\ 1 \end{bmatrix} \ddot{y}_2 \right). \tag{4.28}$$

Hence $x_5 = \dot{x}_2$ and $x_6 = \dot{x}_3$ are the linear functions of $\dot{y}_1$, $\dot{y}_2$ and $\ddot{y}_2$. □

By Theorem 4.2.1, we can further show that scalar output functions in the form of $\bar{y}_{f_1} = x_i$ and $\bar{y}_{f_2} = x_i + c_j x_j + c_k x_k$, where $i, j, k \in \{1, 2, 3\}$ and $i \neq j$, $j \neq k$, $k \neq i$, can be proven as flat output of system (4.17) with proper modification of matrices in conditions (4.20) and (4.21). To check the rank of $\mathbf{Q}$ matrix, the matrix $\mathbf{B}$ is assumed to be known. On the other hand, if one knows the vector relative degree [53] of the system with output function $\mathbf{y}_f$ in which y_{f_1} and y_{f_2} are determined by certain choice of c_2 and c_3, we are able to judge if it is a flat output without knowing $\mathbf{B}$. According to the definition and property of flatness, the problem of finding the flat output for nonlinear systems can also be viewed as a problem of finding an appropriate state feedback control law and a coordinate transformation such that Brunovsky's canonical form can be obtained, which is called State-Space Exact Linearization Problem when we restrict the type of feedback control to regular static state feedback. A well-known lemma [53] has stated the relations between vector relative degree and flatness of the output in this case.

Lemma 4.2.2. *The exact state linearization problem is solvable if and only if there exists a neighborhood* $\mathbf{U}$ *of* $\mathbf{x}^\circ$ *and* m *real-valued functions* $h_1(x), \ldots, h_m(x)$, *defined on* U, *such that the nonlinear system with order of* $2n$ *and* m *independent inputs in the state space given by*

$$\dot{\mathbf{x}} = \bar{\mathbf{F}}(\mathbf{x}) + \bar{\mathbf{G}}(\mathbf{x})\mathbf{u}, \tag{4.29}$$

$$\mathbf{y} = \bar{\mathbf{H}}(\mathbf{x}), \tag{4.30}$$

has some vector relative degree $\{n_1, \cdots, n_m\}$ *at* $\mathbf{x}^\circ$ *and* $n_1 + n_2 + \cdots + n_m = 2n$, *where* $\mathbf{x} \in \mathbb{R}^{2n\times 1}$, $\mathbf{u} \in \mathbb{R}^{m\times 1}$, $\bar{\mathbf{F}}(\mathbf{x}) \in \mathbb{R}^{2n\times 1}$ *and* $\bar{\mathbf{G}}(\mathbf{x}) \in \mathbb{R}^{2n\times m}$, $\bar{\mathbf{H}}(\mathbf{x}) = [h_1(x), h_2(x), \cdots, h_m(x)]^T \in \mathbb{R}^{m\times 1}$ *are real-valued smooth vector fields defined on an open set of* $\mathbb{R}^{2n}$.

Lemma 4.2.3. *If there exist* m *real-valued outputs* $h_1(\mathbf{x}), \cdots, h_m(\mathbf{x})$ *defined on* $\mathbf{U}$ *for* $2n$*-dimensional linear controllable system*

$$\dot{\mathbf{x}} = \bar{\mathbf{A}}\mathbf{x} + \bar{\mathbf{B}}\mathbf{u} \tag{4.31}$$

with m *independent inputs with relative degrees* $\{n_1, n_2, \cdots, n_m\}$ *and* $\sum_{i=1}^{m} n_i = 2n$, *the vector* $\mathbf{y}_f = [y_{f_1}, y_{f_2}, \cdots, y_{f_m}]^T$ *is a flat output where*

$$\begin{aligned} y_{f_1} &= h_1(\mathbf{x}), \\ y_{f_2} &= h_2(\mathbf{x}), \\ &\vdots \\ y_{f_m} &= h_m(\mathbf{x}). \end{aligned} \tag{4.32}$$

Proof. According to Lemma 1, it is sufficient to solve the state-space exact linearization problem of $2n$-dimensional MIMO linear controllable system with a vector of relative degrees $\{n_1, n_2, \cdots, n_m\}$ and $\sum_{i=1}^{m} n_i = 2n$. It implies a set of functions

$$\phi_k^i(\mathbf{x}) = L_{\tilde{\mathbf{A}}}^{k-1} h_i(\mathbf{x}), \tag{4.33}$$

for $1 \leq k \leq n_i$, $1 \leq i \leq m$, completely define the local coordinate transformation $\mathbf{\Phi} = [\phi_1^1, \cdots, \phi_{n_1}^1, \phi_1^2, \cdots, \phi_{n_2}^2, \cdots, \phi_{n_m}^m]^T$, which is invertible around $\mathbf{x}^\circ$, and the transformed new system, after applying a proper static state linearizing feedback, can be rewritten by m sets of equations of the form

$$\begin{aligned} \dot{\xi}_1^i &= \xi_2^i, \\ &\vdots \\ \dot{\xi}_{n_i-1}^i &= \xi_{n_i}^i, \\ \dot{\xi}_{n_i}^i &= v_i, \end{aligned} \tag{4.34}$$

where $\xi_k^i = \phi_k^i(\mathbf{x})$. Define $y_{f_i} = \xi_1^i$. Since $\mathbf{\Phi}$ is invertible, the state $\mathbf{x}$ can be represented as

$$\mathbf{x} = \Phi^{-1}[y_{f_1}, \dot{y}_{f_1}, \ldots, y_{f_1}^{(n_1-1)}, y_{f_2}, \ldots, y_{f_2}^{(n_2-1)}, \ldots, y_{f_m}, \ldots, y_{f_m}^{(n_m-1)}], \tag{4.35}$$

and the control input vector $\mathbf{u}$ can be written as

$$\mathbf{u} = \Psi[y_{f_1}, \dot{y}_{f_1}, \ldots, y_{f_1}^{(n_1)}, y_{f_2}, \ldots, y_{f_2}^{(n_2)}, \ldots, y_{f_m}, \ldots, y_{f_m}^{(n_m)}], \tag{4.36}$$

hence, $\mathbf{y}_f = [y_{f_1}, y_{f_2}, \cdots, y_{f_m}]^T$ is a flat output. □

When the sum of entries in the vector relative degree is equal to the order of the system or the dimension of the state space, the vector of the output is shown to be flat. We can apply this lemma to system (4.17) and obtain the sufficient condition to characterize flat output, which is shown by next theorem

Theorem 4.2.4. *Given real-valued output vector $\mathbf{y}_f = [y_{f_1}, y_{f_2}]^T$ in which $y_{f_1} = x_1$, $y_{f_2} = x_1 + c_2 x_2 + c_3 x_3$, $c_2 \neq 0$, $c_3 \neq 0$, $c_2 \in \mathbb{R}$, $c_3 \in \mathbb{R}$, $\mathbf{y}_f$ can be a flat output with some choice of c_2 and c_3 if reduced linearized system of MIMO nonlinear UMS in the form of Equation (4.17) has a vector relative degree $\{n_1, n_2\}$, and $n_1 + n_2 = 6$.*

Proof. Differentiating y_{f_1} twice, either u_1 or u_2 shows up in the result so the relative degree n_1 associated with y_{f_1} is 2 because at least one of b_{11} and b_{12} is nonzero. Then y_{f_2} has relative degree $n_2 = 4$. Equations (4.20) and (4.21) must be satisfied, which gives

$$\begin{aligned} \ddot{y}_{f_2} &= (a_{11} + c_2^* a_{21} + c_3^* a_{31}) x_1 \\ &\quad + (a_{12} + c_2^* a_{22} + c_3^* a_{32}) x_2 + (a_{13} + c_2^* a_{23} + c_3^* a_{33}) x_3 \\ &= q_1 x_1 + q_2 x_2 + q_3 x_3. \end{aligned} \tag{4.37}$$

where c_2^* and c_3^* must be chosen as the solution of Equations (4.20) and (4.21), and matrix $\mathbf{K} = \begin{bmatrix} b_{21} & b_{31} \\ b_{22} & b_{33} \end{bmatrix}$ must be nonsingular. $\mathbf{y}_f$ and its finite time derivatives define an invertible local coordinates transformation $\mathbf{\Phi}$

$$\mathbf{y} = \mathbf{\Phi}\mathbf{x}, \tag{4.38}$$

$$\mathbf{y}_t = \begin{bmatrix} y_{f_1} \\ \dot{y}_{f_1} \\ y_{f_2} \\ \dot{y}_{f_2} \\ \ddot{y}_{f_2} \\ \dddot{y}_{f_2} \end{bmatrix} = \begin{bmatrix} 1 & 0 & 0 & 0 & 0 & 0 \\ 0 & 0 & 0 & 1 & 0 & 0 \\ 1 & c_2^* & c_3^* & 0 & 0 & 0 \\ 0 & 0 & 0 & 1 & c_2^* & c_3^* \\ q_1 & q_2 & q_3 & 0 & 0 & 0 \\ 0 & 0 & 0 & q_1 & q_2 & q_3 \end{bmatrix} \begin{bmatrix} x_1 \\ x_2 \\ x_3 \\ x_4 \\ x_5 \\ x_6 \end{bmatrix}. \tag{4.39}$$

Now define the matrix $\mathbf{Q}$ as

$$\mathbf{Q} = \begin{bmatrix} c_2^* & c_3^* \\ q_2 & q_3 \end{bmatrix} \tag{4.40}$$

is singular, which implies the row vectors $\mathbf{q}_{r_1} = [c_2^*, c_3^*]$ and $\mathbf{q}_{r_2} = [q_2, q_3]$ are linearly dependent. Let $\mathbf{q}_{r_2} = \lambda \mathbf{q}_{r_1}$, $\lambda \in \mathbb{R}$, and $\lambda \neq 0$. We rewrite Equation (4.37) as

$$\begin{aligned} \ddot{y}_{f_2} &= q_1 y_{f_1} + \lambda c_2^* x_2 + \lambda c_3^* x_3 \\ &= q_1 y_{f_1} + \lambda (y_{f_2} - y_{f_1}) \end{aligned} \tag{4.41}$$

Differentiating $\ddot{y}_{f_2}$ twice gives

$$\begin{aligned} y_{f_2}^{(4)} &= q_1 \ddot{y}_{f_1} + \lambda (\ddot{y}_{f_2} - \ddot{y}_{f_1}) \\ &= (q_1 - \lambda)\ddot{y}_{f_1} + \lambda (q_1 x_1 + q_2 x_2 + q_3 x_3) \\ &= (q_1 - \lambda)(a_{11} x_1 + a_{12} x_2 + a_{13} x_3 + b_{11} u_1 + b_{12} u_2) \\ &+ \lambda (q_1 x_1 + q_2 x_2 + q_3 x_3) \\ &= \bar{w}_1 x_1 + \bar{w}_2 x_2 + \bar{w}_3 x_3 + (q_1 - \lambda) b_{11} u_1 + (q_1 - \lambda) b_{12} u_2. \end{aligned} \tag{4.42}$$

where $\bar{w}_1, \bar{w}_2, \bar{w}_3$ are scalar coefficients and $(q_1 - \lambda) \neq 0$, as the vector relative degree is $\{2, 4\}$. The transformed system becomes

$$\ddot{y}_{f_1} = a_{11} x_1 + a_{12} x_2 + a_{13} x_3 + b_{11} u_1 + b_{12} u_2, \tag{4.43}$$

$$y_{f_2}^{(4)} = \bar{w}_1 x_1 + \bar{w}_2 x_2 + \bar{w}_3 x_3 + (q_1 - \lambda) b_{11} u_1 + (q_1 - \lambda) b_{12} u_2. \tag{4.44}$$

Since the new system can also be written as

$$\dot{\mathbf{y}}_t = \mathbf{\Phi}\bar{\mathbf{A}}\mathbf{\Phi}^{-1}\mathbf{y}_t + \mathbf{\Phi}\bar{\mathbf{B}}\mathbf{u} = \bar{\mathbf{A}}_y \mathbf{y}_t + \bar{\mathbf{B}}_y \mathbf{u}, \tag{4.45}$$

the new control influence vector $\bar{\mathbf{B}}_y$ becomes

$$\bar{\mathbf{B}}_y = \mathbf{\Phi}\bar{\mathbf{B}} = \begin{bmatrix} 0 & 0 \\ b_{11} & b_{12} \\ 0 & 0 \\ 0 & 0 \\ 0 & 0 \\ (q_1-\lambda)b_{11} & (q_1-\lambda)b_{12} \end{bmatrix} \tag{4.46}$$

and the rank of $\bar{\mathbf{B}}_y$ is 1, which contradicts the fact that $\bar{\mathbf{B}}$ has full rank 2, or two independent input channels exist. Therefore the matrix $\mathbf{Q}$ must be invertible. According to Theorem 4.2.1, we conclude $\mathbf{y}_f$ is a flat output of reduced linearized system (4.17). The parametrization of the state vector $\mathbf{x}$ is given by

$$\begin{aligned} &x_1 = y_{f_1}, x_4 && = \dot{x}_1 = y_{f_1}, \\ &x_2 = \chi_2(y_{f_1}, y_{f_2}, \ddot{y}_{f_2}), \quad x_5 &&= \dot{\chi}_2 = \eta_2(\dot{y}_{f_1}, \dot{y}_{f_2}, \dddot{y}_{f_2}), \\ &x_3 = \chi_3(y_1, y_2, \ddot{y}_2), x_6 && = \dot{\chi}_3 = \eta_3(\dot{y}_{f_1}, \dot{y}_{f_2}, \dddot{y}_{f_2}), \end{aligned} \tag{4.47}$$

where η_2 and η_3 are some linear functions. □

From Theorem 4.2.4, the vector relative degree of system (4.17) is an efficient indicator characterizing the flatness of the output in the form of Equations (4.22) and (4.23) without checking the rank of $\mathbf{K}$ and $\mathbf{Q}$. The reduced linearized model greatly simplifies the composition of the flat output components by the means of neglecting all the terms relevant to generalized velocities in the model. The numbers in the set of controllability indices of the reduced model may also be changed compared to the case when all the states in $\mathbf{x}$ are involved. Such simplification is extremely useful in tracking control because certain components of the flat output, for instance, $y_{f_1} = x_1$ of the system we just discussed, could have a simple linear function of a single state and undisturbed by other states during trajectory planning and tracking.

The reduced linearized model can be transformed into the Brunosky's canonical form if a proper static state feedback is applied. The resulting input-to-flat output system is given by,

$$\begin{aligned} \ddot{y}_{f_1} &= a_{11}y_{f_1} + a_{12}\chi_1(y_{f_1}, y_{f_2}, \ddot{y}_{f_2}) \\ &\quad + a_{13}\chi_2(y_1, y_2, \ddot{y}_2) + b_{11}u_1 + b_{12}u_2 \\ &= \mu_1(\mathbf{y}_t) + b_{11}u_1 + b_{12}u_2, \\ y^{(4)}_{f_2} &= w_1 y_{f_1} + w_2\chi_1(y_{f_1}, y_{f_2}, \ddot{y}_{f_2}) \\ &\quad + w_3\chi_2(y_1, y_2, \ddot{y}_2) + l_{21}u_1 + l_{22}u_2 \\ &= \mu_2(\mathbf{y}_t) + l_{21}u_1 + l_{22}u_2. \end{aligned} \tag{4.48}$$

where

$$\begin{aligned} w_1 &= q_1 a_{11} + q_2 a_{21} + q_3 a_{31}, \\ w_2 &= q_1 a_{12} + q_2 a_{22} + q_3 a_{32}, \\ w_3 &= q_1 a_{13} + q_2 a_{23} + q_3 a_{33}, \\ l_{21} &= q_1 b_{11} + q_2 b_{21} + q_3 b_{31}, \\ l_{22} &= q_1 b_{12} + q_2 b_{22} + q_3 b_{32}. \end{aligned} \tag{4.49}$$

Consider two time-varying terms $\rho_1(t)$ and $\rho_2(t)$ for each subsystem that contain the unmodeled dynamics, internal and external disturbances, error caused by linearization, which is the notion of total disturbance from active disturbance rejection control and disturbance-observer based control. The compensated system dynamics can be generally described as

$$\begin{aligned} \ddot{y}_{f_1} &= \Omega_1(t) + b_{11} u_1 + b_{12} u_2, \\ y_{f_2}^{(4)} &= \Omega_2(t) + l_{21} u_1 + l_{22} u_2. \end{aligned} \tag{4.50}$$

where $\Omega_1(t) = \mu_1(\mathbf{y}_t) + \rho_1(t), \Omega_2(t) = \mu_2(\mathbf{y}_t) + \rho_2(t)$. Since the transformation $\mathbf{\Phi}$ is invertible, it is always possible to introduce a static state feedback

$$\mathbf{u} = \begin{bmatrix} b_{11} & b_{12} \\ l_{21} & l_{22} \end{bmatrix}^{-1} \begin{bmatrix} v_1 - \Omega_1(t) \\ v_2 - \Omega_2(t) \end{bmatrix}, \tag{4.51}$$

and hence the Brunosky's canonical form is given by

$$\ddot{y}_{f_1} = v_1, \quad y_{f_2}^{(4)} = v_2. \tag{4.52}$$

The control design of systems in the form of Equation (4.50) can be naturally dealt with in the framework of ADRC, disturbance-observer based control and neural network-based control in which various strategies for online estimation or adaptive approximation of the unknown disturbance term $\Omega_1(t)$ and $\Omega_2(t)$ are proposed.

4.3 Problem Formulation

The characterization of the flatness of nonlinear systems is generally not straightforward, and the problem of finding corresponding flat outputs is also intractable even the accurate mathematical model is given. For linearized system, due to the relations between controllability and flatness, linear flat outputs that transform the system into controllability canonical form are the common choices. When only measurement of outputs are available, the local flatness of nonlinear MIMO systems is possible to be determined by data-driven techniques that construct discrete controllability matrix or equivalently check the rank condition of some matrices. The reduced linearized model of MIMO systems can further simplify the structure

of local flat output. With identified local flat outputs, the uncertainties and approximation made by linearization and model reduction can be compensated by disturbance-observer-based control technique, such as ADRC and neural-network-based observer control. The local flatness greatly expedites the tracking control design of a class of nonlinear MIMO UMSs.

Therefore, we next focus on finding a special type of linear locally flat output $\mathbf{y}_f$ in the form of Equations (4.22) and (4.23) for MIMO nonlinear system (4.7) without relying on the concrete mathematical equations. Based on the reduced linearized model, $\mathbf{y}_f$ can be efficiently identified with linear combination of a few number of states, and the error caused by approximation will be efficiently compensated through a feedforward channel in the control design. The identification of the parameterization of original state can be carried out, after $\mathbf{y}_f$ is found, by applying parametric estimation, with all or partial signals of $\mathbf{y}_f$ and its finite number of time derivatives available in the library. The problem in this chapter can be formalized as follows.

Problem 3. *Given measurements of the state x_1, x_2 and x_3, find the locally flat output $\mathbf{y}_f$ in the form given by Equations (4.22) and (4.23) for MIMO nonlinear UMS around its equilibrium p and hence transform it into controllable canonical form.*

4.4 Identification of Flat Output for MIMO systems

4.4.1 Introduction of Modified FOID (MFOID) Algorithm

Flat output identification (FOID) is a data-driven algorithm that identifies the locally flat output of the nonlinear systems given measurements of the outputs and control input. For SIMO system, the locally flat output exists if any output with relative degree equal to order of the controllable linearization of nonlinear system, or full relative degree, exists around its equilibrium. The algorithm presents the relation between control input and different combination of outputs by calculating the periodograms and evaluate the relative degree from the corresponding transfer functions obtained. The relative degree, in this context, can be viewed as the 'distance' from non-flat output to flat output, and the flatness of the output can be characterized when the relative degree is full. The candidates of flat output are the linear combination of the outputs and the dimension of search space in which possible candidates lie in can be configured, as a result of compromise between the availability of measured outputs and computational cost. However, FOID itself has the limitation that the candidate output has simply one component for SIMO system, and therefore the form of candidate flat output might not be true for MIMO system. The relative degree condition involves more than one output in cases of MIMO systems and one can not perform FOID for single output to find the flat output. In fact, since the number of components of flat output of MIMO systems

equates the number of control input channels, the flat outputs, even the linear ones, becomes more amorphous.

As we have shown in Section 4.2, the relation between vector relative degree and local flatness of nonlinear MIMO UMSs is similar as we found for SIMO UMS, although the number of component of flat output now is more than one. The modified FOID (MFOID) algorithm is developed to fit the problem of finding locally flat output for MIMO UMSs without leveraging the mathematical models in details. The major difficulty to accommodate MIMO situation in FOID is that there are a variety of choices of flat outputs, and one must determine what linear combination is going to be used in identification. Thanks to Theorems 4.2.1 and 4.2.4, an off-the-shelf solution can be found by setting the output function in the form of Equations (4.22) and (4.23) are treating the nonlinear system as linear one near an equilibrium. MFOID is designed to evaluate the vector relative degree and systematically calculate the unknown coefficients c_2 and c_3 in Equations (4.20) and (4.21) without leveraging the details of mathematical equations. The first part of the algorithm focuses on the evaluation of relative degree of simple outputs like y_1 in Equation (4.22). The second part of the algorithm aims to find a proper compound output in the form of y_2 that satisfies the vector relative degree condition in Theorem 4.2.4.

4.4.2 Relative Degree Evaluation of Simple Outputs

The relative degree of simple outputs which only consists of one state can be conveniently determined by inspecting the estimated transfer functions. For linearized reduced model (4.17), the output y_1 in Equation (4.22) is simple, and process of estimating the relative degree of y_1 for control inputs u_1 and u_2 complies with the procedures in FOID shown as follows:

- Data Preprocessing

  The signal of control inputs $u_1(t)$ and $u_2(t)$ and output $y_1(t)$ of the nonlinear system operating in a 'linear' range are first resized and used to calculate the cross power spectral density. The transfer functions from inputs $u_1(t)$ and $u_2(t)$ to the output $y_1(t)$ are estimated as $G_1(j\omega)$ and $G_2(j\omega)$, with some proper filtering, by calculating the periodogram using H_1 estimator.

- Frequency Band Selection

  A frequency range needs to be selected to evaluate the relative degree from the transfer function. It is desirable to have the frequency response in the linear range of system. Such selection can be done manually at the data preprocessing stage or automatically by providing a lower and upper frequency bounds based on the physical property of the system, and removing resonances near the Nyquist frequency.

- Regression

  The data in the selected frequency band can be used to perform regression so that the relative degree is viewed as the absolute value of the slope of the fitted line in log-log plot. Different schemes of regression, such as least mean square method and ridge regression, are adopted for different cases. The norm of residual of LMS or loss function are evaluated to judge the quality of regression. To represent the relative degree as an integer, the estimated slope will be rounded off or truncated.

- Segmentation

  There may be more than one collection of the data suitable for regression, that is, more than one line can be found in the selected frequency band. The data within the selected band can be further divided into subsets. The data in each subset shares the same linear relation with the frequencies. As a result, multiple values of slope will be generated by different subsets of the data. Abnormal results will be discarded. Generally the maximum absolute value of all the slopes of the subsets is chosen as the estimate of the relative degree of the candidate output.

In the case of Equation (4.22), the relative degree of y_1 for both inputs $u_1(t)$ and $u_2(t)$ are expected to be 2 if b_{11} and b_{12} are nonzero. Otherwise, at least one of the coefficients is zero or extremely small. The output chosen as one of the states has two advantages. First, the implementation of the identification would become extremely efficient because the transfer function for the output y_1 is determined beforehand without extra steps. Second, it makes control design more straightforward so that one can directly set the output that needs to be controlled as the flat output component. To complete the identification, the similar steps will be applied for flat output y_2 where some modifications are needed to adapt the situation of multiple input and output measurements.

4.4.3 Relative Degree Evaluation of Compound Outputs

To satisfy the condition that the sum of vector relative degree is equal to the dimension of the state space, the second component must have a relative degree 4. The problem is now converted to finding the coefficients c_2 and c_3 such that Equation (4.23) can have relative degree 4, that is, taking derivatives with respect to time up to four times before either input u_1 or u_2 appears. The number of output considered hence decreases to one. We are able to use the idea in FOID to validate the relative degree for single function. The remaining issue is that the solution of coefficients that makes relative degree become 4 for each input is not unique, and it is generally hard to find them directly and satisfy both equations (4.20) and (4.21) simultaneously by random search in the given range.

Let assume we have a simple first component of flat output chosen as $y_1 = x_1$. The candidate of second component y_2 is then a linear combination of x_1, x_2 and x_3. The estimated transfer functions from input $u_1(t)$ and $u_2(t)$ to x_2 and x_3 are estimated as $G_1^2(j\omega)$, $G_2^2(j\omega)$, $G_1^3(j\omega)$ and $G_2^3(j\omega)$ with some proper filtering, using the same H_1 estimator. The candidates y_2 have the form of $y_2 = x_1 + c_2x_2 + c_3x_3$, so the estimated transfer functions with respect to both u_1 and u_2 are given in the form of $H_i(j\omega) = G_i(j\omega) + c_2G_i^2(j\omega) + c_3G_i^3(j\omega)$ $(i = 1, 2)$.

Since the modified algorithm needs to deal with the identification of relative degree of two inputs, we can implement the estimation of both periodograms in parallel to evaluate the transfer functions $H_1(j\omega)$ and $H_2(j\omega)$. This process is the similar to FOID, but with a new parallel loop to deal with extra estimation.

Next, we look for suitable coefficients c_2 and c_3 to meet the requirement that the relative degree for both inputs is 4 at the same time. If either of them is not 4, the vector relative degree will not lead to a local flatness. However, we notice that for each input, it is impossible to determine the unique solution as the coefficient has infinitely many solutions if one iterates the coefficient over the search range. For example, to satisfy that second component y_2 has relative degree 4 with respect to the first input u_1, Equation (4.20) must be satisfied. This is not solvable because we have only one linear equation and the coefficient of b_{11}, b_{21} and b_{31} are unknown. For u_1, the second component y_2 has to satisfy another set of equations for u_2 with unknown coefficient in the matrix B. Nevertheless, through the FOID algorithm, if we designate c_2 first, then c_3 can be estimated by matching the coefficient in the search space. Implementing the process repeatedly gives a series of data which consists of pairs of possible solution (c_2, c_3). Another set of solution can be found by doing this to the second input. Two series of data provide us with the possibility to solve for the unique solution of the system of linear equations.

Although the coefficients in input matrix are unknown, it is possible to estimate the intersection of the two data sets such that the unique solution is obtained. After collecting the data which makes y_2 have relative degree 4 for either u_1 and u_2, the operation of linear regression can be implemented to generate the function of line in the 2D-plane that fits the data points. Finally, the flat output identification is completed with the unique interpolation solution obtained which is from the predictions of the fitted function relations between c_2 and c_3. Figure 4.1 shows the procedure to implement the MFOID finding local flat output in the chosen search space. Parallel computing introduced in the second part can improve the efficiency.

4.5 Numerical Simulation

We present two numerical simulation examples to demonstrate the feasibility and efficiency of the proposed MFOID algorithm.

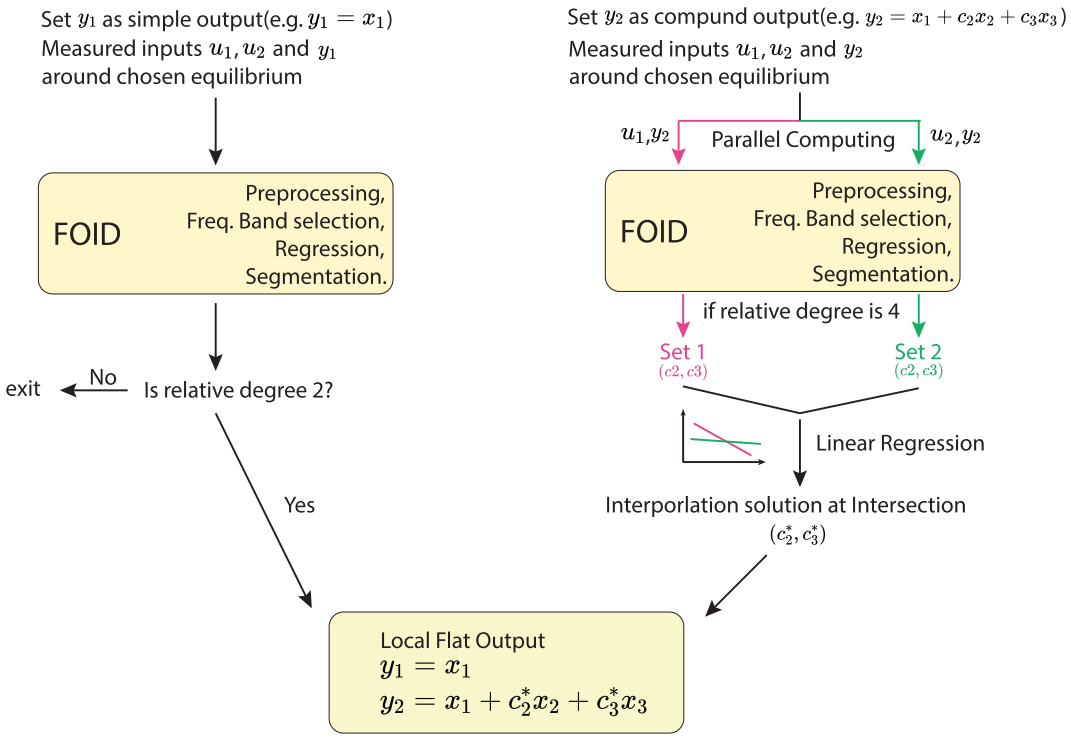

Figure 4.1: Flow chart of the MFOID algorithm.

4.5.1 A Simple Nonlinear MIMO UMS

Consider the equation of motion of a nonlinear underactuated mechanical system is given as follows:

$$\begin{aligned}
\ddot{x}_1 &= -49.452x_1 - 34.4652x_2 + 14.334x_3 - 0.658\dot{x}_1 \\
&\quad - 0.2186\dot{x}_2 - 0.1607\dot{x}_3 + 0.7363x_1^3 + 0.5604u_1 + 0.1862u_2, \\
\ddot{x}_2 &= -30.414x_1 - 47.267x_2 + 27.219x_3 - 0.3723\dot{x}_1 \\
&\quad - 0.1025\dot{x}_2 - 0.1753\dot{x}_3 + 0.3592\sin(x_3) + 0.3717u_1 + 0.0233u_2, \\
\ddot{x}_3 &= -42.599x_1 - 30.362x_2 + 7.113x_3 - 0.8928\dot{x}_1 \\
&\quad - 0.4\dot{x}_2 - 0.557\dot{x}_3 + 0.9588\sin(x_1)x_2 + 0.2747u_1 + 0.2576u_2.
\end{aligned} \tag{4.53}$$

The system has three degrees of freedom, and x_1, x_2 and x_3 are the corresponding generalized coordinates. The dynamics of each generalized coordinate is affected by some linear terms, nonlinear functions of x_i, $i = 1, 2, 3$, and two independent inputs u_1 and u_2. The outputs of the system are measured as $h_1(x) = x_1$, $h_2(x) = x_2$ and $h_3(x) = x_3$. Figures 4.2 and 4.3 show the simulated response of the system and random inputs. To find the locally flat output of the system, we use the MFOID for two components since the number of input is known. The form of the locally flat output is assumed by Equations (4.22) and (4.23).

The goal is to find the proper coefficients c_2 and c_3 that satisfy the vector relative degree condition. We first focus on the first component y_1. To verify if the output y_1 has relative degree 2 for both inputs, the relative degree with respect to the input $u_1(t)$ and $u_2(t)$ are directly estimated by the periodogram generated by measured input and output data. We manually choose the frequency band between 1 Hz to 100 Hz to estimate the slope of the estimated transfer function. The random signal for the estimation follows the normal distribution $N(0, 0.01)$. Figures 4.4 and 4.5 show the result of estimated transfer function for two distinct input $u_1(t)$ and $u_2(t)$. In Figure 4.4, three segments are generated for relative degree evaluation after two antiresonance peaks are removed. The segment 1 and 2 are not considered further because the number of points in each set is lower than the threshold 15% set by algorithm. The points in Segment 3 is used in linear regression and the slope is calculated as -1.9996 per decades in frequency, which indicates the relative degree is approximately 2. Figure 4.5 includes two segments and only segment 2 is considered valid. Therefore the component $y_1 = x_1$ has relative degree 2 as slopes shown in two figures are approximated around 2. It can easily verified from the equations above that it indeed can differentiate y_1 twice to get both inputs appeared.

The second part of MFOID is to find the best set of coefficients to maximize the relative degree of y_2. The relative degree estimation of y_2 is similar to FOID, but there are two individual processes for two inputs. For each process, the value of c_2 iterates over a certain given interval. They are now chosen as same by $[10, 20]$ with step size only 1. This choice gives us a series of coefficient c_2 and hence help

generate two sets of c_3 that makes the second output has relative degree 4. Linear regression is applied to the two sets of c_2 and c_3 and the intersection is assumed to be the solution of flat output finding problem. Figures 4.6 and 4.7 show the estimated result of c_3 when $c_2 = 1$. In Figure 4.6, the candidate y_2 will have relative degree of 4 when c_3 is chosen within $[-3.90, -3.82]$ with step size 0.01. The height of bars are assigned with value of confidence rate or relative data usage [52] which is a measure of how much portion of data points is used in each estimation when c_3 iterates, and the best value of c_3 should be chosen when confidence rate is highest. In this case, all estimates within $[-3.90, -3.82]$ use the same amount of data points so the best c_3 also follows the rule of least absolute value, that is -3.82. The corresponding estimated transfer function is shown in Figure 4.7 with three segments are generated. Due to the drastic change of slope in transfer functions from inputs to y_2, the threshold of picking segments are chosen 5% to avoid skipping some values of c_3 in iteration and improve the accuracy. Segment 2 is chosen for linear regression since the slope is the largest and it is not close to the Nyquist frequency. The same example for input 2 when $c_2 = 1$ is shown by Figures 4.8 and 4.9. After generating the full sets of (c_2, c_3) for both inputs, Figure 4.10 shows that the solution is $c_2 = -1.0324$ and $c_3 = -0.6336$ by finding the intersection of two fitted lines. It can be shown that the linearized system of equation above around origin gives:

$$\begin{aligned}
\ddot{x}_1 &= -49.4521x_1 - 34.4652x_2 + 14.3340x_3 - 0.6580\dot{x}_1 \\
&\quad - 0.2186\dot{x}_2 - 0.1607\dot{x}_3 + 0.5604u_1 + 0.1862u_2, \\
\ddot{x}_2 &= -30.4147x_1 - 47.2673x_2 + 27.2193x_3 - 0.3723\dot{x}_1 \\
&\quad - 0.1025\dot{x}_2 - 0.1753\dot{x}_3 + 0.3717u_1 + 0.0233u_2, \\
\ddot{x}_3 &= -42.5996x_1 - 30.3623x_2 + 7.1132x_3 - 0.8928\dot{x}_1 \\
&\quad - 0.4002\dot{x}_2 - 0.5570\dot{x}_3 + 0.2747u_1 + 0.2576u_2.
\end{aligned} \tag{4.54}$$

One possible locally flat output for this system, rendering full vector relative degree, is indeed very close to the result of identification,

$$\begin{aligned}
y_1 &= x_1, \\
y_2 &= x_1 - 1.0432x_2 - 0.6285x_3.
\end{aligned} \tag{4.55}$$

One important application of the flat output is for control design. For example, we point out that the control design within ADRC framework can be formalized by using the following input-to-flat output relations:

$$\begin{aligned}
\ddot{y}_1 &= \Omega_1(t) + b_1u_1 + b_2u_2, \\
y_2^{(4)} &= \Omega_2(t) + l_1u_1 + l_2u_2.
\end{aligned} \quad , \tag{4.56}$$

where b_1, b_2, l_1, l_2 are nominal input gains chosen, and $\Omega_1(t)$ and $\Omega_2(t)$ are time-varying terms include unknown system dynamics, real-time disturbances and model

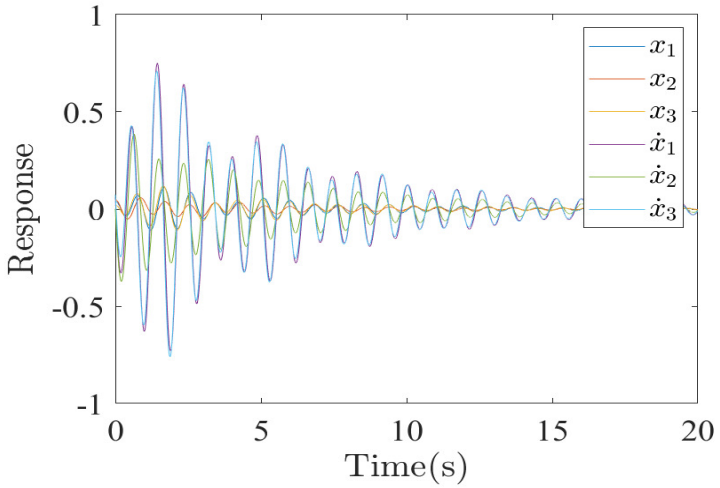

Figure 4.2: Open-loop response of the simple nonlinear UMS.

error caused by choosing nominal gains. An extended state observer (ESO) can be designed to estimated so-called unknown total disturbance $\Omega_1(t)$ and $\Omega_2(t)$ respectively. The MIMO control design is straightforward by cancelling the estimated terms. Note that the relations between states and flat output y_1 and y_2 need to be identified using input-output measured data for leveraging the flatness-based control design, as we have done in Chapter 3.

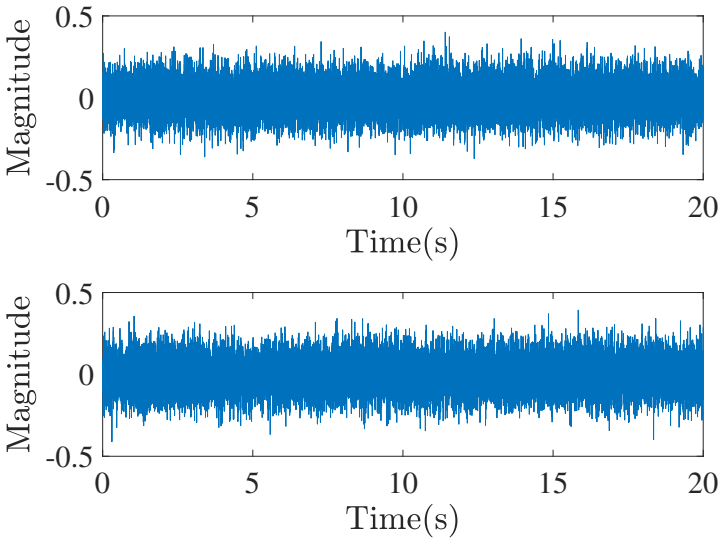

Figure 4.3: Random inputs u_1 (top) and u_2 (bottom).

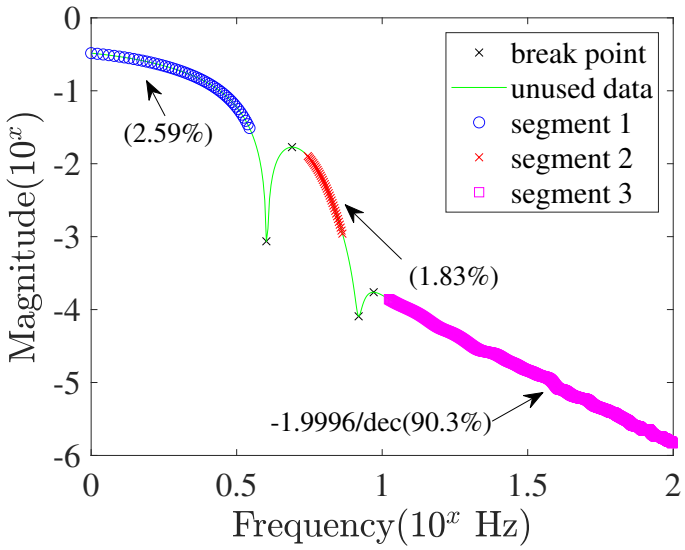

Figure 4.4: The estimated transfer function from u_1 to y_1.

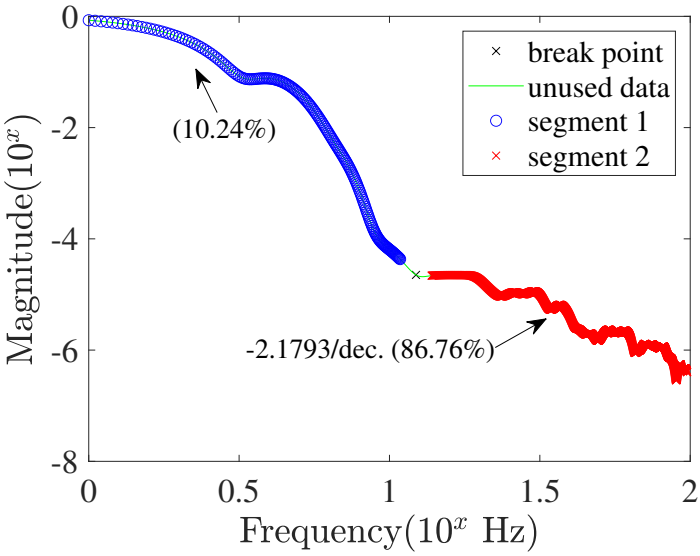

Figure 4.5: The estimated transfer function from u_2 to y_1.

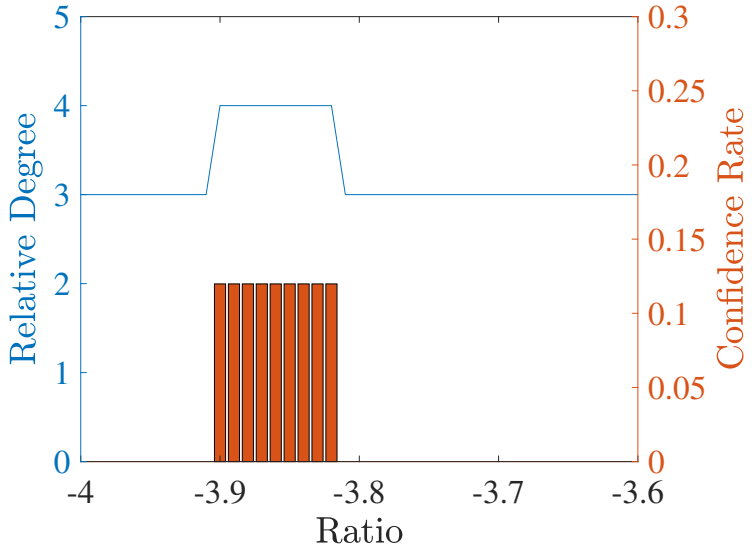

Figure 4.6: Identification of relative degree of y_2 with input u_1.

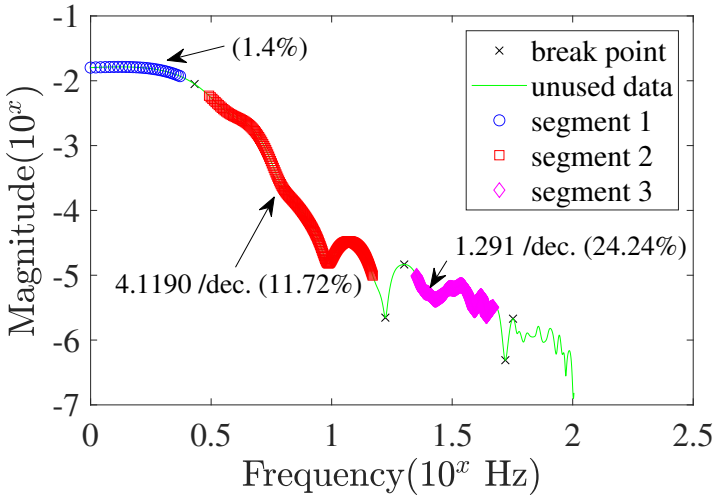

Figure 4.7: The estimated transfer function when $c_2 = 1$ and $c_3 = -3.82$ indicating the relative degree is 4.

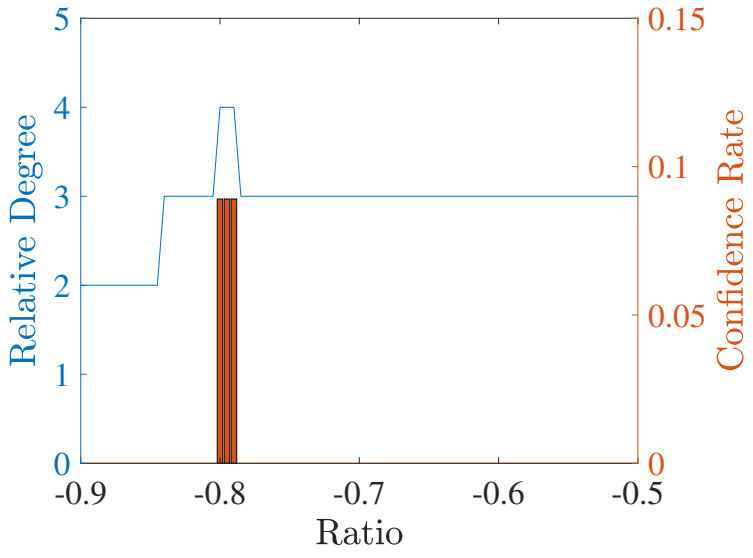

Figure 4.8: Identification of relative degree of y_2 with input u_2.

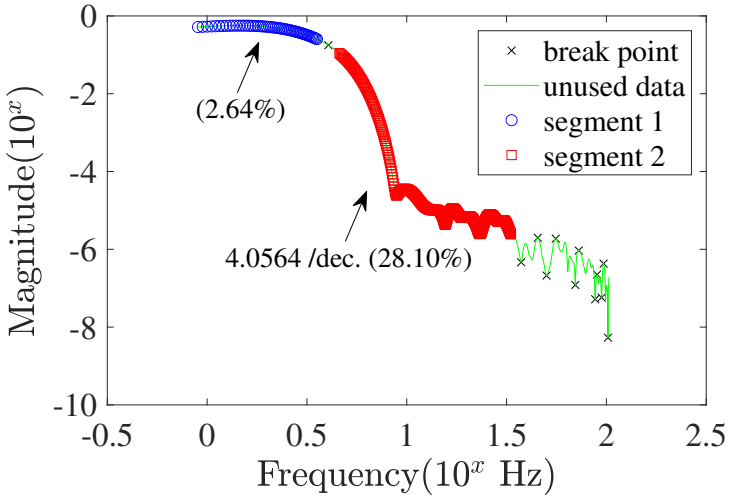

Figure 4.9: The estimated transfer function when $c_2 = 1$ and $c_3 = -0.78$ indicating the relative degree is 4.

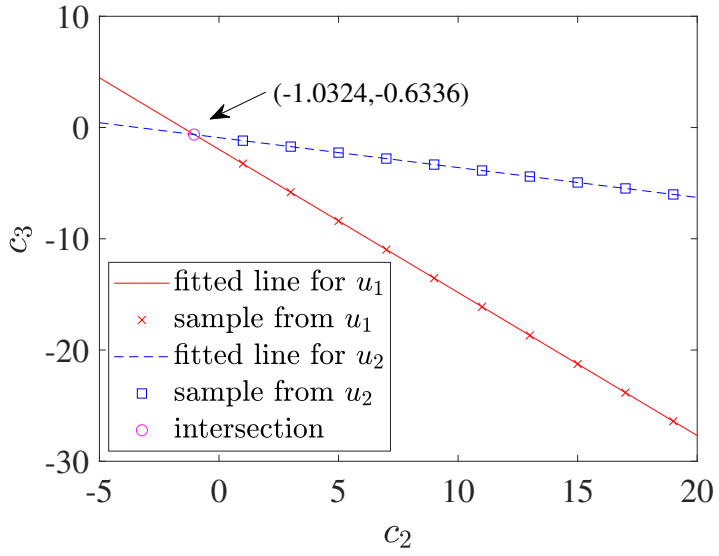

Figure 4.10: The estimated coefficients c_2 and c_3 for flat output.

4.5.2 Three-degree-of-freedom Mass-Spring-Damper System

Consider a nonlinear mass-spring-damper system with 3 degrees of freedom as shown in Figure 4.11.

$$\begin{aligned}&\begin{bmatrix} m_1 & & \\ & m_2 & \\ & & m_3 \end{bmatrix}\begin{bmatrix} \ddot{x}_1 \\ \ddot{x}_2 \\ \ddot{x}_3 \end{bmatrix} + \begin{bmatrix} d_2 & -d_2 & 0 \\ -d_2 & d_2+d_3 & -d_3 \\ 0 & 0 & 0 \end{bmatrix}\begin{bmatrix} \dot{x}_1 \\ \dot{x}_2 \\ \dot{x}_3 \end{bmatrix} \\ &+ \begin{bmatrix} d_1\left|\dot{x}_1\right|\dot{x}_1 \\ 0 \\ d_3\left|\dot{x}_2\right|\left(\dot{x}_3-\dot{x}_2\right) \end{bmatrix} + \begin{bmatrix} k_1+k_2 & -k_2 & 0 \\ -k_2 & k_2+k_3 & -k_3 \\ 0 & -k_3 & k_3 \end{bmatrix}\begin{bmatrix} x_1 \\ x_2 \\ x_3 \end{bmatrix} = \begin{bmatrix} \tau_1 \\ \tau_2 \\ \tau_3 \end{bmatrix},\end{aligned} \tag{4.57}$$

where m_1, m_2 and m_3 are the mass of the carts, k_1, k_2 and k_3 are the stiffness of three springs connecting the carts, and τ_1, τ_2 and τ_3 are the forces generated by DC motors. d_1, d_2 and d_3 are damping coefficients. The first and third dampers are nonlinear as shown by the nonlinear damping matrix. The three inputs τ_i are dependent given by

$$\begin{aligned}\tau_1 &= b_{11}u_1 + b_{12}u_2, \\ \tau_2 &= b_{21}u_1 + b_{22}u_2, \\ \tau_3 &= b_{31}u_1 + b_{32}u_2,\end{aligned} \tag{4.58}$$

where u_1 and u_2 are two independent control voltages, and b_{ij} are the non-zero weight coefficients. The system is underactuated. The state-space representation is given by,

$$\begin{aligned}\dot{x}_1 &= x_4, \\ \dot{x}_2 &= x_5, \\ \dot{x}_3 &= x_6, \\ \dot{x}_4 &= -\frac{k_1+k_2}{m_1}x_1 + \frac{k_2}{m_1}x_2 - \frac{d_2}{m_1}x_4 \\ &\quad + \frac{d_2}{m_1}x_5 - \frac{d_1\left|x_4\right|}{m_1}x_4 + \frac{b_{11}}{m_1}u_1 + \frac{b_{12}}{m_1}u_2, \\ \dot{x}_5 &= \frac{k_2}{m_2}x_1 - \frac{k_2+k_3}{m_2}x_2 + \frac{k_3}{m_2}x_3 + \frac{d_2}{m_2}x_4 \\ &\quad - \frac{d_2+c_3}{m_2}x_5 + \frac{d_3}{m_2}x_6 + \frac{b_{21}}{m_2}u_1 + \frac{b_{22}}{m_2}u_2, \\ \dot{x}_6 &= \frac{k_3}{m_3}x_2 - \frac{k_3}{m_3}x_3 + \frac{d_3\left|x_5\right|}{m_3}x_5 - \frac{d_3\left|x_5\right|}{m_3}x_6 \\ &\quad + \frac{b_{31}}{m_3}u_1 + \frac{b_{32}}{m_3}u_2,\end{aligned} \tag{4.59}$$

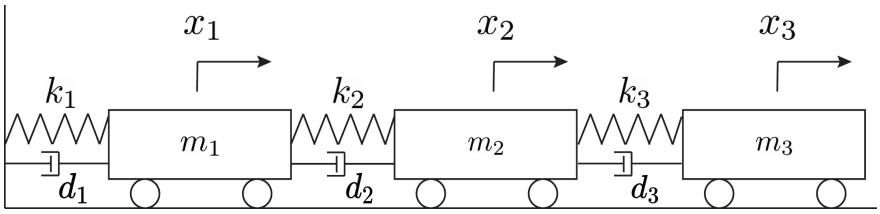

Figure 4.11: A nonlinear mass-spring-damper system with 3 degrees of freedom.

where x_i $(1 < i < 6)$ are the states. $m_1 = 100kg$, $m_2 = 200kg$ and $m_3 = 300kg$. The spring constants are $k_1 = 100N/m$, $k_2 = 150N/m$, $k_3 = 200N/m$. d_1, d_2 and d_3 are $20N \cdot s/m$. The coefficients b_{ij} are $b_{11} = 50$, $b_{12} = 15$, $b_{21} = 22$, $b_{22} = 13$, $b_{31} = 16$, $b_{32} = 38$. We apply the MFOID to this example with inputs as u_1 and u_2. The assumed form of the locally flat output is given in Equations (4.22) and (4.23).

To find the proper coefficients c_2 and c_3 that satisfy the vector relative degree condition, we apply the same settings as in the first simulation example and choose the same frequency band for analysis. The open-loop responses are shown in Figure 4.12. Figures 4.13 and 4.14 show the estimated transfer functions for two inputs $u_1(t)$ and $u_2(t)$. The output $y_1 = x_1$ has relative degree 2 as the slopes shown in two figures are approximately 2, which can be verified from the equations above. The second part of MFOID is to find the best set of coefficients to maximize the relative degree of y_2. With the same procedures, Figure 4.15 shows that the solution is $c_2 = -5.2535$ and $c_3 = -1.5318$. It can be shown that the linearized system around the origin without considering the damping effect would be given by:

$$\begin{aligned} \ddot{x}_1 &= -2.5x_1 + 1.5x_2 + 0.5u_1 + 0.15u_2, \\ \ddot{x}_2 &= 0.75x_1 - 1.75x_2 + x_3 + 0.11u_1 + 0.065u_2, \\ \ddot{x}_3 &= 0.6667x_2 - 0.6667x_3 + 0.0533u_1 + 0.1267u_2, \end{aligned} \tag{4.60}$$

One possible locally flat output for this system, rendering the full vector relative degree, is indeed very close to the identified result,

$$\begin{aligned} y_1 &= x_1, \\ y_2 &= x_1 - 5.2866x_2 - 1.5287x_3. \end{aligned} \tag{4.61}$$

The procedures of control design using ADRC are similar to the one in the previous example. We shall not present the control design for this example.

4.6 Conclusions

A modified flat output identification (MFOID) algorithm is presented in this chapter from experimental data of a dynamic system of known order. The system can be nonlinear, MIMO and underactuated. No detailed mathematical model of

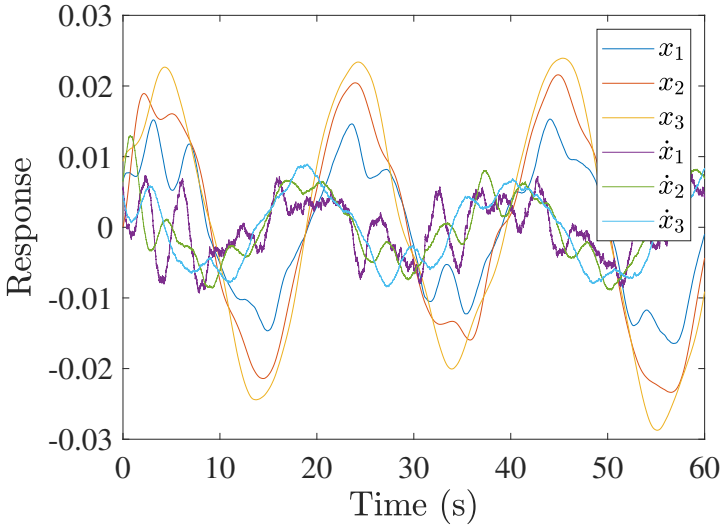

Figure 4.12: Open-loop responses of nonlinear mass-spring-damper system.

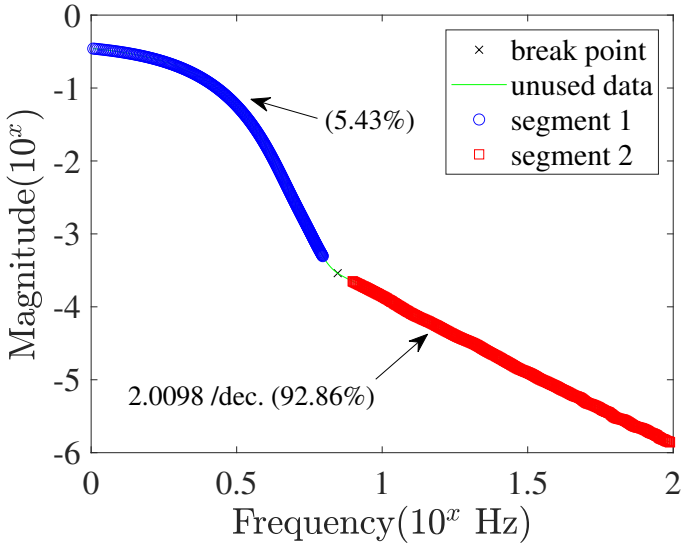

Figure 4.13: The estimated transfer function of chosen output $y_1 = x_1$ to input u_1.

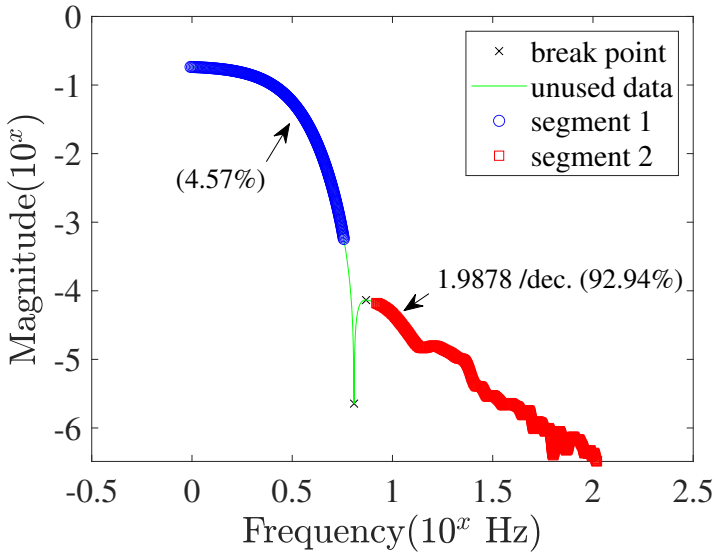

Figure 4.14: The estimated transfer function of chosen output $y_1 = x_1$ to input u_2.

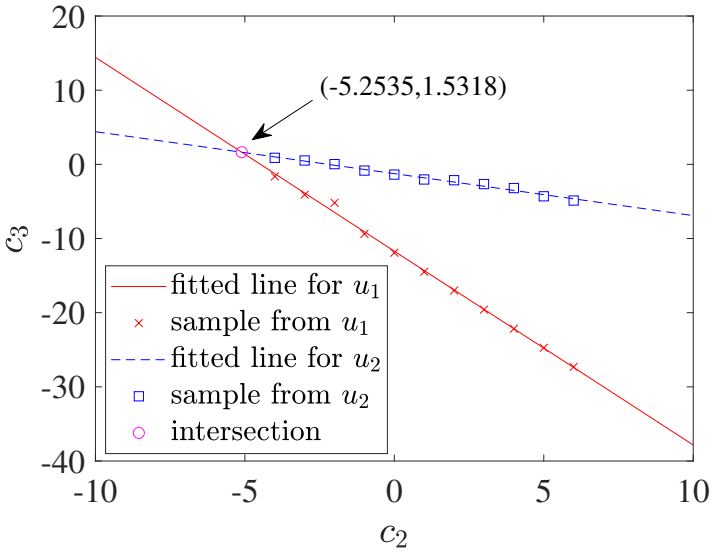

Figure 4.15: The coefficients for y_2 to become locally flat: the intersection indicates the relative degree conditions are both satisfied.

the system is needed. Trial output is written as a linear combination of measured outputs. An optimization problem is proposed to search for the linear combination that leads to the highest relative degree of the trial output. The identification is done in the frequency domain by taking advantage of the asymptotic behavior of transfer functions of linearized systems. Various data handling strategies have been developed to achieve the best estimate of the relative degree in the presence of measurement noise, high frequency dynamics and Nyquist digitization effect. The MFOID algorithm has been tested with two numerical examples of nonlinear dynamic systems.

Chapter 5

FOID-NET: A NEURAL NETWORK FRAMEWORK IDENTIFYING LINEAR DIFFERENTIALLY FLAT OUTPUT USING MEASUREMENTS

In this chapter we introduce a new framework based on neural network aiming to identify linear differentially flat output only using measurements from linear or nonlinear systems. We have seen the powerfulness of flatness in trajectory tracking control design, and also know that the general characterization of flat output highly relies on the mathematical equations of system dynamics. FOID and MFOID algorithm were proposed in the previous chapters to solve the problem of finding locally flat output and make data-driven flatnes-based control feasible. However, the control design based on the framework still requires several additional processes, like characterization of relations between states and flat outputs as we have seen in chapter 3. The FOID-Net, or flat output identification neural network, in this chapter works as a function approximator to automatically construct the best mapping between system's original states and expected flat outputs. Using neural network model has been shown more concise and understandable in solving the FOID problem. For single-input systems, the solution also leads to a well-known result for linear systems, that is, controllability canonical form.

The basics of linear flat output and neural networks will be discussed in Section 5.1. Section 5.2 discusses the structure of FOID-Net and its variants according to systems. In Section 5.3, we propose the several training methods of FOID-Net and emphasize their importance. In Section 5.4, numerical examples are presented to support the efficiency and accuracy of the identification from FOID-Net. The chapter is concluded in Section 5.5.

5.1 Linear Flat Output and Neural Networks

The flat output of the tangent linearization of nonlinear systems near certain equilibrium, or linear flat output alternatively, is generally a vector of functions that consist of linear combination of the original states. As it is mentioned in the previous chapters, the mapping between original states and flat outputs have become purely linear, hence making the identification process much more efficient and feasible. In the case of single-input system, the linear flat output becomes a linear scalar

function of states, which renders a clear relation between states and flat outputs for trajectory tracking control design. Leveraging the property of such local flatness and online disturbance compensators, like extended-state observers from ADRC, the problem of trajectory tracking control of a class of nonlinear systems can be solved straightforwardly.

Neural network is a popular and emerging machine learning and deep learning model because of its capabilities to capture and learn the underlying feature or pattern in large sets of data, approximate strong nonlinear relations between inputs and outputs, and predict time series data. Laying out neural networks in engineering applications is a megatrend for the future. At the same time, however, its interpretability is a challenge in many specific engineering problems. With respect to the problem of flat output identification, neural networks can be used to perform function approximation to help us identify the coordinate transformation from state to flat output, but in the meantime, the nonlinear relationships brought by general neural networks will not allow these results to be 'written out' in mathematical expressions explicitly. To circumvent this issue, in the case of linear flat output identification, we use a purely linear neural network without bias terms, i.e., all network layers satisfy a linear proportional relationship between their inputs and outputs, to carry out the identification process. This method not only helps us to find the corresponding flat output solely by the measured data from systems, but also to figure out the mathematical relationship between the flat output, its successive time derivatives and the states. All these relations will be linear, thanks to the linearity of the network, which can be written in mathematical expressions and completely interpretable. In the next following sections, identification of the linear flat outputs of SIMO nonlinear mechanical systems will be discussed using neural network model.

5.2 FOID-NET Structure

We consider a class of nonlinear mechanical systems interested with single-input that have dynamical equations as Equation (2.1). The controllability of tangent linearization of these system around chosen equilibrium are assumed positive, which is held true for many mechanical systems [39,54,55]. Many applications of control theory, such as system identification and feedback control, need the underlying system to be necessarily controllable. [56] proposes the data-driven controllability test to determine whether a discrete-time linear time-invariant system is controllable. [57] develops a data-driven algorithm that estimates finite-time controllability gramians of linear time-invariant systems, which also provides a way to check the controllability of linear systems without dynamical equations. With the aid of data-driven test of controllability, one may confirm the locally flatness of the system in

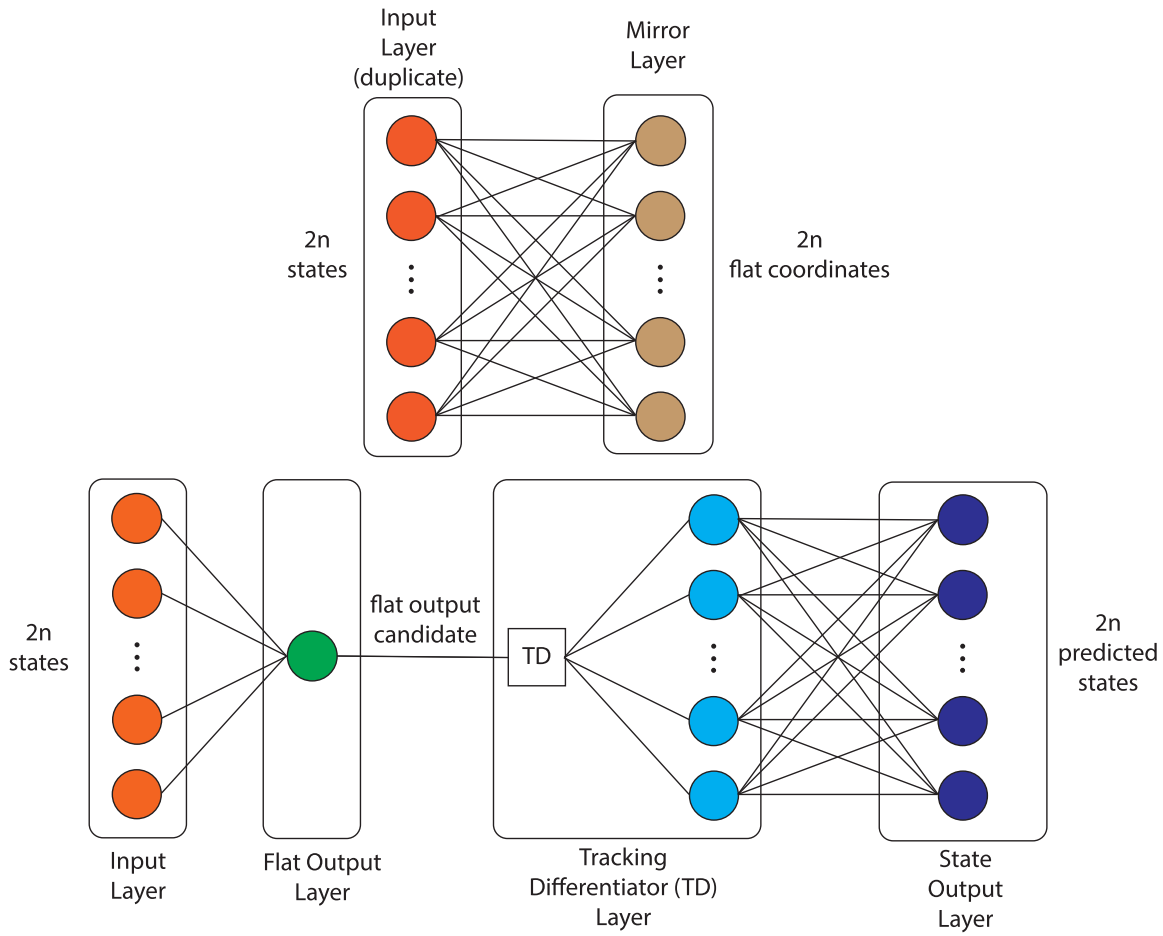

Figure 5.1: General Structure of FOID-Net

the first place before the flat out identification. FOID-Net identifies linear flat output and associated relations between original states for the linearized mechanical system on the basis of its controllability, i.e., flatness.

5.2.1 Basic Structure

The general structure of FOID-Net is shown by Figure 5.1, which is built based on the fact that the linear flat output of single-input linearized system is a linear function of states, and the original state-space states can be recovered using another inversed mapping from flat coordinates if a proper flat output can be found. As shown in Figure 5.1, the input layer has $2n$ input size, where n is the number of degrees of freedom, and the flat output layer follows with only one neuron inside. The output of the flat output layer is a purely linear function of inputs, indicating the flat output candidate would be the product of the weights

of flat output layer and $2n$ states from input layer. The candidate is assumed to have successive time derivatives, up to order of $2n-1$, to complete the expected flat coordinate. To generate time derivatives of the candidate function, a tracking differentiator is placed in the next layer. The task of tracking differentiator is not only to estimate the high-order time derivatives, but also to filter the signal passing through and attenuate the measurement noises and external disturbances. The type of tracking differentiator should be chosen according to the dimension $2n$, as the performance of different tracking differentiators, with linear or nonlinear kernels, varies from case to case. The state output layer predicts the original $2n$ states from the output of TD layer using fully connected $2n$ neurons. The activation function of state output layer is still purely linear. One necessary condition for obtaining a good flat output candidate is that the error between predicted states and original states are minimized as much as possible. In case of finding the flat output for the underlying linearized system, a mirror layer is introduced and fully connected to a duplicate of input layer. The output mirror layer is a linear function of input states, and it is supposed to reproduce the flat coordinates after training. The mirror layer is served as a validation layer, and its weights also characterize the linear mapping between states and flat coordinates, which can be taken as the result for flatness-based control design. The detailed discussion of some specific layers are given in following subsections.

5.2.2 Input State Layer

The FOID-Net needs $2n$ state signals as inputs to implement the identification. For general linear or nonlinear systems, the full-state availability is usually not satisfied, and for this reason, the FOID-Net is not useful to the problems in which states cannot be measured directly or estimated by algorithms. But for mechanical systems with dynamical equations as Equation (2.2), the generalized coordinates chosen are usually angles and displacement, which can be measured by various sensors directly and nicely. Their first-order time derivatives, angular velocities or velocities, are also measurable in case where gyroscope, tachometer or other velocity sensors exist. So do the second order derivatives of them. There are some state estimators or tracking differentiators to estimate the velocities or acceleration, or higher-order time derivatives of generalized coordinates even if those states were not measured from sensors. For these systems, the relations between states are clear and understandable, and they can be used in improving the prediction and identification performance of FOID-Net. Therefore, $2n$ states can be divided into two sets: n generalized coordinates and their n generalized velocities. In following context, the full-state availability is assumed with n generalized coordinates measured, and the rest n states are well-estimated accordingly using a differentiator, as next subsection shows.

5.2.3 TD Layer

The choices of tracking differentiator in FOID-Net remains open. Related work can be found in [58–61]. They can either estimate the remaining n states in input layer, or form the expected flat coordinates in TD layer. Although high-order derivatives of good quality (order greater than 3) are generally hard to obtain due to noise and disturbances, one can still seek the common filter method for ad hoc solution. When the input signals do not fluctuate rapidly with time and noise level is controlled relatively well, the filter expressed by following transfer function $G_D(s)$ handles the derivatives estimation problems:

$$G_D(s) = \frac{r_f^4}{(s + r_f)^4}. \tag{5.1}$$

The fourth-order linear filter with parameter r affecting the position of poles can be also expressed in state-space representation [62]:

$$\begin{aligned} \dot{x}_1 &= x_2, && (5.2)\\ \dot{x}_2 &= x_3, \\ \dot{x}_3 &= x_4, && (5.3)\\ \dot{x}_4 &= f, \\ f &= -r_f(r_f(r_f(r_f(x_1 - v(t)) + 4x_2) + 6x_3) + 4x_4), \end{aligned}$$

where $v(t)$ is the input of the filter, state x_1, x_2, x_3, x_4 are the filtered $v(t)$ and its time derivatives up to order of 3. The function f itself can be viewed as the fourth-order time derivatives of $v(t)$ if needed. The parameter r can be tuned to satisfy better performance while balancing the effect of noise, however overlarge r could cause numerical issue during computation. Implementing such filter during neural network is time-consuming and computationally expensive. In next section, some data preprocessing techniques are adopted to optimize the training process and accelerate the updating of the weights.

5.2.4 State Output Layer

The weights of state output layers form a $2n \times 2n$ matrix that maps flat output candidate and its time derivatives to original states. The linear activation function guarantees the interpretability of the mapping in concrete mathematical expressions. If the $2n$ states are from mechanical systems and have direct differential relations as stated before, the weight matrix can have some special structures that contain some zeros entries and repeated patterns, and hence becomes relatively sparse. This feature indicates that the predicted states are linear functions of selective flat coordinates. So in the actual training process, the state output layer needs not to be a single layer with $2n$ neurons, but may split into several layers with

fewer number of neurons. In next section, an example of fourth-order linearized mechanical system is given to discuss this issue further.

5.2.5 Mirror Layer

The mirror layer and the duplicate input layer constitute a network that validates the correctness of flat coordinates and provides the linear relation between these two layers. The weights of mirror layer is also a $2n \times 2n$ matrix and it is exactly the inverse matrix of weights of state output layer. The output of first neuron in mirror layer should be exactly the output of the flat output layer, that is, the flat output candidate. Therefore, the first row or column (depending on how it lays out) of weight matrix of mirror layer should equal to the weight vector of flat output layer. These constraints all contribute to the design of loss functions, which we shall continue to discuss next. The weights of the mirror layer is the essential information for designing tracking trajectories in flatness-based control, as we have done in Chapter 3.

5.3 Training FOID-NET

The training process of neural network plays an important role in guaranteeing its satisfactory prediction performance and fast convergence. The FOID-Net has customized TD layer that requires heavy computation during training , and hence non-optimized training process could cause extremely slow convergence and may also trap neural network into undesirable local optimal solution. Data preprocessing method is proposed in this section to improve the efficiency of training. The loss functions and optimizer are also given. Due to the non-convexity of the problem and the large number of training parameters, we use a stepwise training approach to approximate the global optimal solution. FOID-Net will be trained several times, and the constraints of the weight parameters will be released step by step, and the initial values of each training can be inherited to the next training until the loss function reaches a preset level.

5.3.1 Data Preprocessing

Assume $2n$ state signals are inputs to FOID-Net. For every update of the weights of flat output layer, the TD block re-computes the $2n$ potential flat coordinates, for example, using the proposed fourth-order filter. However, it is possible to avoid implementing TD block repeatedly by preparing the derivatives of states before training starts. Due to the linearity of the flat output candidate function, denoted by y_f, the i-th time derivatives of y_f can be written as

$$y_f^{(i)} = \mathbf{W}_f^{\mathrm{T}} \mathbf{x}^{(i)}, 0 \leqslant i \leqslant 2n-1, \tag{5.4}$$

where $\mathbf{W}_f$ is the weight vector of flat output layer, and $\mathbf{x} = \begin{bmatrix} x^1 & x^2 & \dots & x^{2n-1} \end{bmatrix}^T$ is the original $2n$ state vector. The TD block can be implemented few times to get $\mathbf{x}^{(i)}$ and the derivatives of y_f are computed by Equation (5.4) directly. Therefore, the TD layer is actually implemented indirectly with data matrices for $\mathbf{x}^{(i)}$ precomputed. These raw data can pass through additional filters to further attenuate noises with specific band of frequency. So the result of data preprocessing stage is that filtered state matrix $\mathbf{W}_\mathbf{x} \in N \times 2n$ and their derivatives matrices $\mathbf{W}_{\mathbf{x}^{(i)}}, 1 \leqslant i \leqslant 2n-1$ are generated for computing the flat output candidate and its time derivatives.

5.3.2 Loss Functions

The loss functions are several criteria defined for FOID-Net to reach optimized performance. The goal of training is to find the proper weight vector of flat output layer that characterizes the flat output for the underlying system, and also the weight matrix of state output layer and mirror layer for mathematical relations between states and flat coordinates. Let $\mathbf{x}_p$ denote the output, predicted state vector, of the state output layer, and the predicted states are $x_p^1, x_p^2, ..., x_p^{2n}$. The loss function $\mathcal{L}_1$ is defined to measure the error of state prediction as follows:

$$\mathcal{L}_1 = \text{MSE}(\mathbf{x}, \mathbf{x}_p) = \frac{1}{2n}\sum_{i=1}^{2n}(x^i - x_p^i)^2. \tag{5.5}$$

Denote the $2n \times 2n$ weight matrix defined by state output layer by $\mathbf{W}_p$, the output vector, flat coordinates, of TD layer by $\mathbf{y}_f$. The loss function $\mathcal{L}_1$ above can be also given by,

$$\mathcal{L}_1(\mathbf{W}_p; \mathbf{x}) = \text{MSE}(\mathbf{x}, \mathbf{W}_p\mathbf{y}_f) = \frac{1}{2n}\sum_{i=1}^{2n}(x^i - \mathbf{w}_p^i\mathbf{y}_f)^2,$$

where $\mathbf{w}_p^i$ is the i-th row of $\mathbf{W}_p$. The loss function $\mathcal{L}_2$ is defined for error between $\mathbf{y}_m$, the output of mirror layer and $\mathbf{y}_f$:

$$\begin{aligned} \mathcal{L}_2(\mathbf{W}_m, \mathbf{W}_f; \mathbf{x}, \dot{\mathbf{x}}, ..., \mathbf{x}^{(i-1)}) &= \text{MSE}(\mathbf{y}_m, \mathbf{y}_f) \\ &= \text{MSE}(\mathbf{W}_m\mathbf{x}, \mathbf{y}_f) \\ &= \frac{1}{2n}\sum_{i=1}^{2n}(\mathbf{w}_m^i\mathbf{x} - y_f^{(i-1)})^2 \\ &= \frac{1}{2n}\sum_{i=1}^{2n}(\mathbf{w}_m^i\mathbf{x} - \mathbf{W}_f^{\mathrm{T}}\mathbf{x}^{(i-1)})^2. \end{aligned} \tag{5.6}$$

Ideally, the mirror layer should duplicate the flat coordinates and the weights should be adjusted to express the inversed mapping of $\mathbf{W}_p$. Therefore this introduces another loss function:

$$\mathcal{L}_3(\mathbf{W}_m, \mathbf{W}_p) = \text{MSE}(\mathbf{W}_m\mathbf{W}_p, I_{2n\times 2n}). \tag{5.7}$$

The structure of $\mathbf{W}_p$ satisfies some special feature that one can make use of to save the cost of training. Since first n states for the interested mechanical systems are integrated signals of last n states, the expression of them in flat coordinates must not contain derivative terms of y_f that have order higher than $2n-2$. A clear example when $n=2$ is illustrated. The predicted states should be a function of flat coordinates. Let the first and second state be the generalized coordinate we choose, then they can be written by

$$x^1 = w^1_{p1} y_f + w^1_{p2} \dot{y}_f + w^1_{p3} \ddot{y}_f \tag{5.8}$$

$$x^2 = w^2_{p1} y_f + w^2_{p2} \dot{y}_f + w^2_{p3} \ddot{y}_f, \tag{5.9}$$

where w^i_{pj} is the element of i-th row and j-th column of $\mathbf{W}_p$. The rest 2 states x^3, x^4 are the time derivative of them, which are given by

$$x^3 = w^3_{p2} \dot{y}_f + w^3_{p3} \ddot{y}_f + w^3_{p4} \dddot{y}_f = \dot{x}^1 = w^1_{p1} \dot{y}_f + w^1_{p2} \ddot{y}_f + w^1_{p3} \dddot{y}_f \tag{5.10}$$

$$x^4 = w^4_{p2} \dot{y}_f + w^4_{p3} \ddot{y}_f + w^4_{p4} \dddot{y}_f = \dot{x}^2 = w^2_{p1} \dot{y}_f + w^2_{p2} \ddot{y}_f + w^2_{p3} \dddot{y}_f, \tag{5.11}$$

This information indicates that $\mathbf{W}_p$ has zero elements, or zero weights that does not require training. The matrix $\mathbf{W}_p$ shows a 'shifted' structure since the coefficients for first and last n states do not change:

$$\mathbf{W}_p = \begin{bmatrix} w^1_{p1} & w^1_{p2} & w^1_{p3} & 0 \\ w^2_{p1} & w^2_{p2} & w^2_{p3} & 0 \\ 0 & w^1_{p1} & w^1_{p2} & w^1_{p3} \\ 0 & w^2_{p1} & w^2_{p2} & w^2_{p3} \end{bmatrix}, \text{when } n = 2. \tag{5.12}$$

The special structure also inspires us to create a new single layer, with number of neurons equal to $2n-1$, to replace state output layer to predict the $2n$ states respectively. The layer should have $2n-1$ inputs and is supposed to have n outputs. The input signals of this layer are first and last $2n-1$ elements of $\mathbf{y}_f$. In this way, the number of trainable weights in $\mathbf{W}_p$ is decreased and hence improve the performance of FOID-Net. Another loss function $\mathcal{L}_4$ we design to involve the weight vector of the flat output layer $\mathbf{W}_f$ directly is aimed to double check the accuracy of the predicted states and $\mathbf{W}_p$:

$$\mathcal{L}_4(\mathbf{W}_p^{-1}, \mathbf{W}_f) = \text{MSE}(\mathbf{w}^1_{ip}, \mathbf{W}_f^{\mathrm{T}}), \tag{5.13}$$

where $\mathbf{w}^1_{ip}$ is the first row of the $\mathbf{W}_p^{-1}$. The total loss function could be the sum of all loss functions defined before, with different weights assigned if necessary:

$$\mathcal{L} = \mathcal{L}_1 + \mathcal{L}_2 + \mathcal{L}_3 + \mathcal{L}_4. \tag{5.14}$$

The adaptive moment estimation, or Adam, optimizer is used in training FOID-Net, which is the most popular stochastic optimization method in machine

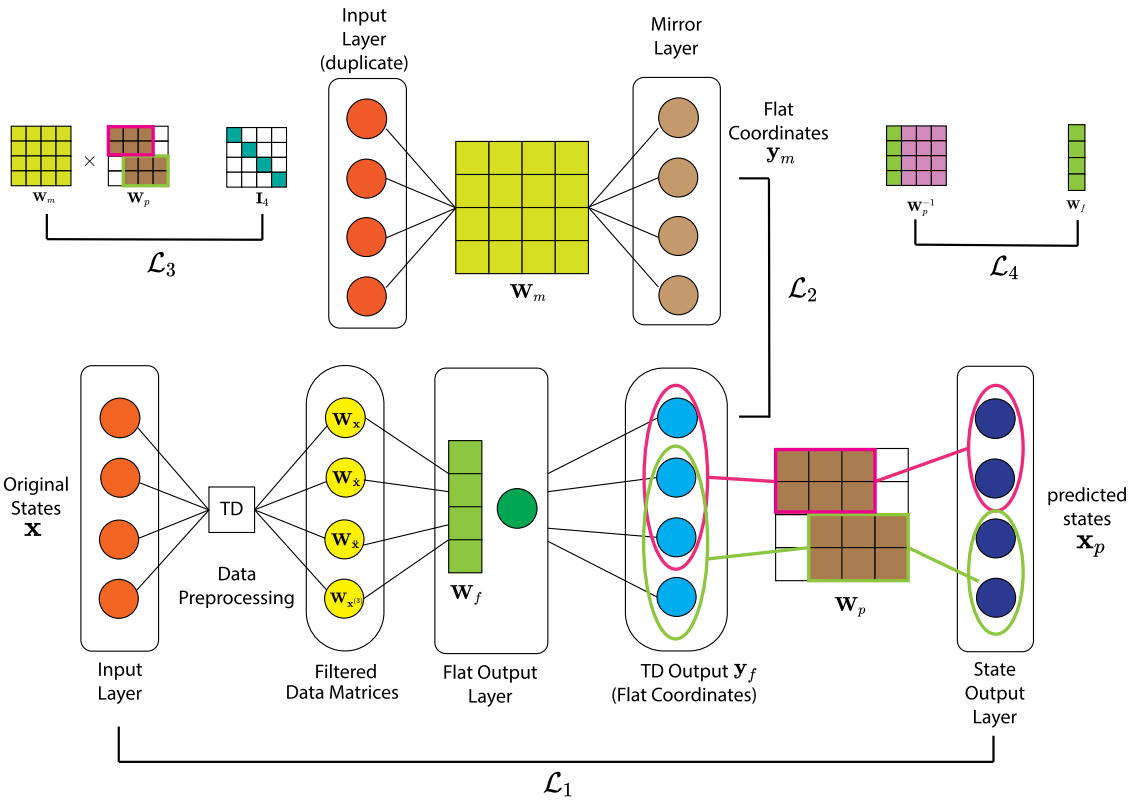

Figure 5.2: The structure and loss functions of FOID-Net for two degrees-of-freedom underactuated mechanical systems.

learning and deep learning community. The details of Adam optimization can be found in [63]. Traditional stochastic gradient descent(SGD) algorithm maintains a single learning rate to update all weights, and the learning rate does not adaptively change during the training process. In contrast, Adam provides each trainable weight with its own adaptive learning rate by computing first-order moment estimates and second-order moment estimates of the gradient. The gradient needed for Adam will be calculated from the partial derivatives of loss function $\mathcal{L}$ for all trainable weights in corresponding weight matrix. Figure 5.2 shows the actual structure when implementing the FOID-Net and illustrates the loss function definition.

5.3.3 Re-initialization with Weight Constraints

There are infinitely many solutions for a flat output candidate of single-input system even if the system has low dimension in state-space model. Therefore, many sets of weights in flat output layer, or the elements in $\mathbf{W}_f$, can theoretically minimized the loss functions, which are all considered correct. When n is getting larger, the number of trainable weights in each layer grow so that the training task gets extremely hard and the neural network could trap itself into local minima even if with numerous training epochs. The different result of initialization of the weights in each layer could cause cause them to converge locally to undesirable values. If n is relatively not that large ($n = 2, 3$), we introduce the re-initialization technique which re-trains the FOID-Net with initial weights immigrated from previous pre-trained FOID-Net. More specifically, we put some weight constraints to the weight vector of flat output layer $\mathbf{W}_f$ that last n weights that represent the coefficients of generalized velocities in expression of flat output candidate are set to zero in the first-time training, which agrees with our assumption of reduced linearized model. Many flat output of linearized mechanical systems have dominant components with generalized coordinates, i.e., first n states. When the damping and Coriolis force effect can be ignored, the flat output would be purely a linear combination of generalized coordinates, as we have shown in Chapter 3. After the first training reaches the expected loss, the trained weights are immigrated to initialize next training, where the weight constraints for $\mathbf{W}_f$ are released. In this way, the training is going to hit the endpoint with satisfactory results better than the one from random initialization and large-epoch iteration.

5.4 Numerical Simulation

5.4.1 Furuta Pendulum

5.4.1.1 Simulation Setting

We use Furuta pendulum model from Chapter 2 to generate the data of states for FOID-Net training. The dynamic equations are given by Equation (2.16) and

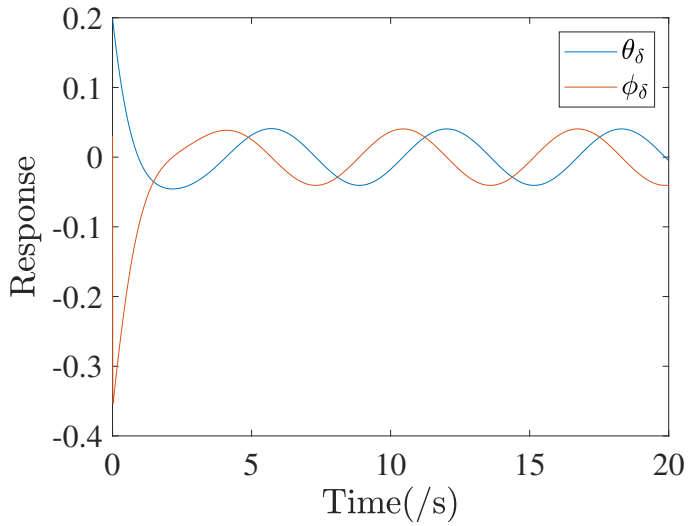

Figure 5.3: Closed-loop Response of Furuta Pendulum with θ_δ and ϕ_δ outputs.

Equation (2.17). The four gains of the LQR control is given by

$$K_e = \begin{bmatrix} 33.4754 & 11.9579 & -1.0000 & -1.9512 \end{bmatrix}.$$

As we have mentioned before, such closed-loop control does not change the flat output or flatness of the system. The input signal is a simple signal $u(t) = \sin(t) + \cos(t)$, which alleviates the burden of TD to calculate the derivatives of output states and improve the accuracy of the result. The output equation is given as Equation, so only two states, ϕ_δ and θ_δ, are assumed to be measurable. The sample frequency f_s is 1kHz, the data length for each output state is of 20 second simulation time. The closed-loop responses collected for data preprocessing is shown in Figure 5.3.

The FOID-Net structure is designed as Figure 5.2 has shown. The filter described by Equation (5.3) is adopted to retrieve the first-order derivatives of ϕ_δ and θ_δ, completing the full-state assumption, and to estimate the data matrices $\mathbf{W}_{\mathbf{x}^{(i)}}$ for constructing the flat coordinates. The parameter r_f is chosen 150 by inspecting the output of filter before training, and this number should not be too large to prevent numerical instability issue. The initial stepsize or learning rate α of Adam optimizer is chosen as 0.5. FOID-Net is built and tested in the environment of Tensorflow v2.7.0 using APIs from Keras module.

5.4.1.2 Simulation results

Two trainings with different initialization of weights can be carried out. The first initialization is set up by random normalized numbers from Keras API, alias 'random normal'.The learning rate α are decreased from 0.5 to 0.001 in second

Table 5.1: Result of 1st training FOID-Net for Furuta Pendulum

Description	Value
Number of Epochs	2500
learning rate α	0.5
Best Ratio C_r	-0.8969067931175232
Min Total Loss $\mathcal{L}$	$2.0981655 \times 10^{-10}$
Loss $\mathcal{L}_1$	$5.681606574103881 \times 10^{-11}$
Loss $\mathcal{L}_2$	$1.0597643596010897 \times 10^{-10}$
Loss $\mathcal{L}_3$	$4.584249299610654 \times 10^{-11}$
Loss $\mathcal{L}_4$	$1.1815586486649265 \times 10^{-12}$
$\mathbf{W}_f^{\mathrm{T}}$	$\begin{bmatrix}-0.07344062, 0.12577936, 0, 0\end{bmatrix}$
$\mathbf{W}_p$	$\begin{bmatrix}-2.079355, -0.3350958, -0.97297806, 0 \\ 4.9324055, -1.0919425, -1.2145464, 0 \\ 0, -2.079355, -0.3350958, -0.97297806 \\ 0, 4.9324055, -1.0919425, -1.2145464\end{bmatrix}$
$\mathbf{W}_m$	$\begin{bmatrix}-0.15758981, 0.14609472, -0.00404385, 0.01143858 \\ -0.0509068, -0.01741791, -0.16682577, 0.13230194 \\ -0.63749486, -0.10790826, 0.16682497, -0.04175542 \\ 0.37350577, 0.01207666, -0.86133194, -0.23466454\end{bmatrix}$
Weights Initialization	Random Normal

training. In the first training, we manually set the last 2 weights of $\mathbf{W}_f$ to zero. The ratio of first two states and value of loss function is observed. For each epoch, we feed the whole batch of data of length 19800 to FOID-Net. First 200 elements of each column of the data matrices $\mathbf{W}_{\mathbf{x}^{(i)}}$ are cut because of the common bad transition behavior of the TD. The minimum value of loss function and the corresponding ratio and weight matrices are recorded for each training.

Table 5.1 shows the result of first training after 2500 epochs. We trained first two weights to some level where the total loss $\mathcal{L}$ reaches a local minimum at 645-th epoch and it maintains the minimum for next 1500 epochs. Therefore an early stop of training is called because the minimum loss is already at a low value and overtraining the neural network may cause overfitting problem since we have two trainable weights in $\mathbf{W}_f$ set to be zeros. The results are used to initiate next training where we use smaller learning rate for Adam. Figure 5.4 and Figure 5.4 manifest the ratio change and the epoch in which value of $\mathcal{L}$ hits the local minimum during the training.

Table 5.2 shows the result of second training after 3250 epochs. The learning

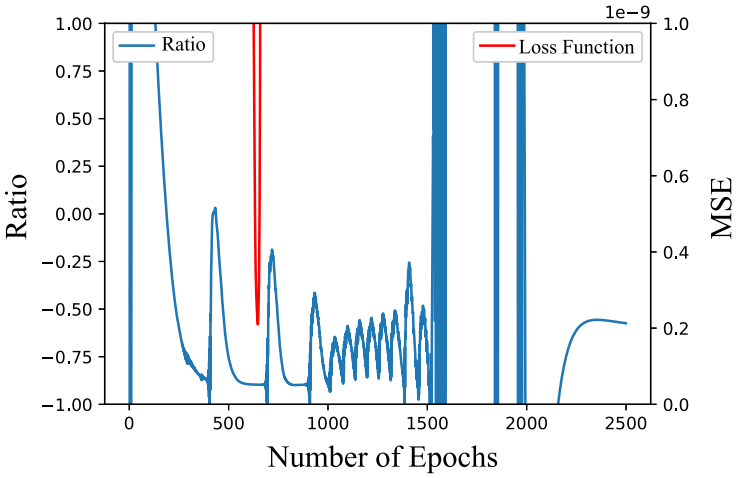

Figure 5.4: Ratio between first 2 weights in $\mathbf{W}_f$ within $(-1, 1)$ and Value of Loss function $\mathcal{L}$ within 2500 epochs. At 645-th epoch, value of $\mathcal{L}$ reaches the minimum.

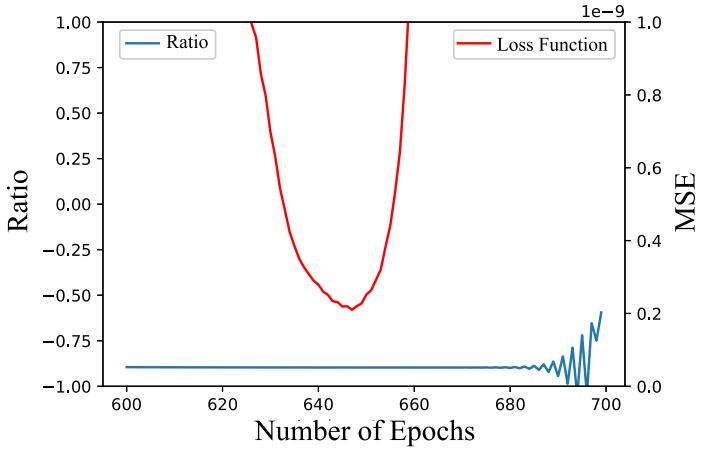

Figure 5.5: Ratio between first 2 weights in $\mathbf{W}_f$ within $(-1, 1)$ and Value of Loss function $\mathcal{L}$ between 600 and 700 epochs. At 645-th epoch, value of $\mathcal{L}$ reaches the minimum. Zoom view of Figure 5.4.

rate is decreased because we are expected to search a solution based on our baseline model, the model with our previous trained $\mathbf{W}_f^{\mathrm{T}}, \mathbf{W}_p, \mathbf{W}_m$. In the second training, we let the 4 weights in $\mathbf{W}_f^{\mathrm{T}}$ become trainable and may add a optional new penalty term in loss function to 'punish' the norm of last two weights, which is based on our knowledge of the system that it is lightly damped. In the simulation case, we have linearized the Furuta pendulum around the origin, so the damping terms are actually removed from the dynamics, which has been validated by the result shown in the Table 5.2. Figure 5.6 and Figure 5.7 gives the ratio change and value of loss function close to the minimum. We rearrange the order of states and write out the matrices of closed-loop state-space representation of the linearized Furuta pendulum with all variables substituted:

$$\mathbf{x} = \begin{bmatrix} \theta_\delta \\ \phi_\delta \\ \dot{\theta}_\delta \\ \dot{\phi}_\delta \end{bmatrix}, \mathbf{A} = \begin{bmatrix} 0 & 0 & 1 & 0 \\ 0 & 0 & 0 & 1 \\ -611.4987 & 19.2397 & -230.0666 & 37.5404 \\ -571.2377 & 17.2605 & -206.3995 & 33.6786 \end{bmatrix}, \mathbf{B} = \begin{bmatrix} 0 \\ 0 \\ 19.2397 \\ 17.2605 \end{bmatrix}. \tag{5.15}$$

The transformation matrix for $\mathbf{x}$ to become flat coordinates can be found through process of transforming controllable pair $(\mathbf{A}, \mathbf{B})$ into controllability canonical form $(\mathbf{A}_c, \mathbf{B}_c)$. Let $\mathbf{y}_f = \mathbf{T}\mathbf{x}$, the transformation matrix $\mathbf{T}$ and its inverse $\mathbf{T}^{-1}$ are given by

$$\mathbf{T} = \begin{bmatrix} 0.0021 & -0.0023 & 0 & 0 \\ 0 & 0 & 0.0021 & -0.0023 \\ 0.0520 & 0 & 0 & 0 \\ 0 & 0 & 0.0520 & 0 \end{bmatrix}, \tag{5.16}$$

$$\mathbf{T}^{-1} = \begin{bmatrix} 0 & -0.0001 & 19.2397 & 0 \\ -435.6687 & 0.0001 & 17.2605 & 0 \\ 0.0520 & 0 & -0.0001 & 19.2397 \\ 0 & -435.6687 & 0.0001 & 17.2605 \end{bmatrix}. \tag{5.17}$$

One can immediately get the one of the flat output of the linearized Furuta pendulum is

$$y_f = 0.0021\theta_\delta - 0.0023\phi_\delta = 0.0023(-0.8971\theta_\delta + \phi_\delta). \tag{5.18}$$

$\mathbf{W}_f^{\mathrm{T}}$ trained is $\left[0.20245, -0.22568, -1.2678 \times 10^{-6}, 1.2313 \times 10^{-6}\right]$, which is roughly 100 times of the first row of $\mathbf{T}$. It gives us another flat output of the form:

$$y_{fnn} = 0.20245\theta_\delta - 0.22568\phi_\delta - 1.2678 \times 10^{-6}\dot{\theta}_\delta + 1.2313 \times 10^{-6}\dot{\phi}_\delta \approx 100 y_f. \tag{5.19}$$

$\mathbf{W}_m$ is the identified matrix of $\mathbf{T}$, it also satisfies that $\mathbf{W}_m \approx 100\mathbf{T}$. And $\mathbf{W}_p$, the estimate of the $\mathbf{T}^{-1}$, is around $1/100\mathbf{T}^{-1}$. Hence we could prove that identified y_{fnn} is indeed a linear flat output of the Furuta pendulum near origin.

Table 5.2: Result of 2nd training FOID-Net for Furuta Pendulum

Description	Value
Number of Epochs	3250
learning rate α	0.001
Best Ratio C_r	-0.8971047401428223
Min Total Loss $\mathcal{L}$	9.639888×10^{-14}
Loss $\mathcal{L}_1$	$9.009180493367141 \times 10^{-15}$
Loss $\mathcal{L}_2$	$7.182695735928613 \times 10^{-14}$
Loss $\mathcal{L}_3$	$1.499903750734697 \times 10^{-14}$
Loss $\mathcal{L}_4$	$5.637120731007616 \times 10^{-16}$
$\mathbf{W}_f^{\mathrm{T}}$	$\begin{bmatrix} 0.20245, -0.22568, -1.2678 \times 10^{-6}, 1.2313 \times 10^{-6} \end{bmatrix}$
$\mathbf{W}_p$	$\begin{bmatrix} -3.9985 \times 10^{-7}, -6.8630 \times 10^{-7}, 0.19568, 0 \\ -4.4311, -2.7582 \times 10^{-5}, 0.17554, 0 \\ 0, -3.9985 \times 10^{-7}, -6.8630 \times 10^{-7}, 0.19568 \\ 0, -4.4311, -2.7582 \times 10^{-5}, 0.17554 \end{bmatrix}$
$\mathbf{W}_m(\times 10^{-8})$	$\begin{bmatrix} 2.0245 \times 10^{7}, -2.2568 \times 10^{7}, -111.31, 143.56 \\ -3072.6, -10.289, 2.0245 \times 10^{7}, -2.2568 \times 10^{7} \\ 5.1104 \times 10^{8}, -47.308, 327.68, -126.40 \\ 2.2089 \times 10^{-5}, 4.1427 \times 10^{-8}, 5.1103, -5.5076 \times 10^{-7} \end{bmatrix}$
Weights Initialization	$\mathbf{W}_f^{\mathrm{T}}, \mathbf{W}_p, \mathbf{W}_m$ from previous training

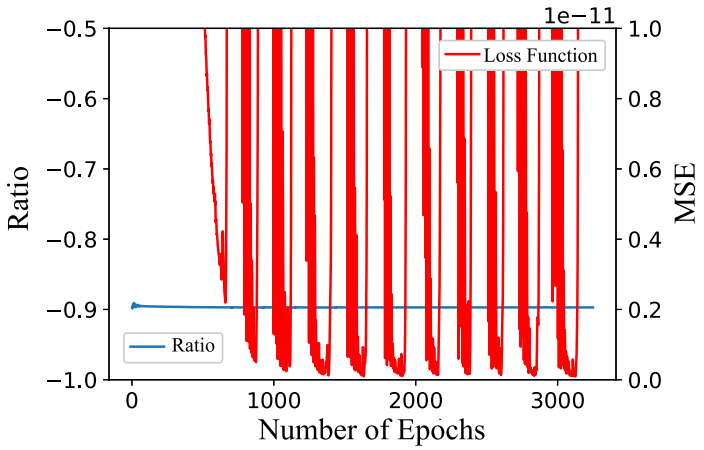

Figure 5.6: Ratio between first 2 weights in $\mathbf{W}_f$ within $(-1, -0.5)$ and Value of Loss function $\mathcal{L}$ within 3250 epochs. At 3122-th epoch, value of $\mathcal{L}$ reaches the minimum.

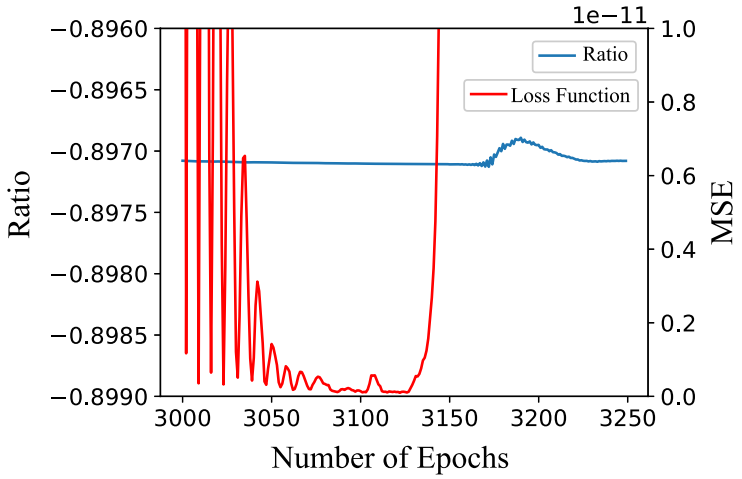

Figure 5.7: Ratio between first 2 weights in $\mathbf{W}_f$ within $(-0.8990, -0.8960)$ and Value of Loss function $\mathcal{L}$ between 3000 and 3250 epochs. At 3122-th epoch, value of $\mathcal{L}$ reaches the minimum.

5.4.2 A Nonlinear Fourth-Order UMS

We consider a two degrees-of-freedom nonlinear UMS. The linearized system is controllable near the origin. By defining the first two states x_1, x_2 as its two generalized coordinates, the state-space equations are given by

$$\begin{aligned}
\dot{x}_1 &= x_3, \\
\dot{x}_2 &= x_4, \\
\dot{x}_3 &= -15.4737x_1 + 27.13x_2 + 13.5185x_3 + 16.8618x_4 \\
&\quad + 0.8751x_1^3 + 0.422\sin(x_2)x_2 - u(t), \\
\dot{x}_4 &= 18.7105x_1 - 34.1949x_2 - 17.2778x_3 - 22.7927x_4 \\
&\quad + 0.4080\sin(x_3) + 0.1280x_4^3 + 1.5u(t),
\end{aligned}$$

where $u(t)$ is the input signal. Signals of first two states as outputs are collected from simulation. The sample frequency f_s is 1kHz and the simulation time is 20 seconds. The input signal is chosen $u(t) = 0.1H$, where H is unit step function. The system is slightly stimulated around the origin to get the linearized state information. In this simulation, we assume the outputs are measured with some level of noise. The occurrence of noise in FOID-Net certainly would affect the performance of identification to some degree. We set the singal-to-noise ratio level of output channel to 80dB. The responses of first two outputs are given by Figure 5.8. At the data preprocessing stage, we use the proposed fourth-order filter to filer the these two signals, and generate their first-order derivatives. The phase is compensated by

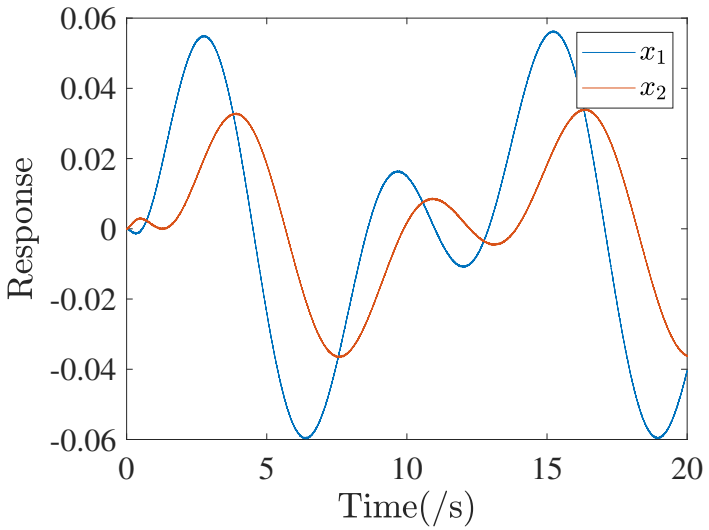

Figure 5.8: Open-loop response x_1, x_2 of a fourth-order nonlinear UMS

shifting the 4 outputs of the filter until the phase of original states can match with the filtered states. The r is set to 10 because the level of noise is high.

We totally perform 2 trainings to identify the best flat output for the given fourth-order system. Table 5.3 and Table 5.4 have shown the result of two consecutive trainings. We set the last two states to zero in the first training, and release the constraint in the second training. The results show that the flat output candidate is

$$y_f = 2.9593787x_1 + 1.9837099x_2 - 0.13599189x_3 - 0.08895281x_3 \tag{5.20}$$

To verify the accuracy of this flat output candidate function. We find the best linearized system assosciated with y_f

$$\mathbf{A}_y = \begin{bmatrix} 0 & 0 & 1 & 0 \\ 0 & 0 & 0 & 1 \\ -15.564 & 27.202 & 13.419 & 16.865 \\ 18.764 & -34.194 & -16.743 & -22.747 \end{bmatrix}, \mathbf{B}_y = \begin{bmatrix} 0 \\ 0 \\ -0.9786 \\ 1.4955 \end{bmatrix},$$

where

$$\mathbf{W}_m\mathbf{A}_y\mathbf{W}_m^{-1} \approx \begin{bmatrix} 0 & 1 & 0 & 0 \\ 0 & 0 & 1 & 0 \\ 0 & 0 & 0 & 1 \\ -22.099 & -34.369 & -27.193 & -9.342 \end{bmatrix}, \frac{1}{30.8642}\mathbf{W}_m\mathbf{B}_y = \begin{bmatrix} 0 \\ 0 \\ 0 \\ 1 \end{bmatrix}.$$

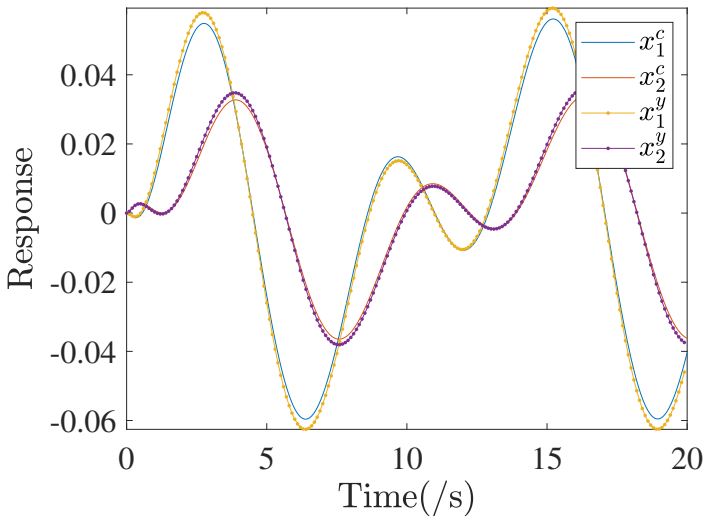

Figure 5.9: The response of system $(\mathbf{A}_y, \mathbf{B}_y)$ with outputs x_1^y, x_2^y and of system $(\mathbf{A}_c, \mathbf{B}_c)$ with outputs x_1^c, x_2^c when input is chosen as $u(t) = 0.1(\sin(t) + \cos(\frac{1}{2}t))$

Therefore we know $\mathbf{W}_m$ tranforms system $(\mathbf{A}_y, \mathbf{B}_y)$ to controllability canonical form. We compare the open-loop responses from system $(\mathbf{A}_y, \mathbf{B}_y)$ with one from linearized system $(\mathbf{A}_c, \mathbf{B}_c)$ around origin of original nonlinear system given by,

$$\mathbf{A}_c = \begin{bmatrix} 0 & 0 & 1 & 0 \\ 0 & 0 & 0 & 1 \\ -15.4737 & 27.13 & 13.5185 & 16.8618 \\ 18.7105 & -34.1949 & -16.8698 & -22.7927 \end{bmatrix}, \mathbf{B}_c = \begin{bmatrix} 0 \\ 0 \\ -1 \\ 1.5 \end{bmatrix}.$$

Figure 5.9 has shown the simulation difference between system $(\mathbf{A}_y, \mathbf{B}_y)$ and linearized system $(\mathbf{A}_c, \mathbf{B}_c)$. We can see y_f defines a canonical transformation for system $(\mathbf{A}_y, \mathbf{B}_y)$ and their responses are pretty close, which proves the choice of y_f is excellent. We further find that the canonical transformation matrix of linearized system $(\mathbf{A}_c, \mathbf{B}_c)$ is

$$T_c = \begin{bmatrix} 0.1051 & 0.0704 & -0.0024 & -0.0016 \\ 0.0072 & -0.0104 & 0.0997 & 0.0664 \\ -0.2990 & 0.4318 & 0.2336 & 0.1557 \\ -0.7008 & 1.0122 & 0.2317 & 0.8212 \end{bmatrix} \approx \frac{1}{30.8642}\mathbf{W}_m.$$

Such relationship between them again validates y_f.

.

Table 5.3: Result of 1st training FOID-Net for 4D UMS

Description	Value
Number of Epochs	15000
learning rate α	0.5
Best Ratio C_r	1.439252495765686
Min Total Loss $\mathcal{L}$	7.050812×10^{-5}
Loss $\mathcal{L}_1$	$2.2563683899079479 \times 10^{-7}$
Loss $\mathcal{L}_2$	$6.911051605129614 \times 10^{-5}$
Loss $\mathcal{L}_3$	$1.1718325367837679 \times 10^{-6}$
Loss $\mathcal{L}_4$	$1.3576725854669291 \times 10^{-10}$
$\mathbf{W}_f^{\mathrm{T}}$	$\begin{bmatrix} 3.1899514, 2.2163947, 0, 0 \end{bmatrix}$
$\mathbf{W}_p$	$\begin{bmatrix} 0.21257, 0.078292, -0.033500, 0 \\ 0.14524, -0.11268, 0.048215, 0 \\ 0, 0.21257, 0.078292, -0.033500 \\ 0, 0.14524, -0.11268, 0.048215 \end{bmatrix}$
$\mathbf{W}_m$	$\begin{bmatrix} 3.1900, 2.2164, -1.4047 \times 10^{-6}, -7.6989 \times 10^{-5} \\ -1.1735 \times 10^{-3}, -4.1814 \times 10^{-3}, 3.1867, 2.2217 \\ -9.6222, 1.4022, 7.4215, 5.2362 \\ -22.4910, 32.753, 7.7297, 26.317 \end{bmatrix}$
Weights Initialization	Random Normal

Table 5.4: Result of 2nd training FOID-Net for 4D UMS

Description	Value
Number of Epochs	15000
learning rate α	0.001
Best Ratio C_r	1.4918404817581177
Min Total Loss $\mathcal{L}$	6.444609×10^{-6}
Loss $\mathcal{L}_1$	$1.8805332047122647 \times 10^{-7}$
Loss $\mathcal{L}_2$	$6.386674067471176 \times 10^{-5}$
Loss $\mathcal{L}_3$	$3.895050895152963 \times 10^{-7}$
Loss $\mathcal{L}_4$	$1.7926575779370069 \times 10^{-9}$
$\mathbf{W}_f^{\mathrm{T}}$	$\begin{bmatrix}2.9593787, 1.9837099, -0.13599189, -0.08895281\end{bmatrix}$
$\mathbf{W}_p$	$\begin{bmatrix}0.23190, 0.094644, -0.031693, 0\\ 0.15815, -0.11820, 0.048464, 0\\ 0, 0.23190, 0.094644, -0.031693\\ 0, 0.15815, -0.11820, 0.048464\end{bmatrix}$
$\mathbf{W}_m$	$\begin{bmatrix}2.9594, 1.9837, -0.13599, -0.088947\\ 0.44390, -0.65242, 2.6268, 1.7183\\ -8.5725, 12.536, 6.8313, 4.4821\\ -22.356, 32.700, 8.0806, 25.957\end{bmatrix}$
Weights Initialization	$\mathbf{W}_f^{\mathrm{T}}, \mathbf{W}_p, \mathbf{W}_m$ from previous training

5.5 Conclusions

In this chapter, a novel neural network framework called FOID-Net is proposed to solve FOID problem for tangent linearized UMSs. We use the time series of data and their derivatives, generated by tracking differentiator, to train a autoencoder-like neural network. The basic structure of FOID-Net, definitions of loss functions and training techniques are discussed. The numerical simulations have shown that FOID-Net can identify the flat output of linear system and locally flat output of nonlinear systems around equilibrium point. It has good capability of rejecting noise as long as the TD has strong noise rejection feature. A convincing result can be obtained if sufficient training is available. As the dimension of the underlying systems grows, a more systematic training method needs to be developed in the future.

Chapter 6

SUMMARY AND FUTURE WORK

6.1 Concluding Remarks

This thesis mainly discusses how data-driven approach can be used to identify the flat output of a nonlinear UMSs at the equilibrium point. The identification method involves transfer function estimation in the frequency domain, data fitting and regression, sparse identification, algebraic method dealing with high-order derivatives estimation, and the construction and training of neural networks. The results of the identification can be combined with the ADRC framework, or other disturbance-observer-based control for the tracking control design of the UMS. This set of approaches allow the trajectory tracking control of many UMSs that are not inherently differentially flat to be handled using properties of differentially flat systems, which greatly simplifies the control design of this special class of mechanical systems. Moreover, the data-driven framework does not rely heavily on model information, which reduces the difficulty of control design to a large extent further, even if it has not achieved completely model-free control yet. For fully actuated systems, this approach can still be applied, which is one of the advantages of this framework. A lot of significant research problems, such as implementation of high-order ESO in practical control application, can be derived from the topic. We believe the data-driven thoeries and methods on flatness-based control and ADRC could be further developed in a bright future.

6.2 Future Work

6.2.1 FOID-Net For MIMO System

It is not hard to extend the current FOID-Net to MIMO system, while the training of network may become extremely hard when the number of inputs increases. Indeed, the number of trainable weights may become too large for one to find a satisfactory solution from the network. Nevertheless, the MIMO version of FOID-Net has a chance to work for lower number of inputs, for example, 2 or 3. The flat output is no longer a single function but has two components that are functions of all states. MIMO FOID problem may be solved with practical training approaches in the future work.

6.2.2 Nonlinear Flat Output Identification

Nonlinear flat output, due to its complex mathematical expression in terms of states, is not the primary function aimed to be identified in this thesis. With structure of FOID-Net, we may use nonlinear activation function in flat output layer and state output layer to approximate the nonlinear mapping between states and flat coordinates. Then the nonlinear mapping needs to be reinterpreted by new function approximators or a neural network that provide us with better mathematical interpretability. For example, if polynomials of states can approximate the identified nonlinear mapping well, we may replace the trained nonlinear mapping with a simpler and more understandable expression between state and flat coordinates. In this way, a data-driven nonlinear flat output identification can be done.

BIBLIOGRAPHY

[1] Liu Y, Yu H (2013) A survey of underactuated mechanical systems. *IET Control Theory & Applications* **7**(7), 921–935

[2] Krafes S, Chalh Z, Saka A (2018) A review on the control of second order underactuated mechanical systems. *Complexity* **2018**

[3] Emran BJ, Najjaran H (2018) A review of quadrotor: An underactuated mechanical system. *Annual Reviews in Control* **46**, 165–180

[4] He B, Wang S, Liu Y (2019) Underactuated robotics: a review. *International Journal of Advanced Robotic Systems* **16**(4), 1729881419862,164

[5] Fliess M, Lévine J, Martin P, Rouchon P (1995) Flatness and defect of nonlinear systems: introductory theory and examples. *International Journal of Control* **61**(6), 1327–1361

[6] Murray R, Rathinam M, Sluis W (1995) Differential flatness of mechanical control systems: A catalog of prototype systems

[7] Sira–Ramírez H, Zurita-Bustamante EW, Hernández-Flores E (2017) On the adrc of non-differentially flat, underactuated, nonlinear systems: An experimental case study. *ASME 2017 International Design Engineering Technical Conferences and Computers and Information in Engineering Conference*

[8] Lévine J, Nguyen DV (2003) Flat output characterization for linear systems using polynomial matrices. *Systems & Control Letters* **48**(1), 69–75

[9] Charlet B, Lévine J, Marino R (1989) On dynamic feedback linearization. *Systems & Control Letters* **13**(2), 143–151

[10] Charlet B, Lévine J, Marino R (1991) Sufficient conditions for dynamic state feedback linearization. *SIAM Journal on Control and Optimization* **29**(1), 38–57

[11] Aranda-Bricaire E, Moog CH, Pomet JB (1995) A linear algebraic framework for dynamic feedback linearization. *IEEE Transactions on Automatic Control* **40**(1), 127–132

[12] Rathinam M, Murray RM (1998) Configuration flatness of lagrangian systems underactuated by one control. *SIAM Journal on Control and Optimization* **36**(1), 164–179

[13] Chetverikov VN (2001) New flatness conditions for control systems. *IFAC Proceedings Volumes* **34**(6), 191–196

[14] Schlacher K, Schöberl M (2007) Construction of flat outputs by reduction and elimination. *IFAC Proceedings Volumes* **40**(12), 693–698

[15] Antritter F, Lévine J (2010) *Flatness characterization: Two approaches*. Springer, Berlin, Heidelberg

[16] Lévine J (2011) On necessary and sufficient conditions for differential flatness. *Applicable Algebra in Engineering, Communication and Computing* **22**(1), 47–90

[17] Yong SZ, Paden B, Frazzoli E (2015) Computational methods for mimo flat linear systems: Flat output characterization, test and tracking control. *2015 American Control Conference (ACC)* pp 3898–3904

[18] Campbell SL, Terrell WJ (1995) Determining flatness for complex nonlinear systems. In: *Proceedings of IEEE Southeastcon'95: Visualize the Future*, pp 118–122

[19] Sira-Ramírez H, Oliver-Salazar MA (2012) On the robust control of buck-converter dc-motor combinations. *IEEE Transactions on Power Electronics* **28**(8), 3912–3922

[20] Ramírez-Neria M, e L García-Antonio J, Sira-Ramírez H, Velasco-Villa M, Castro-Linares R (2013) An active disturbance rejection control of leader-follower thomson's jumping rings. *Control Theory & Applications* **30**(12), 1564–1572

[21] Sira-Ramírez H, Linares-Flores J, García-Rodríguez C, Contreras-Ordaz MA (2014) On the control of the permanent magnet synchronous motor: an active disturbance rejection control approach. *IEEE Transactions on Control Systems Technology* **22**(5), 2056–2063

[22] Huang C, Sira-Ramírez H (2015) Flatness-based active disturbance rejection control for linear systems with unknown time-varying coefficients. *International Journal of Control* **88**(12), 2578–2587

[23] Ramírez-Neria M, Sira-Ramírez H, Garrido-Moctezuma R, Luviano-Juarez A (2014) Linear active disturbance rejection control of underactuated systems: The case of the Furuta pendulum. *ISA Transactions* **53**(4), 920–928

[24] Ramŕez-Neria M, Sira-Ramŕez H, e Garrido-Moctezuma R, Luviano-Juárez A (2016) On the linear control of underactuated nonlinear systems via tangent flatness and active disturbance rejection control: The case of the ball and beam system. *Journal of Dynamic Systems, Measurement, and Control* **138**(10), 104,501

[25] Ramírez-Neria M, Sira-Ramírez H, Garrido-Moctezuma R, Luviano-Juárez A (2019) Active disturbance rejection control of the inertia wheel pendulum through a tangent linearization approach. *International Journal of Control, Automation and Systems* **17**(1), 18–28

[26] Ramírez-Neria M, Gao Z, Sira-Ramírez H, Garrido-Moctezuma R, Luviano-Juarez A (2020) On the tracking of fast trajectories of a 3dof torsional plant: A flatness based adrc approach. *Asian Journal of Control* **https://doi.org/10.1002/asjc.2300**

[27] Sira-Ramírez H, Zurita-Bustamante E, Hernandez-Flores E, Aguilar-Orduña MA (2018) On a linear input–output approach for the control of nonlinear flat systems. *International Journal of Control* **91**(9), 2131–2146

[28] Brunton SL, Proctor JL, Kutz JN (2016) Discovering governing equations from data by sparse identification of nonlinear dynamical systems. *Proceedings of the national academy of sciences* **113**(15), 3932–3937

[29] Mangan NM, Kutz JN, Brunton SL, Proctor JL (2017) Model selection for dynamical systems via sparse regression and information criteria. *Proceedings of the Royal Society A: Mathematical, Physical and Engineering Sciences* **473**(2204), 20170,009

[30] Fliess M, Sira–Ramírez H (2003) An algebraic framework for linear identification. *ESAIM: Control, Optimisation and Calculus of Variations* **9**, 151–168

[31] Leylaz G, Ma SF, Sun JQ (2020) An optimal model identification algorithm of nonlinear dynamical systems with the algebraic method. *Journal of Vibration and Acoustics* **143**(2)

[32] Fliess M, Lévine J, Martin P, Rouchon P (1999) A Lie-Bäcklund approach to equivalence and flatness of nonlinear systems. *IEEE Transactions on Automatic Control* **44**(5), 922–937

[33] Li Z, Jiang J, Hong L, Sun JQ (2019) On the data-driven generalized cell mapping method. *International Journal of Bifurcation and Chaos* **29**(14), 1950,204

[34] Bendat JS, Piersol AG (1980) *Engineering applications of correlation and spectral analysis*. Wiley-Interscience, New York

[35] Herlufsen H (1984) Dual Channel FFT Analysis (Part I). *Technical Review* **No. 1**

[36] Oppenheim AV, Schafer RW, Buck JR (1999) *Discrete-time signal processing*. Prentice Hall, Upper Saddle River, NJ

[37] Sira-Ramírez H (2018) From flatness, gpi observers, gpi control and flat filters to observer-based adrc. *Control Theory and Technology* **16**(4), 249–260

[38] Sira-Ramírez H, Luviano-Juárez A, Ramírez-Neria M, Zurita-Bustamante EW (2018) *Active disturbance rejection control of dynamic systems: a flatness based approach*. Butterworth-Heinemann, Oxford, United Kingdom

[39] Spong MW (1998) Underactuated mechanical systems. In: *Control Problems in Robotics and Automation*, Springer, pp 135–150

[40] Tibshirani R (1996) Regression shrinkage and selection via the lasso. *Journal of the Royal Statistical Society: Series B (Methodological)* **58**(1), 267–288

[41] Lévine J (2009) *Analysis and control of nonlinear systems: A flatness-based approach*. Springer Science & Business Media

[42] Yoo D, Yau ST, Gao Z (2007) Optimal fast tracking observer bandwidth of the linear extended state observer. *International Journal of Control* **80**(1), 102–111

[43] Han J (2009) From PID to active disturbance rejection control. *IEEE transactions on Industrial Electronics* **56**(3), 900–906

[44] Li S, Yang J, Chen WH, Chen X (2011) Generalized extended state observer based control for systems with mismatched uncertainties. *IEEE Transactions on Industrial Electronics* **59**(12), 4792–4802

[45] Xiong S, Wang W, Liu X, Chen Z, Wang S (2015) A novel extended state observer. *ISA transactions* **58**, 309–317

[46] Zhao ZL, Guo BZ (2017) A nonlinear extended state observer based on fractional power functions. *Automatica* **81**, 286–296

[47] Ramírez-Neria M, Madonski R, Shao S, Gao Z (2020) Robust tracking in underactuated systems using flatness-based adrc with cascade observers. *Journal of Dynamic Systems, Measurement, and Control* **142**(9)

[48] Łakomy K, Madonski R (2020) Cascade extended state observer for active disturbance rejection control applications under measurement noise. *ISA transactions*

[49] Zhang D, Wu Q, Yao X (2018) Bandwidth based stability analysis of active disturbance rejection control for nonlinear uncertain systems. *Journal of Systems Science and Complexity* **31**(6), 1449–1468

[50] Liu C, Luo G, Duan X, Chen Z, Zhang Z, Qiu C (2019) Adaptive ladrc-based disturbance rejection method for electromechanical servo system. *IEEE Transactions on Industry Applications* **56**(1), 876–889

[51] Zheng Q, Gao LQ, Gao Z (2012) On validation of extended state observer through analysis and experimentation. *Journal of Dynamic Systems, Measurement, and Control* **134**(2)

[52] Ma SF, Leylaz G, Sun JQ (2020) Identification of differentially flat output of underactuated dynamic systems. *International Journal of Control* pp 1–27

[53] Isidori A (1995) *Nonlinear Control Systems*. Springer-Verlag London, London, United Kingdom

[54] Mori S, Nishihara H, Furuta K (1976) Control of unstable mechanical system control of pendulum. *International Journal of Control* **23**(5), 673–692

[55] Murray RM, Hauser JE (1991) A case study in approximate linearization: The acrobat example

[56] Banno I, i Azuma S, Ariizumi R, Asai T, i Imura J (2021) Data-driven estimation of finite-time controllability gramians. In: *Proceedings of 2021 60th Annual Conference of the Society of Instrument and Control Engineers of Japan (SICE)*, pp 666–670

[57] Mishra VK, Markovsky I, Grossmann B (2020) Data-driven tests for controllability. *IEEE Control Systems Letters* **5**(2), 517–522

[58] Shi YL, Hou CZ (2008) Design of improved nonlinear tracking differentiator. *Control and Decision* **23**(6), 647–650

[59] Guo BZ, Zhao ZL (2011) On convergence of tracking differentiator. *International Journal of Control* **84**(4), 693–701

[60] Guo BZ, Zhao ZL (2012) Weak convergence of nonlinear high-gain tracking differentiator. *IEEE Transactions on Automatic Control* **58**(4), 1074–1080

[61] Tian D, Shen H, Dai M (2013) Improving the rapidity of nonlinear tracking differentiator via feedforward. *IEEE transactions on industrial electronics* **61**(7), 3736–3743

[62] Han J (2008) *Active disturbance rejection control technique-the technique for estimating and compensating the uncertainties*. National Defense Industry Press, Beijing

[63] Kingma DP, Ba J (2014) Adam: A method for stochastic optimization. *arXiv preprint arXiv:14126980*